Optimisation of CCR7-based cellular models for future use in drug development programmes.

Emily Nicole Pilgrim
BSc Biochemistry

Submitted in fulfilment of requirements for the degree of MScR Cardiovascular Pharmacology.

School of Cardiovascular and Metabolic Health.
College of Medicine, Veterinary and Life Sciences.
University of Glasgow.

Supervisors: Professor George Baillie, Professor Joanne Edwards, Dr Connor Blair

Key Words

CCR7

CCL19

CCL21

Chemokine receptors

Colorectal Cancer

GPCR

HEK293 cells

Immune microenvironment

Kaplan-Meier survival analysis

Lymphatic dissemination

Metastasis

Prognostic biomarker

Contents

Acknowledgements

I would like to express my deepest gratitude to all those who have supported and contributed to this project.

First, I would like to thank Professor George Baillie, Dr Connor Blair, and the entire Lab 535 team for their mentorship, guidance, and continuous support throughout this project. Their expertise, encouragement, and constructive feedback were critical in aiding in troubleshooting challenges, experimental design, and interpreting complex data. A special thanks to Joe Graystone, the previous master's student whose foundational work laid the groundwork for this study, and who generously helped to introduce me to lab techniques and provide a strong starting point for this research.

I am particularly thankful for Susan Baillie and the Glasgow Imaging Facility for providing training and allowing access to their imaging facilities. Their support was instrumental in enabling the experiments presented in this study.

I am also extremely grateful to the Joanne Edwards Research Group at the Garscube Campus for providing access to their Colorectal Cancer RNA-seq datasets. Their assistance with bioinformatic analyses was invaluable and greatly enhanced the scope of this project.

Abbreviations

ADCs	Antibody Drug Conjugates
CCL19	C-C motif chemokine ligand 19
CCL21	C-C motif chemokine ligand 21
CCR7	C-C Chemokine Receptor 7
CLL	Chronic lymphocytic leukaemia
CNS	Central Nervous System
CRC	Colorectal Cancer
CSS	Cancer Specific Survival
CVS	Crystal Violet Stain
DCs	Dendritic Cells
dH_2O	De-ionised water
DMEM	Dulbecco's Modified Eagle Medium
EMT	Epithelial-mesenchymal transition
FBS	Foetal Bovine Serum
GPCR	G protein-coupled receptor
GDP	Guanosine diphosphate
GTP	Guanosine triphosphate
HEK293	Human Embryonic Kidney 293
HEVs	High Endothelial Venules
HPA	Human Protein Atlas
ICC	Immunocytochemistry
mAbs	Monoclonal Antibodies
PBS	Phosphate-Buffered Saline
PDCs	Peptide Drug Conjugates
PFA	Paraformaldehyde
P/S	Penicillin/Streptomycin
TME	Tumour Microenvironment
WB	Western Immunoblot

1. Abstract

C-C Chemokine receptor 7 (CCR7) is a cell surface receptor expressed on a range of immune cells, where it plays a critical role in mediating cell migration, chemotaxis, and immune homeostasis through interactions with its two specific ligands, CCL19 and CCL21. Emerging evidence has demonstrated that cancer cells can exploit CCR7 expression to hijack its natural mechanisms, promoting the metastatic dissemination of malignant cells throughout the body. While CCR7 has been identified as a promising therapeutic target, it also presents significant challenges as targeting this receptor could disrupt immune function and lead to adverse effects, including chronic inflammation and autoimmune diseases.

In this study, CCR7 is evaluated as a potential biomarker in oncology by analysing its expression and functional role across selected cancer models, whilst simultaneously attempting to establish a transient and validated CCR7-expressing cell-based system to support future high-throughput drug screening efforts. These findings provide insights into the oncogenic role of CCR7 and establish a platform for targeted therapeutic discovery, while also addressing the biological implications of modulating this receptor.

2. Introduction

C-C Chemokine receptor 7 (CCR7) is a G protein-coupled receptor (GPCR) that plays a pivotal role in immune cell migration, chemotaxis, and maintaining immune homeostasis [1]. Its biological activity is mediated through interactions with its two primary ligands, C-C motif chemokine ligand 19 (CCL19) and C-C motif chemokine ligand 21 (CCL21) [2]. These ligands are predominantly expressed by stromal cells within lymphoid tissues and establish local chemokine gradients that direct the movement of CCR7-expressing cells to secondary lymphoid organs, where immune responses are initiated [3].

CCL21 is expressed by lymphatic endothelial cells and high endothelial venules (HEVs) within secondary lymphoid organs, including lymph nodes and Peyer's patches [3-5]. This ligand is immobilised on the luminal surface of HEVs and lymphatic vessels, enabling haptotactic migration and recruitment of CCR7-expressing cells [3, 6-8]. In contrast, CCL19 is primarily produced by mature dendritic cells (DCs) in the T-cell zones of lymphoid tissues and functions to attract T cells and other CCR7 expressing immune cells [2,4].

Together, CCL19 and CCL21 orchestrate the migration of CCR7-expressing cells, such as DCs, T cells, B cells, and natural killer (NK) cells, to secondary lymphoid organs, including the lymph nodes and spleen [1,3,6]. This then facilitates antigen presentation, T cell priming, and the initiation of adaptive immune responses [9].

Dysregulated CCR7 signalling can lead to the misguidance of immune cells and result in impaired immune surveillance and adaptive immune responses, contributing to the development of chronic inflammation and various autoimmune diseases [3,9]. Furthermore, increased CCR7 expression has been observed in numerous cancer cells, where it has been identified as playing a key role in driving tumour metastasis [10]. These cancer cells exploit CCR7-mediated chemotactic pathways to migrate towards lymphatic tissues, enabling dissemination and the formation of secondary tumours, particularly in the lymph nodes, thereby driving disease progression [3,9,10].

Metastasis remains the leading cause of cancer related mortality, estimated to be responsible for 90% of cancer deaths, and remains a major challenge in the development of effective cancer treatments. Understanding the molecular mechanisms driving metastasis is essential for identifying therapeutic targets and improving patient outcomes [11]. Hijacking the CCR7 receptor’s natural mechanisms of action in the immune response has emerged as one of the

many pathways involved in facilitating tumour cell migration, survival, and immune evasion [10]. Its involvement in cancer metastasis, especially to lymph nodes, makes it an attractive therapeutic target in the fight against metastatic cancer.

2.1 CCR7 Overview: Structure, Localisation, and Function

2.1.1 Structure

CCR7 is a GPCR comprised of 378 amino acids, characterised by seven transmembrane alpha-helices, an extracellular N-terminal domain involved in ligand recognition and binding, and intracellular regions, including the C-terminal domain, that facilitate its interaction with G-proteins and mediates downstream signal transduction upon ligand binding (Fig. 1,2) [2,4].

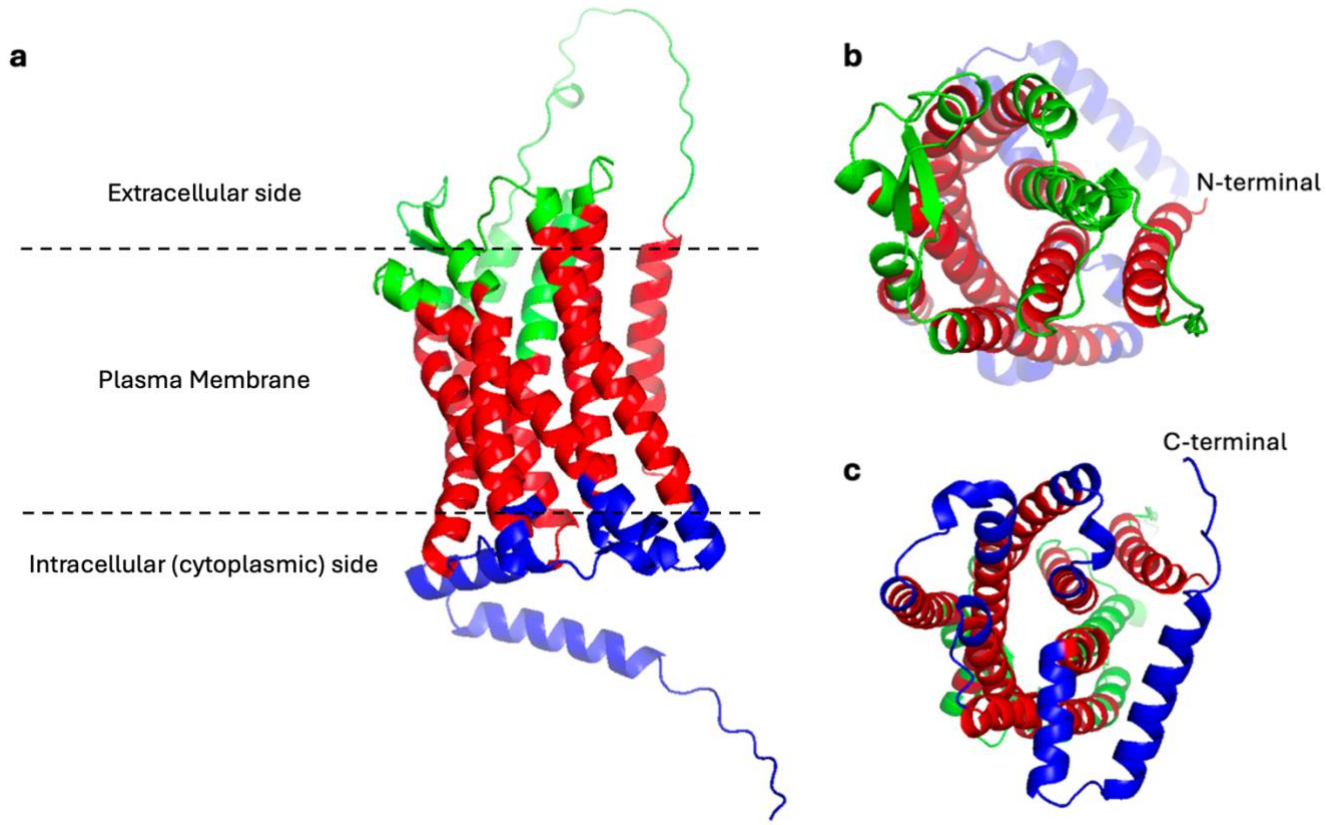

Figure 1 – Predicted three-dimensional structure of the human CCR7 receptor generated using AlphaFold and visualised in PyMOL.

Structural regions are colour coded: extracellular region (green), transmembrane (topological) region (red), and intracellular region (blue).

The N-terminal (residues 1-24) and C-terminal are indicated.

***(a)** Side (lateral) view.*

***(b)** Top-down view from the extracellular side.*

***(c)** Bottom-up view from the intracellular side.*

A unique structural characteristic of CCR7 is its cleavable sequence (24 amino acids long) within the N-terminal domain (Fig. 1), which is essential for trafficking the receptor from the endoplasmic reticulum, where it is synthesised, to the Golgi apparatus via endosomal pathways, ensuring efficient surface membrane localisation and functional ligand interactions [12].

Once imbedded in the cell membrane, CCR7 is able to selectively bind to its two ligands, CCL19 and CCL21 (Fig. 2). Despite their structural similarities, these ligands exhibit distinct functional characteristics and expression patterns that critically influence CCR7-mediated signalling [2,3,13]. CCL19, primarily secreted by DCs, efficiently recruits ß-arrestin, leading to receptor

internalisation via clathrin-coated pits, which then desensitises CCR7 and generates robust, transient, signalling [2,3,13]. In contrast, CCL21 features a unique glycosaminoglycan (GAG)-binding C-terminal tail which allows it to form stable chemokine gradients on lymphatic endothelial surfaces, facilitating haptotactic migration of immune cells [2,13,14]. These complementary functions enable CCR7 to precisely regulate immune cell trafficking and positioning, thus facilitating adaptive immune responses.

2.1.2 Localisation

CCR7 is a membrane bound signalling GPCR that is expressed on a wide range of immune cells, including DCs, naïve B and T cells, T regulatory (T-reg) cells, and central memory T cells, as well as secondary lymphoid organs, such as the lymph nodes, spleen, and mucosal tissues, where it plays a critical role in immune surveillance and response [1-3,12]. It is also minimally expressed in the GI tract and certain cells in the central nervous system (CNS) [14]. Notably, CCR7 expression is upregulated on DCs and NK cells in response to pathogens and in various malignancies, highlighting its role in pathophysiological processes beyond immune homeostasis [1-3]. This upregulation in cancers, particularly in metastatic cancers, highlights its role in tumour progression and immune evasion.

2.1.3 Function

CCR7 guides the migration of immune cells, particularly naïve T cells and DCs, to secondary lymphoid organs where immune responses are initiated [2,3]. Most notably, this migration ensures that antigen-presenting DCs encounter naïve T cells, a vital step required for initiating antigen-specific adaptive immune responses [3,13].

The establishment of local chemokine gradients enables CCR7 to guide immune cells to precise microanatomic locations, facilitating immune cell trafficking and communication [3,6]. The spatial and temporal distribution of CC19 and CCL21 is critical to CCR7's function, and these ligands complement each other's role in this process. CCL19, with its shorter signalling lifespan, fine-tunes immune cell positioning and activation through transient, high-intensity signalling, while CCL21's GAG-binding capacity enables the formation of stable, long-distance gradients on endothelial and stromal cell surfaces, directing immune cell migration along haptotactic cues [2,13]. Together, these ligands enable CCR7 to efficiently direct immune cells to sites where an immune response has been initiated.

Alongside guiding cell migration, CCR7 also contributes to the structural integrity of lymphoid organs through its ability to regulate immune cell positioning, particularly during embryogenesis and postnatal lymphoid tissue development. This positioning optimises immune surveillance by shaping the architecture of lymph nodes and other lymph tissues, ensuring the proper migration and positioning of immune cells within these tissues, and therefore optimising immune responses [3,4,9].

Moreover, CCR7 contributes to resolving inflammation by directing the migration of activated T cells and DCs from inflammatory responses to lymphatic vessels, where they are then cleared from the inflamed tissues. This further highlights CCR7's dual role in both initiating and resolving immune responses, thus maintaining tissue homeostasis and preventing chronic inflammation [3,15].

2.1.4 CCR7-associated pathways

Upon binding of CCL19 or CCL21, CCR7 undergoes a conformational change that enables coupling to heterotrimeric Gi-proteins located on the intracellular surface of the plasma membrane (Fig. 2) [13,15,16]. In its inactive state, the Gα subunit is bound to guanosine diphosphate (GDP) and remains associated with the Gβγ subunits. Ligand binding promotes the exchange of GDP for guanosine triphosphate (GTP) on the Gα subunit, resulting in dissociation of the Gα and Gβγ complexes and subsequent activation of downstream signalling effectors [13,15].

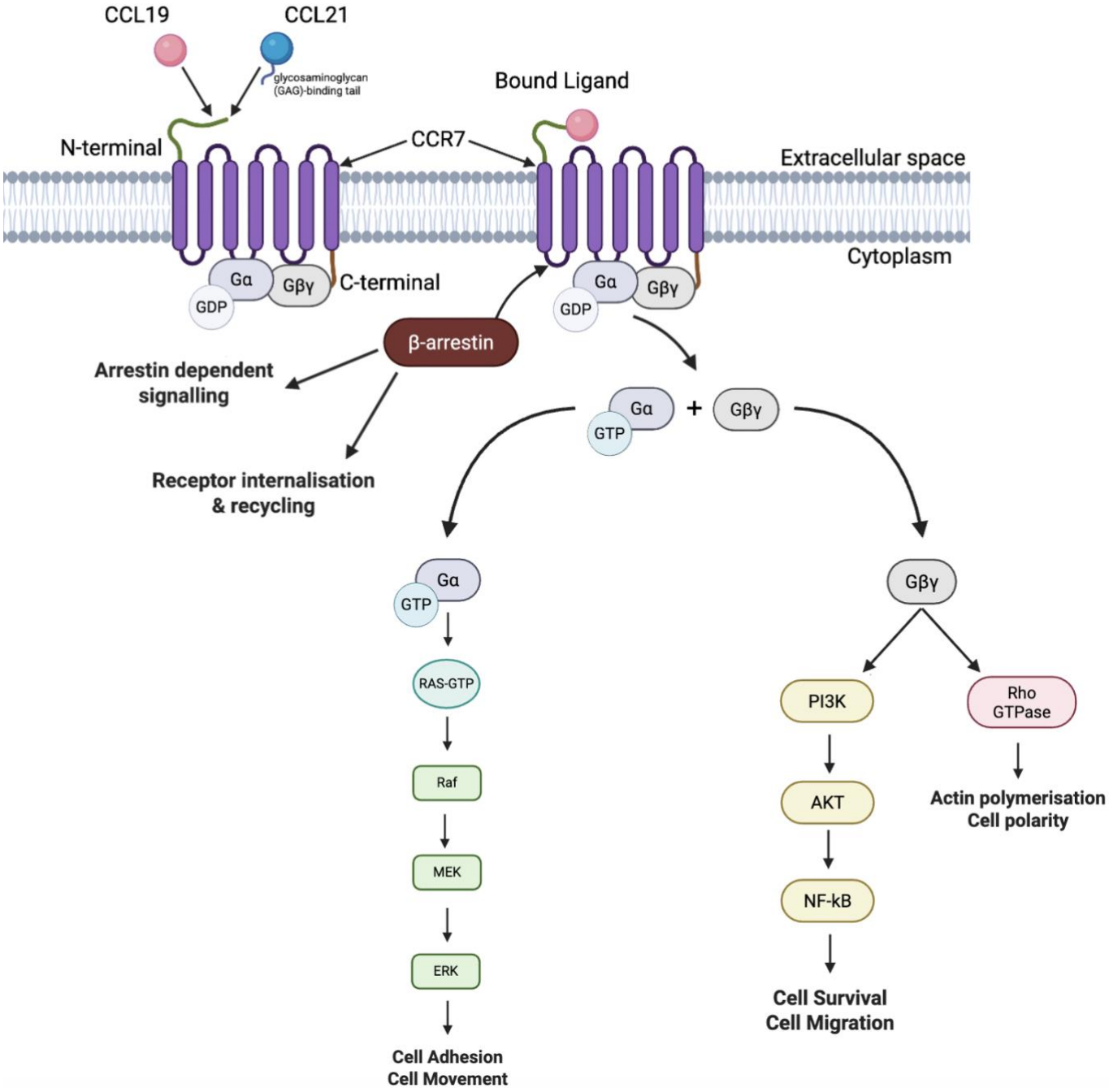

Figure 2 – Localisation and downstream signalling pathways of CCR7 following ligand binding

Image produced using BioRender.

Schematic representation of the chemokine receptor CCR7 localised within the plasma membrane and its activation following binding of the ligands CCL19 and CCL21. Ligand binding induces a conformational change in CCR7, promoting activation of the associated heterotrimeric Gi protein complex. Exchange of GDP for GTP on the Gαi subunit promotes dissociation of the Gi complex into Gαi-GTP and Gβγ subunits, leading to the activation of multiple downstream signalling cascades. These include: PI3K/AKT, ERK/MAPK, and Rho family GTPase signalling pathways, which regulate cell survival, migration, polarity, cytoskeletal remodelling, and transcriptional responses. Recruitment of β-arrestin promotes receptor

desensitisation, internalisation, recycling, and arrestin-dependent signalling. CCL21 additionally contains a positively charged C-terminal extension that facilitates glycosaminoglycan (GAG) binding and contributes to immobilised chemokine gradients. Straight arrows indicate the direction of intracellular signal transduction following CCR7 activation.

***Abbreviations**: ERK, extracellular signal-regulated kinase; PI3K, Phosphatidyl inositide-3-kinase; AKT, protein kinase B; NF-κB, nuclear factor-κB; MAPK, mitogen-activated protein kinase.*

These signalling intermediates activate multiple intracellular signalling cascades, including phosphoinositide 3-kinase (PI3K)/AKT, extracellular signal-regulated kinase (ERK)/mitogen-activated protein kinase (MAPK), and Rho family GTPase signalling, which collectively coordinate cytoskeletal remodelling, chemotaxis, cell survival, and immune cell migration [15–17]. Specifically, the PI3K/AKT pathway promotes cell survival and migration, while the ERK/MAPK pathway induces cytoskeletal changes necessary for changes in cell shape and adhesion during tissue migration [15,16]. Members of the Rho family of GTPases regulate actin polymerisation, cell polarity, and endocytosis, further facilitating immune cell trafficking [15,17]. These signalling pathways operate independently but work in a coordinated manner to ensure cell survival and enable efficient immune responses [13].

CCR7 signalling also overlaps with broader immune regulatory pathways, such as cross-talk with T-cell receptor pathways to enhance T cell activation and differentiation [18]. Furthermore, its interaction with podoplanin, a proteoglycan expressed on lymphatic endothelial and stromal cells, modulates CCL21 presentation and gradient formation, thus facilitating precise immune cell homing and tissue distribution [19].

2.2 CCR7 in Disease

2.2.1 CCR7 in Inflammatory and Autoimmune diseases

CCR7 dysfunction is closely linked to immune dysregulation, contributing to a wide range of pathologies, including autoimmune diseases, chronic inflammatory disorders, and cancer [2,7]. In autoimmune conditions such as rheumatoid arthritis, multiple sclerosis, and systemic lupus erythematosus, aberrant CCR7 expression disrupts the normal trafficking of immune cells [12,13]. This misdirection facilitates the infiltration and accumulation of autoreactive lymphocytes in target tissues, leading to chronic inflammation and progressive tissue damage [7].

In chronic inflammatory diseases, dysregulated CCR7 signalling causes an exaggerated or prolonged immune response, perpetuating tissue damage and the chronicity of the inflammatory response [7]. Conversely, insufficient CCR7 activity can impair the effective clearance of immune cells from inflamed sites, further exacerbating inflammatory responses [7,12,20].

Although CCR7 is essential for maintaining immune homeostasis, its dysregulation can result in a range of serious pathological consequences. This complexity presents significant challenges when it comes to therapeutic targeting, particularly in conditions like cancer where CCR7 can simultaneously support anti-tumour immune responses while also promoting tumour metastasis.

2.2.2 CCR7 in Cancer

CCR7 plays a multifaceted role in cancer biology, primarily through its involvement in promoting cancer metastasis and facilitating immune evasion. CCR7 overexpression has been identified in numerous malignancies, including breast, lung, and colorectal cancers, as well as melanoma, and lymphoma (Fig. 3) [10]. As a result, this receptor is often associated with advanced disease stages, larger tumour sizes, and poor clinical prognosis, making it a reliable biomarker for aggressive tumour behaviour. In many cancers, CCR7 overexpression correlates with increased metastatic potential, particularly to the lymph nodes, which significantly impacts prognosis [1,10].

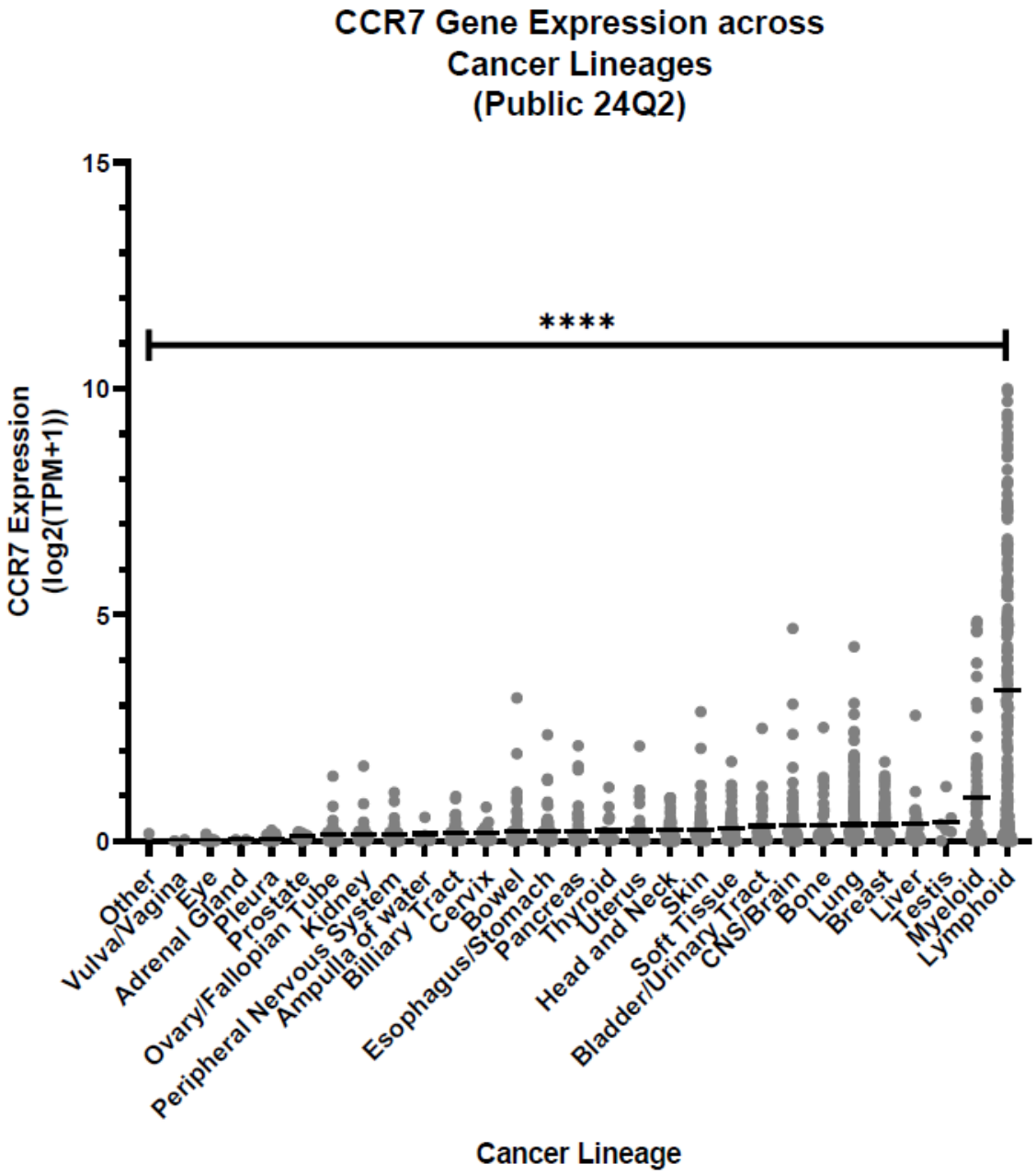

Figure 3 – CCR7 expression across cancer lineages in the DepMap Public 24Q2 dataset.
CCR7 mRNA expression levels were obtained from the DepMap Public 24Q2 transcriptomic dataset and are plotted as $log_2(TPM + 1)$ across annotated cancer lineages. Each point represents a single cell line. Lineages correspond to the tissue of origin classifications provided by DepMap. The log transformation normalises the expression distribution and reduces skew from highly expressed genes.
*The lymphoid lineage exhibited significantly higher CCR7 expression compared to all other lineages (****P < 0.0001, multiple comparisons test).*

CCR7 expression was detected across a wide range of cancer lineages (Fig. 3), with the highest levels observed in lymphoid, myeloid, breast, and lung-derived cancers. Among these, lymphoid

cancers exhibited significantly elevated CCR7 mRNA expression compared to all other lineages (****P < 0.0001, multiple comparisons test). This is consistent with CCR7's established role in immune cell trafficking, particularly in directing lymphocytes to secondary lymphoid organs via chemokine gradients [10]. The data also highlight a strong tissue-specific enrichment, reinforcing the relevance of CCR7 in cancers arising from or interacting with the immune system.

Notably, mutations in CCR7, CCL19, and CCL21 are relatively rare across DepMap cancer cell lines, and do not appear to significantly influence expression levels. This suggests that CCR7 overexpression is likely regulated transcriptionally rather than being mutation-driven.

This elevated expression in lymphoid malignancies suggests that CCR7 has a biological relevance that extends beyond immune surveillance. Given its known function in guiding immune cells along chemokine gradients, this expression pattern raises the possibility that tumour cells similarly exploit CCR7-mediated signalling to promote migration, particularly towards lymphatic structures. As a result, CCR7 presents itself as a promising therapeutic target for inhibiting lymphatic dissemination and improving patient outcomes.

CCR7 facilitates cancer progression through several interconnected mechanisms, including lymph node metastasis, modulation of the tumour microenvironment (TME), and epithelial-mesenchymal transition (EMT) [10,21].

2.2.3 Lymph Node Metastasis

One of CCR7's most characterised roles is in promoting lymphatic dissemination of cancer cells through interactions with its ligands, particularly CCL21 [1,10,21]. Tumour cells expressing CCR7 display enhanced motility and cell adhesion, enabling them to utilise lymphatic pathways to establish metastatic colonies in lymphoid tissues. This interaction between CCR7 and CCL21 both promotes directional migration and activates integrin-mediated adhesion to the lymphatic endothelium, thus promoting tumour cell extravasation into lymph nodes and the colonisation of these tissues [10].

This behaviour has significant clinical implications. In breast cancers, CCR7 expression strongly correlates with lymph node metastasis, particularly in aggressive subtypes such as triple-negative and luminal B cancers. However, in low-grade luminal A tumours, CCR7 expression alone does not always predict lymphatic migration, likely due to interactions with other

regulatory factors like hormones, and inflammatory mediators, such as TNF-α and epidermal growth factor [10]. Therefore, while CCR7 has been identified as a critical driver of lymphatic metastasis, its prognostic significance may vary across cancer types.

CCR7's ability to promote chemotaxis, cell adhesion, and lymphangiogenesis identify the receptor as a critical mediator of lymphatic dissemination as well as a potential target to disrupt metastatic cascades and improve patient outcomes [10,21].

2.2.4 Tumour Microenvironment (TME) Modulation

CCR7 aids in modulating the composition and function of the TME in order to favour tumour progression and immune evasion [22]. It does this by recruiting regulatory immune cells, such as T-regs and myeloid-derived suppressor cells, to promote an immunosuppressive environment and, as a result, prevent effective anti-tumour immune responses. T-regs present in solid TMEs can suppress the function of cytotoxic T cells, which further aids the evasion of tumour cells from immune-mediated destruction [1]. Additionally, CCR7 signalling in DCs impairs their maturation and antigen-presenting abilities, further weakening T-cell-mediated immunity and enabling tumour cells to evade immune surveillance [1,23].

CCR7 facilitates the migration of malignant cells to lymphoid tissues, where interactions with the local stroma enhance tumour survival and immune evasion, particularly in lymphoid cancers such as Hodgkin lymphoma and chronic lymphocytic leukaemia (CLL) (Fig. 4). Malignant cells exploit CCR7 to position themselves in niches that are rich in CCL19 and CCL21. These interactions enable tumour cells to access trophic factors, such as IL-7 and CXCL12, which further support their proliferation and resistance to apoptosis [14].

2.2.5 Epithelial-Mesenchymal Transition (EMT)

The activation of CCR7 has been strongly linked to EMT, an important process required for cancer cell metastasis and drug resistance. During EMT, epithelial cells lose their cell-cell adhesion properties and gain mesenchymal traits, specifically heightened motility and invasiveness. This enables tumour cells to detach from their primary sites to invade surrounding tissues and spread to distant sites around the body [24,25].

CCR7 facilitates this transition by activating signalling pathways, like PI3K/AKT and ERK/MAPK, which upregulate EMT-inducing transcription factors, such as Snail, Twist, and ZEB1 [24]. These transcription factors promote the downregulation of epithelial markers, like E-cadherin, while

also upregulating EMT markers, thus facilitating the detachment of tumour cells from primary sites and their migration to surrounding tissues [10,23,25]. In breast and lung cancers, high CCR7 expression (Fig. 3) correlates with increased EMT marker expression and more aggressive phenotypes [10,23]. Similarly, in gastric cancer, CCR7 enhances TGF-β1-induced EMT, promoting lymph node metastasis and poor survival rates [23].

As a result, targeting CCR7 or its downstream pathways, such as PI3K/AKT, ERK/MAPK, or TGF-β1, presents a promising therapeutic strategy to inhibit EMT, reduce metastasis, and enhance the efficacy of existing treatments.

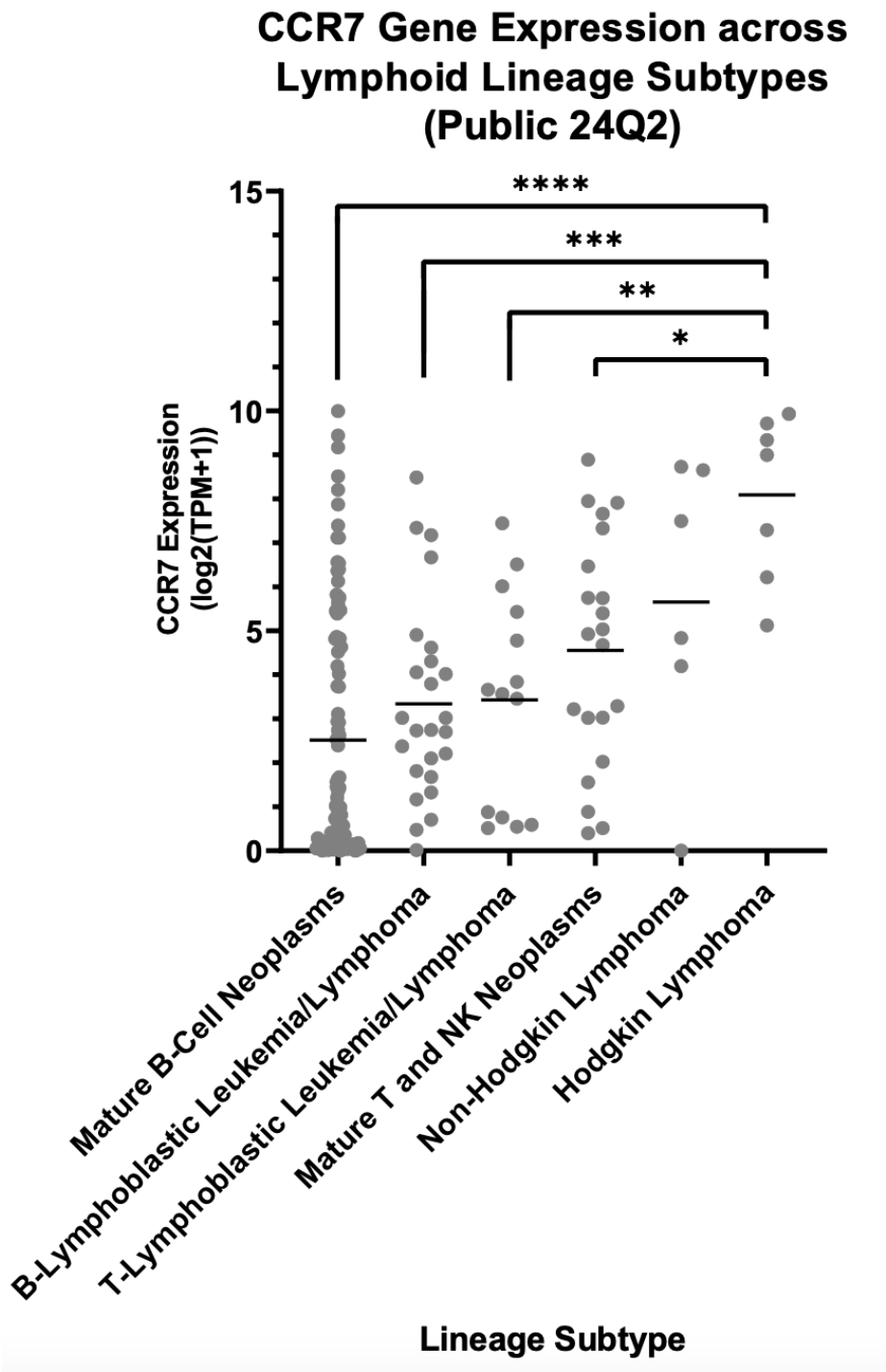

Figure 4 – CCR7 expression across lymphoid lineage subtypes in the DepMap Public 24Q2 dataset.

CCR7 mRNA expression levels were obtained from the DepMap Public 24Q2 transcriptomic dataset and are plotted as $\log_2(TPM + 1)$ across lymphoid-derived cancer lineages. Each data point represents an individual cancer cell line; lineages are grouped by tissue of origin, as classified by DepMap. The log-transformation normalises expression values and reduces skew from outliers.

*Statistical significance between subtypes was assessed and annotated as follows: ****P < 0.0001, ***P < 0.001, **P < 0.01, *P < 0.05.*

The elevated average expression of CCR7 in Hodgkin's lymphoma compared to other subtypes of lymphomas suggests CCR7 plays a key role in its disease progression, particularly in cell metastasis and immune evasion, which are processes commonly associated with high CCR7 expression.

In contrast, the broad range of expression within Mature B-cell neoplasms, despite its overall low average, could point to the heterogeneity of CCR7 expression within this subtype. This variability suggests that CCR7 may have a more significant impact in some patients, making it a potential target for treatments, particularly in cancers where CCR7 is more highly expressed.

While Hodgkin lymphoma shows the highest average CCR7 gene expression among lymphoid subtypes, it is important to note the presence of both high and low expressers across all groups. This bimodal distribution suggests that expression heterogeneity exists within each subtype. Given the relatively small number of cell lines per group, these observed differences in average expression may be influenced by sample size. Therefore, if larger cohorts were available, it would provide a more statistically reliable comparison and may show that a similar range of high and low CCR7 expressers would emerge across other subtypes too.

The statistically significant differences in CCR7 gene expression across lymphoid subtypes suggest that CCR7 may contribute to tumourigenesis and metastasis in a lineage-specific manner. For instance, the significantly higher expression observed in Hodgkin Lymphoma compared to other subtypes indicates that CCR7 has a more prominent role in the progression of this malignancy. This could suggest that Hodgkin lymphoma cells are more reliant on CCR7-mediated signalling pathways for disease progression, including immune evasion, migration to lymph nodes, or interactions with TME.

However, the lack of statistically significant difference in expression levels across other subtypes suggests that factors beyond CCR7 expression, such as the presence of co-factors or alternative signalling pathways within the TME, could also influence cancer progression and metastatic dissemination. This indicates that CCR7's role in these processes may be context-dependent, varying across different malignancies based on additional molecular factors.

Ultimately, Figure 4 highlights CCR7 as a potential biomarker and therapeutic target, particularly in Hodgkin lymphoma, where CCR7 expression levels are significantly higher. However, the heterogeneous expression patterns in other lymphoid malignancies emphasises the need for personalised treatment strategies that account for individual variations in CCR7 activity. To better understand the precise mechanisms by which CCR7 contributes to cancer progression across various lymphoid malignancies, further studies with larger patient cohorts and functional assays are necessary.

2.3 CCR7 as a Therapeutic Target

Despite CCR7 being recognised for its role in cancer progression, the development of therapies that target this receptor have faced challenges in achieving therapeutic specificity, mitigating side effects, and translating preclinical findings into clinically effective treatments [26,27]. The diverse role of CCR7 in biological processes, most notably immune homeostasis and cell trafficking, poses significant challenges when it comes to designing therapeutic targets since systemic inhibition of this receptor may lead to widespread immune disruption and adverse effects such as chronic inflammation or increased susceptibility to infections [28,29].

Unlike other cytokine receptors that share ligands, CCR7 binds exclusively with CCL19 and CCL21, reducing the risk of off-target effects associated with targeted therapies [28]. However, CCR7 can also engage in biased signalling where the downstream pathways activated depend upon the specific ligand that binds, as well as the cellular context, which introduces further complexity [30]. Additionally, the widespread expression of CCR7 across numerous different immune cells and tissues throughout the body poses additional concerns for developing CCR7-targeted therapies [31]. For example, while CCR7 activation can promote anti-tumour immune responses by recruiting cytotoxic T cells to the TME, these pathways can also be hijacked by tumour cells to facilitate the metastasis and dissemination to the lymph nodes and other organs [8,29].

These challenges underscore the urgent need for more precise, context-dependent strategies that can selectively regulate CCR7 activity to harness its therapeutic potential while minimising adverse effects. Several novel approaches are being explored to overcome these challenges associated with CCR7 targeting, offering promising new strategies for the development of effective cancer therapies.

2.3.1 Existing clinical and preclinical therapies

One particular area of focus involves the development of monoclonal antibodies (mAbs) that target chemokines or their receptors to treat a range of cancers, including colon and breast cancer, melanoma, and leukaemia [32]. By specifically targeting CCR7 or its ligands, mAbs can disrupt receptor-ligand interactions, thus impairing the receptor's function and blocking its downstream signalling pathways.

A promising example of this approach is CAP-100, an anti-CCR7 antibody currently undergoing a Phase I clinical trial for relapsed CLL patients (NCT04704323) [33]. This mAb has demonstrated high specificity, disruption of CCR7-mediated migration and survival, and favourable safety compared to existing agents [33-36]. Additionally, mAbs can be engineered as antibody drug conjugates (ADCs), which deliver cytotoxic agents directly to tumour cells overexpressing CCR7. ADCs combine the specificity of mAbs with the potency of cytotoxic drugs, enhancing their therapeutic index while also minimising their off-target effects [28]. An example of this is JHB492, a mAb currently undergoing phase 1 clinical trials (NCT04240704) [38]. This mAb is a first in class CCR7 targeting ADC that can selectively eliminate CCR7-positive tumour cells while sparing healthy tissues [38].

An emerging alternative to ADCs is the use of peptide drug conjugates (PDCs), which allow for the targeted delivery of a cytotoxic payloads to tumour cells that overexpress CCR7, thereby enhancing the efficacy and precision of treatment [39]. PDCs targeting CCR7 offer several advantages over ADCs, including improved tumour penetration, shorter systemic half-life, and reduced off-target toxicity [40].

CCR7-targeting PDCs hold great promise for improving both the efficacy and safety of cancer therapies, especially in cancers characterised by dense stromal environments or deep tissue metastases.

2.3.2 Opportunities for future therapies

CCR7 targeting therapies may be further enhanced by adopting combination approaches that exploit complementary mechanisms of action to overcome the limitations of monotherapies. These strategies hold significant potential for improving therapeutic outcomes by addressing both tumour progression and resistance to current treatments.

One possible approach would be to combine CCR7 targeting therapies with immune checkpoint inhibitors (ICIs), such as anti-PD-1 or anti-CTLA-4, which could enhance T cell-mediated immunity. ICIs are effective in 'hot' tumours, characterised by significant immune cell infiltration, but their efficacy is limited in 'cold' tumours due to immunosuppressive TMEs [41]. CCR7 targeting therapies that inhibit this receptor could facilitate migration of cytotoxic T cells to the TME, converting 'cold' tumours into 'hot' tumours and enhancing ICIs therapeutic benefits [42].

Similarly, the combination of CCR7 targeting therapies with conventional cytotoxic therapies, such as chemotherapy, or advanced modalities like ADCs and PDCs, allows for the selective delivery of cytotoxic payloads to cells overexpressing CCR7, amplifying local drug activity while minimising systemic toxicity [42]. Additional combination therapies with agents targeting angiogenesis, such as VEGF inhibitors, or BTK inhibitors show promise in disrupting tumour vascularisation and B cell-mediated immune evasion in haematological cancers [43].

Another innovative approach is RNA interference (RNAi) therapies, which reduces CCR7 mRNA levels. Preclinical studies, such as those using small interfering RNAs (siRNAs) to target CCR7 in bladder cancer models, have shown promising results. While translating RNAi based therapies into clinical practice has faced many challenges, the use of nanoparticle-based delivery systems, particularly lipid nanoparticles, have demonstrated great potential in stabilising RNA payloads and enabling targeted delivery to cells overexpressing CCR7 [44].

While CCR7 targeting therapies hold significant promise, challenges remain in optimising combination strategies, addressing delivery issues, and ensuring stability and specificity. The heterogeneity of cancer and the variability in CCR7's involvement across different cancer types also complicates therapeutic development. Despite these challenges, the continued evolution of CCR7 targeted approaches has the potential to revolutionise the treatment of metastatic cancers. With further development, these strategies could achieve more precise, effective, and tailored treatments for patients, thus improving clinical outcomes.

2.3.3 Study Aims

CCR7 is a key regulator of immune cell trafficking through its interaction with CCL19 and CCL21, and plays a central role in maintaining immune homeostasis. However, its dysregulation has been implicated in cancer progression, particularly in lymphoid malignancies, where elevated CCR7 expression is associated with increased migration, invasion, and metastasis. These

oncogenic behaviours make CCR7 a compelling candidate for both therapeutic targeting and biomarker development in oncology.

Given the therapeutic potential and biological complexity of CCR7, this study aims to:

1. Interrogate CCR7 as a pro-oncogenic marker across selected cancer contexts, providing insight into its expression patterns and relevance in tumour progression.
2. Develop and optimise a CCR7-Flag overexpression cellular model to enable downstream functional assays and drug development.

The development of this cellular model is particularly important for future downstream applications, including peptide array-based screening approaches, where CCR7-enriched lysates can be used to identify potential binding partners or interaction motifs. Given that CCR7 is a GPCR and not readily amenable to direct immobilisation on peptide arrays, the use of lysates derived from CCR7-overexpressing cells provides a practical alternative for probing protein–peptide interactions. Such approaches could facilitate the identification of peptides capable of disrupting CCR7-mediated signalling, thereby contributing to early-stage therapeutic development.

Together, these aims will establish a foundation for high-throughput screening and contribute to understanding CCR7's role in cancer biology, thus supporting the development of targeted and more effective therapeutic strategies.

3. Materials and Methods

3.1 Materials

3.1.1 Media and Buffers

All reagents and consumables were prepared and stored according to manufacturer guidelines unless otherwise stated. Table 1 lists the commercially sourced reagents used throughout this study.

***Table 1**. Materials used for Media and Buffers in this study.*

Reagent	Supplier	Catalogue Number
Tissue Culture		
Dulbecco's Modified Eagle Medium (DMEM)	Gibco™, ThermoFisher	11965092
10% Foetal Bovine Serum (FBS)	Sigma-Aldrich	F9665
100 U/mL Penicillin/Streptomycin (P/S)	Sigma-Aldrich	P0781
1X Phosphate-Buffered Saline (DPBS)	Gibco™, ThermoFisher	14190094
OptiMEM™ Reduced Serum Medium	Gibco™, ThermoFisher	31985070
Cell Lysis		
cOmplete™, EDTA-Free Protease Inhibitor	Roche	11697498001
phosSTOP™ Phosphotase Inhibitor	Roche	4906837001
Electrophoresis and Immunoblotting		
Blocking Buffer (0.5X Intercept® TBS)	LI-COR	NC1703226

3.1.2 Media and Buffer Preparation

The following solutions were prepared in-house and used as described in the corresponding protocols.

Gel Electrophoresis

- **10X TAE Buffer**: 0.89 M Tris-base, 0.89 M Acetic Acid, 20 mM EDTA (pH 8.3). Diluted to 1X for working concentration.

Western Immunoblotting

- **5X SDS Sample Buffer**: 10% SDS, 300 mM Tris-HCl, 0.05% bromothymol blue, 10% ß-mercaptoethanol.
- **1X TBS**: 20 mM Tris-HCl (pH 7.4), 150 mM NaCl.

- **1X TBS-T**: TBS supplemented with 0.1% Tween-20 (w/v).

Cell Lysis

- **Immunoprecipitation (IP) Buffer**: 25 mM Tris, 150 mM NaCl, 0.1 mM EDTA, 1% NP-40, 5% glycerol, pH 7.4; supplemented with protease and phosphatase inhibitors.
- **RIPA Buffer**: 150 mM NaCl, 50 mM Tris-base, 1% Triton X-100, 0.5% sodium deoxycholate, 0.1% SDS, pH 8.0; supplemented with protease and phosphatase inhibitors.

Transient Transfection

- **DMEM formulations**:
    - DMEM (0% FBS, 100 U/mL P/S)
    - DMEM (5% FBS, 100 U/mL P/S)

3.1.3 Antibodies

All antibodies (Table 2) were stored at -20ºC and diluted using Intercept® T20 (TBS) Antibody Diluent (Li-Cor, #NC1703226). They were used in Western blotting (WB) and Immunocytochemistry (ICC).

***Table 2**. List of Primary and Secondary Antibodies used in this study.*

Target	Host / Type	Application(s)	Dilution	Supplier	Catalogue Number	Fluorophore
Primary Antibodies						
CCR7	Rabbit polyclonal	WB, ICC	1:1000 (WB), 1:250 (ICC)	ProteinTech	25898-1-AP	-
CCR7 (clone SR36-04)	Rabbit monoclonal	WB	1:1000 (WB)	Thermo Fisher Scientific	MA5-31992	-
Anti-DDDDK tag (Binds to FLAG® tag sequence)	Rabbit monoclonal	WB	1:1000 (WB)	Abcam	EPR20018-251	-
FLAG (DDDDK-tag)	Mouse monoclonal	WB, ICC	1:1000 (WB), 1:1000 (ICC)	ProteinTech	66008-4-Ig	-
GAPDH	Mouse monoclonal	WB	1:80,000 (WB)	ProteinTech	60004-1-Ig	-
CCL21	Rabbit polyclonal	WB	1:1000 (WB)	PeproTech®	500-P109-50UG	-
CCL19 / MIP-3β	Rabbit polyclonal	WB	1:1000 (WB)	ProteinTech	13397-1-AP	-
Western Immunoblotting Secondary Antibodies						
Donkey anti-mouse IgG	Donkey, secondary, IRDye 800	WB	1:5000 (WB)	LI-COR	926-32212	-
Donkey anti-rabbit IgG	Donkey, secondary, IRDye 680	WB	1:5000 (WB)	LI-COR	926-68073	-
Immunocytochemistry Secondary Antibodies						
Donkey anti-mouse IgG	Donkey polyclonal	ICC	1:500 (ICC)	Invitrogen	A-21202	Alexa Fluor® 488
Donkey anti-rabbit IgG	Donkey polyclonal	ICC	1:500 (ICC)	Invitrogen	A-31573	Alexa Fluor® 647
DAPI	Chemical stain	ICC (nuclear staining)	Ready-to-use	ThermoFisher Scientific	P36935	Emits blue (~461 nm)

3.1.4 Ligands

All proteins (Table 3) were supplied with carrier and used in Western blotting (WB) and Transwell migration assays.

***Table 3**. Recombinant chemokine ligands used in this study.*

Ligand	Protein Type	Carrier	Application	Supplier	Catalogue Number
CCL19	Recombinant Human CCL19/MIP-3β	With Carrier	WB, Transwell Migration Assay	Bio-Techne / R&D Systems	361-MI-025
CCL21	Recombinant Human CCL21/6Ckine	With Carrier	WB, Transwell Migration Assay	Bio-Techne / R&D Systems	366-6C-025

3.1.5 CCR7 Plasmid

A standard pcDNA3.1(+)-N-DYK expression plasmid encoding the CCR7 gene was obtained from GenScript™. The lyophilised plasmid was reconstituted as per manufacturer instructions and stored at -20ºC for downstream applications.

3.2 Methods

3.2.1 Bacterial Transformation

All stages of bacterial transformation were performed aseptically using a Bunsen burner and sterile equipment.

LB-Ampicillin Agar Plates

LB-agar plates containing 100 µg/mL ampicillin were prepared using the following formulation: 5 g tryptone, 5 g NaCl, 2.5 g yeast extract, and 15 g agar, made up to 500 mL with dH_20. The medium was then sterilised in the autoclave and allowed to cool to approximately 55°C. Ampicillin was then added aseptically to a final concentration of 100 µg/mL, and the medium was poured into 10 cm sterile Petri dishes under aseptic conditions.

Transformation into competent E. coli DH5-α cells

Competent E. coli DH5-α cells (Invitrogen, #18265-017) with the CCR7 plasmid. Transformation reactions were set up using CCR7 plasmid concentrations of 1 ng/µL, 10 ng/µL, and 100 ng/µL. For each transformation, 50 µL of competent cells were mixed gently with the appropriate of plasmid DNA for each concentration on ice and incubated on ice for 30 minutes. Cells were then heat-shocked at 42°C for 45 seconds, followed by immediate incubation on ice for a further 2 minutes.

Plating and Incubation

Following transformation, 50 µL of each reaction mixture was spread onto pre-warmed LB-Ampicillin agar plates. A negative control plate (cells + autoclaved dH_2O) was included to assess background growth. Plates were incubated at 37°C for 16 hours to enable colony formation. Colonies from the 10 ng/µL plate were selected for plasmid extraction due to optimal growth.

3.2.2 CCR7 Plasmid Extraction

Miniprep

Eight DH5-α colonies transformed with 10 ng/µL CCR7 plasmid were aseptically picked and cultured in 5 mL LB broth (5g Tryptone, 5g NaCl, 2.5g Yeast Extract; made up to 500 mL with dH_20. Sterilised by autoclaving). These cultures were incubated overnight at 37°C, 225 RPM. Colony growth was assessed, and plasmid DNA was extracted using the QIAGEN® Plasmid Mini Kit (QIAGEN, #12123) according to the manufacturer's protocol.

Maxiprep

Two DH5α colonies transformed with 10 ng/µL CCR7 plasmid were aseptically picked and cultured into 5 mL LB broth. These starter cultures were incubated overnight at 37ºC, 225 RPM, and subsequently used to culture 250mL LB broth. These larger cultured were incubated overnight at 37ºC, 225 RPM. Plasmid DNA was extracted using the QIAGEN® Plasmid Maxi Kit (QIAGEN, #12126) according to the manufacturer's protocol.

DNA Quantification

DNA concentration and purity were assessed using a Nanodrop spectrophotometer (ThermoFisher Scientific).

3.2.3 PCR Amplification of CCR7 Plasmid

PCR Amplification

A conventional PCR assay was performed as a preliminary validation step to confirm the presence of the CCR7 insert and FLAG-tag region within the pcDNA3.1(+)-N-DYK CCR7 expression plasmid. Rather than amplifying the full CCR7 coding sequence (1137bp excluding restriction sites), primers were designed to target a 743bp internal region encompassing part of the CCR7 open reading frame and the adjacent FLAG-tag sequence. This shorter amplicon was selected to enable reliable amplification and visualisation under standard PCR cycling and agarose gel electrophoresis conditions.

A forward primer (5'–AATGTCGTAACAACTCCGCC–3') and reverse primer (5'–CAGCTTGCTAATCAGCAGC–3') were designed to bind either side of the targeted internal region. Primer binding locations and the amplified region are illustrated in Appendix A. All primers were sourced from Integrated DNA Technologies®, supplied in a lyophilised form, and stored at -20ºC.

A 50 µL reaction was performed for each extracted plasmid, consisting of 25 µL NEB OneTaq® 2X Master Mix with Standard Buffer (NEB# M0482S), 1 µL forward primer, 1 µL reverse primer, CCR7 plasmid concentration of 0.2 ng/µL, then made up to a total volume of 50 µL using nuclease free water.

The PCR reaction was performed using a Biorad PCR machine. The thermal cycler was programmed for 30 s at 94ºC for initial denaturation, followed by 30 cycles of 30 s at 94ºC for denaturation, 30 s at 55ºC for annealing, 45 s at 68ºC for extension, and 5 minutes at 68ºC for the final extension.

Purification

Amplified products were purified enzymatically, using Exonuclease I (Ref: EN0581) and FastAP Thermosensitive Alkaline Phosphatase (Fast AP) (Ref: EF0651). Reactions contained 5 µL PCR product, 0.5 µL Exonuclease I, 0.1 µL Fast AP. Mixtures were incubated at 37ºC for 15 mins, then the enzymes were inactivated by an incubation at 85ºC for 15 mins. DNA concentration and purity was measured using a Nanodrop spectrophotometer (ThermoFisher Scientific).

3.2.4 Gel Electrophoresis

Gel Preparation

PCR products were analysed by agarose gel electrophoresis to verify the amplification of the expected 743 bp CCR7 insert. A 1% (w/v) agarose gel was prepared by dissolving 0.5 g agarose in 50 mL of 1X TAE buffer. The solution was heated in a microwave until fully dissolved. After cooling slightly, 15 µL of SYBR™ Safe DNA Gel Stain (ThermoFisher Scientific, #S33102) was added. The gel was poured into a casting tray with the casting comb added and then allowed to set.

Sample Preparation

Each PCR products was prepared as a 6 µL sample at 60ng/µL, containing 1 µL of Gel Loading Dye, Purple (6X), no SDS (New England Biolabs®, #B7025S) and made up with nuclease-free H_2O. A 1 kb DNA ladder (New England Biolabs®, #N3232S) was used as a molecular weight marker, prepared with 5 µL ladder and 1 µL of loading dye.

Electrophoresis

Electrophoresis was performed in 1X TAE buffer at 100 V for 60 minutes. Agarose gel was visualised using a Dual LED Blue/White Light Transilluminator (Invitrogen).

3.2.5 Sanger Sequencing

For sequencing, 15 µL of purified PCR products (10 ng/µL) was combined with 2 µL of 100 µM sequencing primer. A custom forward sequencing primer (5'–AGCTCTCTGGCTAACTAGAG–3') was designed 51bp downstream of the PCR forward primer to confirm FLAG-tag integrity. Samples were sent to Eurofins Scientific® for Sanger sequencing. Returned sequences were aligned against the original CCR7 FASTA sequence (provided by GenScript®) using the NCBI BLAST tool to confirm sequence identity and confirm the integrity of the FLAG-tag region.

3.2.6 Tissue Culture – HEK293 Cell Culture

All tissue culture procedures were performed aseptically in Class II biosafety cabinets (ThermoFisher Scientific), using sterile equipment, reagents, and consumables. Human Embryonic Kidney 293 (HEK293) cells were cultured in 10 mL DMEM supplemented with 10% FBS and 100 U/mL P/S in T75 tissue culture flasks. Cultures were maintained in a humidified incubator at 37ºC with 5% CO_2 and passaged at 80-90% confluence.

All media used on cells was room temperature or warmed in a 37ºC water bath prior to culturing.

Cell Passaging

Cells were passaged using standard trypsinisation protocols. Once HEK293 cells reached 80–90% confluence, culture media (DMEM (10% FBS, 100 U/mL P/S) was aspirated out, and the cell monolayer was washed twice with 10mL of PBS to remove residual serum. To detach the cells from the flask, 2 mL of 0.05% Trypsin-EDTA (Gibco™, #25300054) was added and the flask returned to the incubator for 3 minutes. After incubation, the cells were visualised using an optical microscope to ensure detachment, and gentle tapping was applied if necessary. The trypsin was then inactivated by adding 8 mL of DMEM (10% FBS, 100 U/mL P/S), and the cell suspension was transferred to a 15 mL falcon tube.

Cells were pelleted via centrifugation at 1000 RPM for 3 minutes at room temperature and the resulting supernatant was aspirated out. The pellet was then resuspended in an appropriate volume of fresh DMEM (10% FBS, 100 U/mL P/S). For routine passaging, a 1:10 split ratio was used for bi-weekly splitting.

Cell Counting and Seeding

Cell concentration was determined using a haemocytometer. Following resuspension after centrifugation, 10 µL of the cell suspension was loaded onto the haemocytometer chamber, after cleaning using 70% ethanol, and a coverslip was placed over top. The haemocytometer was placed under an optical microscope, and cells in four outer squares were counted. An average was obtained from these values, which was then multiplied by 10,000 to give the overall cell concentration (cells per mL).

To determine the volume of cell suspension to add to each well of a plate, the desired cell density (Table 4) was divided by the calculated cell concentration. Cells were then seeded accordingly. Following seeding, plates or flasks were returned to the incubator and cultured under standard conditions until ready to use.

***Table 4**. Seeding density used in tissue culture plates depending on experiment.*

Plate	Application	Seeding Density (cell/mL)
6-well	WB	500,000
6-well	ICC	50,000
6-well	Transwell Migration Assay	200,000
12-well	WB	100,000

3.2.7 Transient Transfection of CCR7 Plasmid in HEK293 Cells

HEK293 cells were seeded at appropriate densities (Table 4) and incubated for 24 h at 37ºC with 5% CO_2, to allow for cell adherence prior to transfection. Cells were transfected when they reached ~60% confluence.

Collagen Coating

In specified experiments, tissue culture plates were coated with a layer of Collagen I, Rat Tail (Gibco, #A10483–01) prior to seeding to promote adherence. Collagen was diluted to 50 µg/mL in 20mM acetic acid and sterile water. Each well of a 6-well plate received 1 mL of this dilution (0.5 mL per well of a 12-well plate) and was incubated at 37ºC with 5% CO_2 for one hour. Wells were aspirated and washed three times using PBS, then left to air dry prior to cell seeding.

Transient Transfection

HEK293 cells were transfected at ~60% confluence. Transient transfection was performed using increasing concentrations of CCR7 plasmid DNA (0.5–8.0 µg), and two different transfection reagents: Lipofectamine LTX with Plus™ Reagent (ThermoFisher®, #15338100), and Lipofectamine 3000 Transfection Reagent (ThermoFisher®, #L3000008), following manufacturer protocols.

For transfections using Lipofectamine LTX with Plus™ Reagent, CCR7 plasmid DNA was first diluted in half the final reaction volume of transfection media, while the LTX and Plus reagents were diluted in the remaining half-volume of transfection media. These two mixtures were then combined and mixed gently, then left to incubate at room temperature for 10 minutes to allow complex formation.

Seeded plates were retrieved from the incubator and media aspirated out. Following incubation, the resulting transfection complexes were added dropwise to each of the wells, ensuring not to disturb the adhered cell monolayer.

Transfection reactions were carried out in a total volume of 1 mL or 2 mL per well in 6-well plates. Mock-transfected controls were included and received the Lipofectamine reagent mix without plasmid DNA, while untreated wells served as negative controls (media only).
An identical protocol was used for transfections using Lipofectamine® 3000, with lipofectamine reagent volumes adjusted according to manufacturer instructions.
The media used during transfection was either OptiMEM, DMEM (0% FBS, 100 U/mL P/S), or DMEM (5% FBS, 100 U/mL P/S), depending on experimental design.
Transfected cells were incubated at 37ºC with 5% CO_2 for varying time periods (24, 48, 72 hours) post-transfection.

Transient Transfection for ICC

For ICC experiments, the transient transfection protocol was carried out the same as above, however prior to seeding, a 0.13mm round glass coverslip (TheromFisher, # 174950) was placed into each well. These coverslips were sterilised using pure ethanol, washed three times with PBS, then left to air dry prior to seeding. Cells were seeded as per previously described protocol.

3.2.8 Cell Lysis and Protein Quantification

Following post-transfection incubation, HEK293 cells were lysed and processed for downstream protein analysis. All lysis procedures were carried out on ice or at 4ºC to minimise protein degradation. All reagents, including PBS and lysis buffers, were pre-chilled on ice prior to use.

Cell Lysis

Cells were placed on ice, and growth media was carefully aspirated from each well, being careful not to disturb the adherent cell monolayer. Cells were washed twice using 1 mL PBS to remove serum proteins and residual media. After aspiration, 80 µL of lysis buffer (IP or RIPA) was added directly to each well and the plate was placed on an orbital shaker and incubated for 10 minutes on ice. Cells were then scraped using the back end of a pipette and the lysates transferred to pre-chilled, labelled centrifuge tubes. Tubes were then placed on a rotator at 4ºC for 30 minutes to complete lysis. Samples were then centrifuged at 15,000 RPM for 20 minutes at 4ºC, the supernatants collected and stored in a new, pre-chilled and labelled centrifuge tubes. Cell pellets were discarded. Protein lysates were kept on ice for immediate use or stored at -20ºC.

Protein Quantification

Protein lysate concentration was determined using the Bradford Protein Assay (Bio-Rad, #5000006) according to the manufacturer's protocol. Samples were prepared for each lysate and loaded into a 96-well plate in triplicate, and Bovine Serum Albumin (BSA) serial dilution standards (0-1000 µg/mL) were also pipetted in triplicate to produce a standard curve. Bradford reagent was diluted 1:5 in dH2O and 200 µL was loaded into each well. Absorbance was measured at 595 nm using a spectrophotometer. All measurements were performed in technical triplicates, and average values were used for final concentration calculations. Protein samples were then normalised for downstream application.

3.2.9 SDS-PAGE and Western Immunoblotting

Sample Preparation

Protein lysate concentrations were determined via Bradford Assay and equal amounts of total protein were prepared for electrophoresis. Lysates were diluted in 15 µL 5X SDS sample buffer and the same lysis buffer used during cell lyses (IP or RIPA). Samples were then denatured by boiling at 95ºC for 10 minutes and stored at room temperature until use.

SDS-PAGE Gel

Protein samples were resolved on NuPAGE™ Bis-Tris Mini Protein Gels, 4–12%, 1.0–1.5 mm (Invitrogen, #NP0321BOX). Prior to loading, the comb and plastic tape were removed from the pre-cast gels, which were then placed into a ThermoFisher Mini Gel Tank filled with 1× NuPAGE™ MOPS SDS Running Buffer (ThermoFisher, #NP0001). Each well was loaded with 40 µL of sample, and 2 µL of Precision Plus Protein Standards (BioRad, #161-0373) for downstream analysis. Gels were run under a stepwise voltage programme at 80 V for 10 minutes, 120 V for 15 minutes, and 150 V for 35 minutes.

Protein Transfer

Following electrophoresis, proteins were transferred onto Cytiva Amersham™ Protran™ Premium NC Nitrocellulose Blotting Membrane (Fisher Scientific, #10600003) using the wet transfer method in a Mini Blot Module (ThermoFisher, #B1000) as per the manufacturer's protocol. Blotting pads, filter papers, and membranes were soaked in 1X NuPAGE™ Transfer Buffer (ThermoFisher, #NP0002) supplemented with 20% (v/v) methanol. Transfers were run at 30 V for 1 h.

Blocking and Antibody Probing

Following transfer, membranes were blocked using 0.5X Intercept® TBS Blocking Buffer (LI-COR, #NC1703226) for 1 h at room temperature with gentle agitation. After blocking, membranes were incubated overnight at 4 °C in primary antibody diluted in Intercept® T20 (TBS) Antibody Diluent (Li-Cor, #NC1703226) (table 2).

Following incubation, membranes were washed three times in TBS-T for 10 minutes and incubated in appropriate secondary antibody (LI-COR, 1:1000) (table 2) for 1 hour at room temperature in the dark, with gentle agitation. Membranes were again washed three times in TBS-T for 10 minutes before being visualised using the Odyssey CLx Imaging System (LI-COR). Analysis was performed using ImageJ software.

Membranes were sequentially probed with anti-CCR7, anti-FLAG, and GAPDH primary antibodies. Antibodies and working dilutions are listed in Table 2.

3.2.10 Immunocytochemistry

Transient transfection of HEK293 cells was performed as previously described, with the modification that sterile 0.13 mm glass coverslips were placed into each well prior to seeding to allow for immunocytochemical analysis.

Following desired transfection protocol, coverslips were washed three times with PDBS for 5 minutes, fixed in 4% paraformaldehyde (PFA) for 10 minutes with gentle agitation, and permeabilised using 0.1% Triton X-100 in PBS for 4 minutes with gentle agitation. Cells were then washed again three times in PBS for 5 minutes and blocked for 1 hour at room temperature in blocking buffer (10% donkey serum, 2% BSA in PBS) with gentle agitation.

Primary antibodies, anti-CCR7 (Proteintech #25898-1-Ap) and anti-FLAG (Proteintech #66008-4-Ig), were diluted 1:500 in ICC antibody dilutant (5% donkey serum, 1% BSA in PBS) and applied to samples overnight at 4°C in a humidified chamber. Following incubation, coverslips were washed three times in PBS for 5 minutes, and incubated in secondary antibodies, Alexa Fluor 647-conjugated donkey anti-rabbit [1:500] and Alexa Fluor 488-conjugated donkey anti-mouse secondary antibodies [1:500], for 1 hour at room temperature in a humidity chamber. Coverslips were then washed three times in PBS for 5 minutes with gentle agitation and covered with foil to prevent antibody degradation. The nuclei were counterstained with ProLong™ Gold Antifade Mountant with DNA Stain DAPI (ThermoFisher #P36935), and coverslips were mounted onto 76 mm x 26 mm glass microscope slides (Fisherbrand™, #MCG01012).

Samples were imaged using a Zeiss LSM 880 confocal laser scanning microscope, controlled by the Zeiss ZEN imaging software, with a 63X imaging objective. Images were captured under appropriate excitation and emission wavelengths for Alexa Fluor 488, Alexa Fluor 647, and DAPI. Channels were imaged sequentially to avoid spectral overlap. Image acquisition parameters

(laser intensity, gain, and exposure) were kept consistent across samples for comparative analysis using ImageJ (Wayne Rasband and contributors National Institutes of Health, USA).

3.2.11 Transwell Migration Assay

HEK293 cells were first transiently transfected, as previously described, in two 6-well plates; one under optimised CCR7 transfection conditions, and one as a mock-transfected control.
23 h post-transfection, cells were serum-starved for 1 h in DMEM (0% FBS, 100 U/mL P/S) prior to migration setup (Fig. 5).
Transwell assays were performed using 24-well plates Nunc™ Cell Culture Inserts in Carrier Plate Systems (ThermoFisher, #141006), which have 8 µm pore polycarbonate membrane inserts. Recombinant human CCL19/MIP-3β (R&D Systems, #361-MI-025) and CCL21/6Ckine (R&D Systems, #366-6C-025) were diluted in DMEM (100 U/mL P/S) containing either 0% or 1% FBS to achieve final concentrations of 0, 50, 100, and 200 ng/mL in the lower chamber.
The upper chambers were seeded with 50,000 cells per well of either mock-transfected or CCR7-transfected HEK293 cells in the corresponding media. Each ligand concentration was tested in triplicate for both cell types, with separate plates used for CCL19 and CCL21. Plates were incubated for 24 h at 37°C in a humidified 5% CO_2 atmosphere to allow for migration.
After incubation, non-migrated cells on the upper membrane surface were gently removed using cotton swabs. Media in the lower chamber was aspirated out, and the cells were washed three times in PBS. Migrated cells on the lower surface were then fixed using 4% PFA for 5 minutes, washed three more times, and then stained using Crystal Violet Solution (Abcam, Cat. #ab246820) for 10 minutes. The cells were rinsed in PBS until all excess dye had been removed (~ 3 washes), and air dried.
Membranes were imaged at 4X magnification using a NIS-Elements microscope equipped with a Canon digital camera. Images were collected under consistent illumination and magnification settings across all samples.
For quantitative analysis, bound dye was solubilised using the Crystal Violet Solubilisation Solution (Abcam, Cat. #ab232855) from the Crystal Violet Assay Kit. Solubilised samples were transferred to a 96-well plate in triplicate, and absorbance was measured at 595 nm using a spectrophotometer plate reader. Mean absorbance values were calculated from technical triplicates, standardised against the solubilisation solution, and expressed as relative migration.

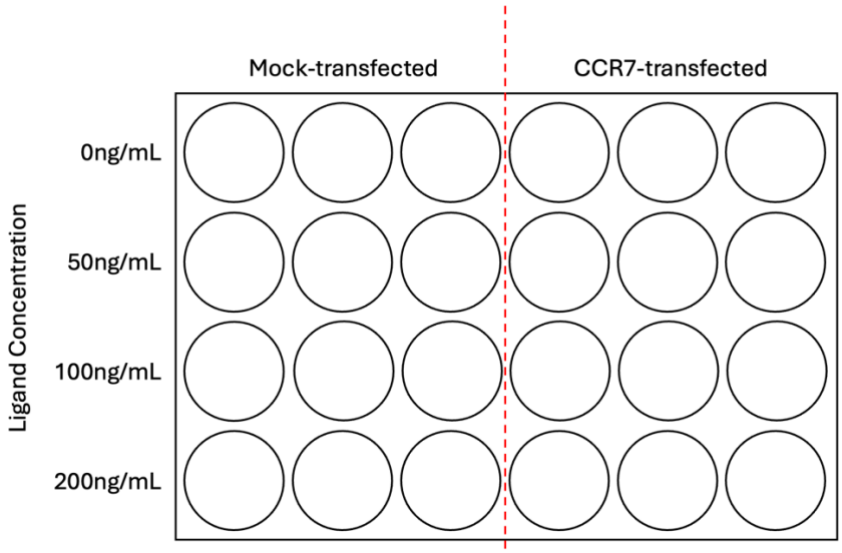

Figure 5 – Transwell Migration Assay Plate Layout.

Each row corresponds to a different ligand concentration (0–200 ng/mL), with three columns per condition (mock-transfected and CCR7-transfected HEK293 cells). Separate plates were used for CCL19 and CCL21 conditions.

4. Results

4.1 Clinical and Bioinformatic Analysis of CCR7 Gene Expression

4.1.1 CCR7 Gene Expression and Prognostic Analysis of Colorectal Cancer Cohorts

CCR7 gene expression in colorectal cancer (CRC) was analysed using clinical and pre-clinical datasets provided by Joanne Edwards Research group at Garscube Campus. RNA-seq data from the CRC patients was processed and analysed using R, focusing on gene expression patterns, survival outcomes, and biological relevance, particularly with respect to CCR7's potential as a biomarker. This dataset comprised a total of 271 patients (Full Cohort), with a subset of 63 rectal cancer patients (Rectal Subset).

Analysis included unsupervised clustering (k-means) (Fig. 6) to explore CCR7 expression patterns, and Kaplan-Meier survival analysis to assess associations with cancer-specific survival (CSS) (Fig. 7). As k-means clustering is an unsupervised algorithm, the resulting cluster labels (Group 1 and Group 2) were assigned arbitrarily and did not inherently correspond to biologically defined high- or low-expression groups. Cluster identity was therefore interpreted post hoc based on the relative CCR7 expression profiles observed within each cohort. Additionally, a cutpoint optimisation algorithm (survminer) was applied to explore the most statistically effective threshold for stratifying CCR7 expression levels (Fig. 8).

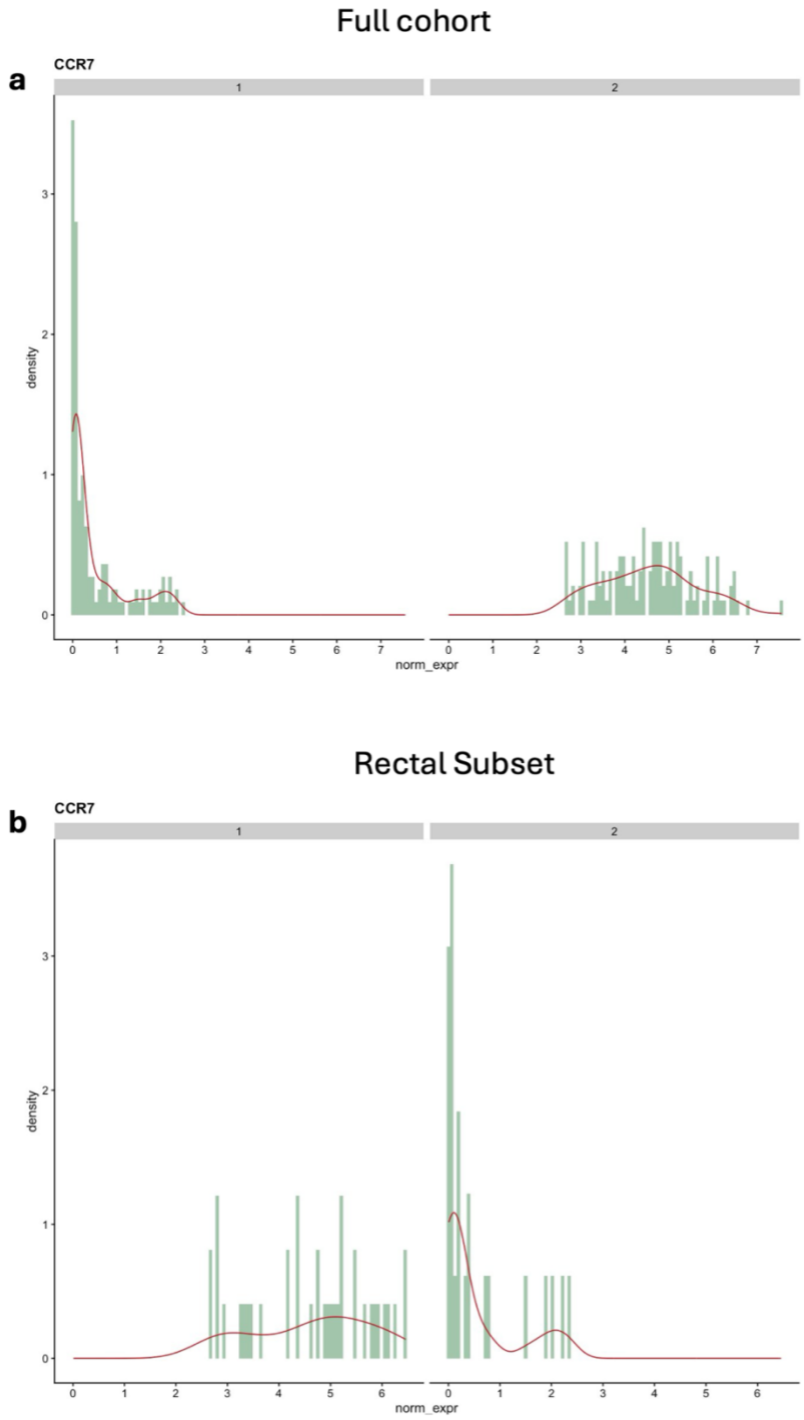

Figure 6 – CCR7 expression-based clustering in colorectal cancer.
*K-means clustering of CCR7 RNA expression in the **(a)** full cohort and **(b)** rectal subset, showing distinct high and low expression groups.*

K-means clustering revealed a clear separation between high and low CCR7 RNA expression in both the full CRC cohort (n = 271) and the rectal subset (n = 63) (Fig. 6). In the full cohort (Fig. 6a), clustering divided samples into two distinct expression groups with Group 1 showing tightly clustered low expression levels (peak density ~0-1 normalised expression units), while Group 2

displayed a broader range of moderate expression levels (peak density ~3-5 normalised expression units). In the rectal subset (Fig. 6b), this separation was less defined, with Group 1 corresponding to relatively higher CCR7 expression across a broader distribution (~2.5-6 normalised expression units), while Group 2 displayed a dense peak at the lower end (~0-1 normalised expression units), suggesting a more skewed expression profile.

These stratified expression groups were subsequently used for downstream expression analysis to investigate the prognostic relevance of CCR7 expression in relation to CSS (Fig. 7).

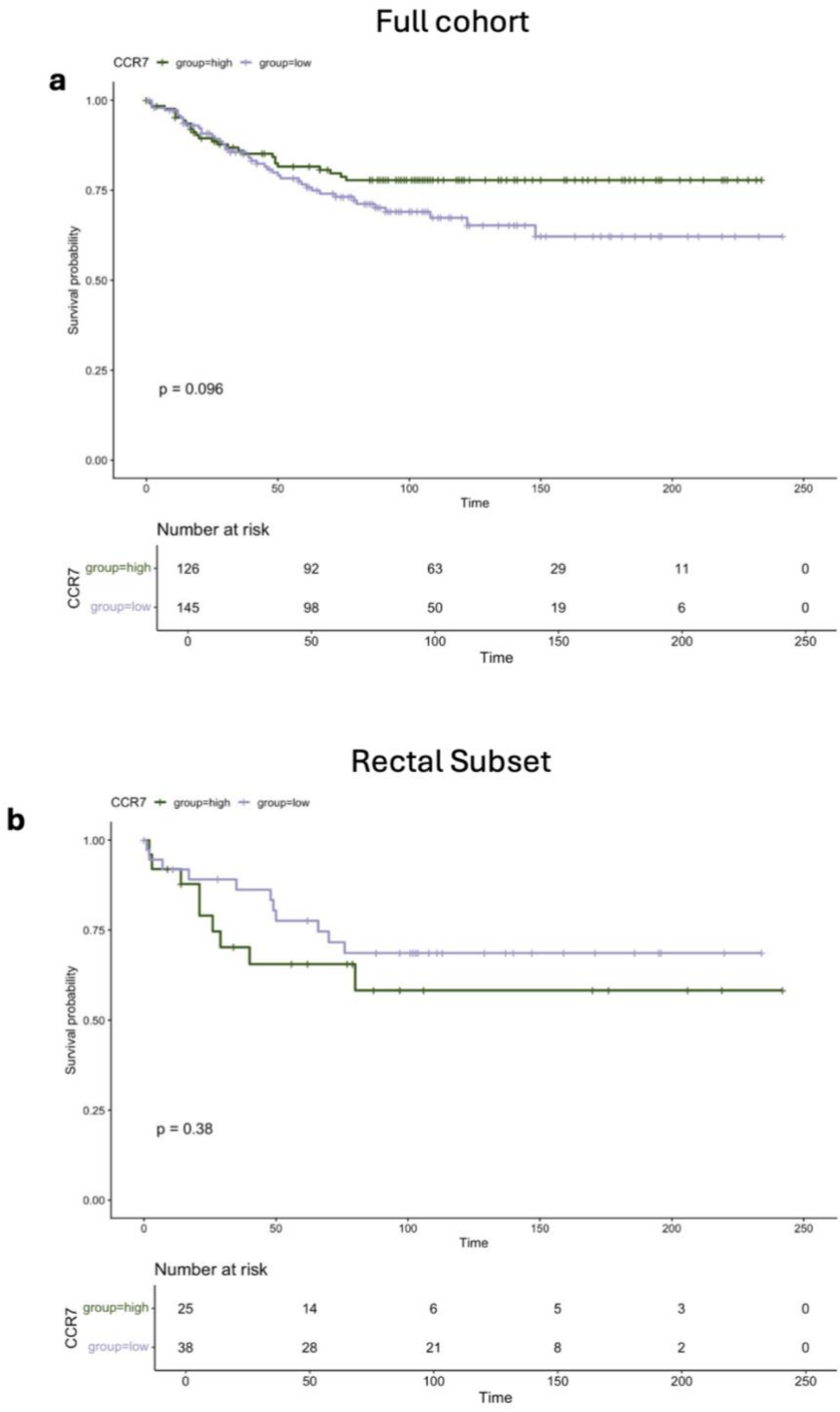

Figure 7 – Cancer Specific Survival by CCR7 expression group.

Kaplan-Meier curves for CSS comparing high vs low CCR7 expression in the ***(a)*** *full cohort and* ***(b)*** *rectal-only cohort, showing non-significant (p = 0.096 and 0.38, respectively) survival trends related to CCR7 expression.*

Kaplan-Meier survival analysis showed trends suggestive of prognostic relevance, however statistical significance between high CCR7 expression and low CCR7 expression and survival probability was not reached (Fig. 7). In the full cohort, higher CCR7 expression (Fig. 6a, Group

1) was associated with improved CSS (HR = 0.82, p = 0.11) (Fig. 7a), while in the rectal subset, higher CCR7 expression (Fig. 6b, Group 2) was linked with worse CSS (HR = 0.74, p = 0.20) (Fig. 7b). These opposing trends suggest potential cohort-specific variability, but neither reached conventional thresholds for significance (p = 0.096 and 0.38, respectively).

To explore the prognostic potential of CCR7 more precisely, a data-driven cutpoint optimisation approach was applied using the survminer package, and Kaplan-Meier curves were produced (Fig. 8).

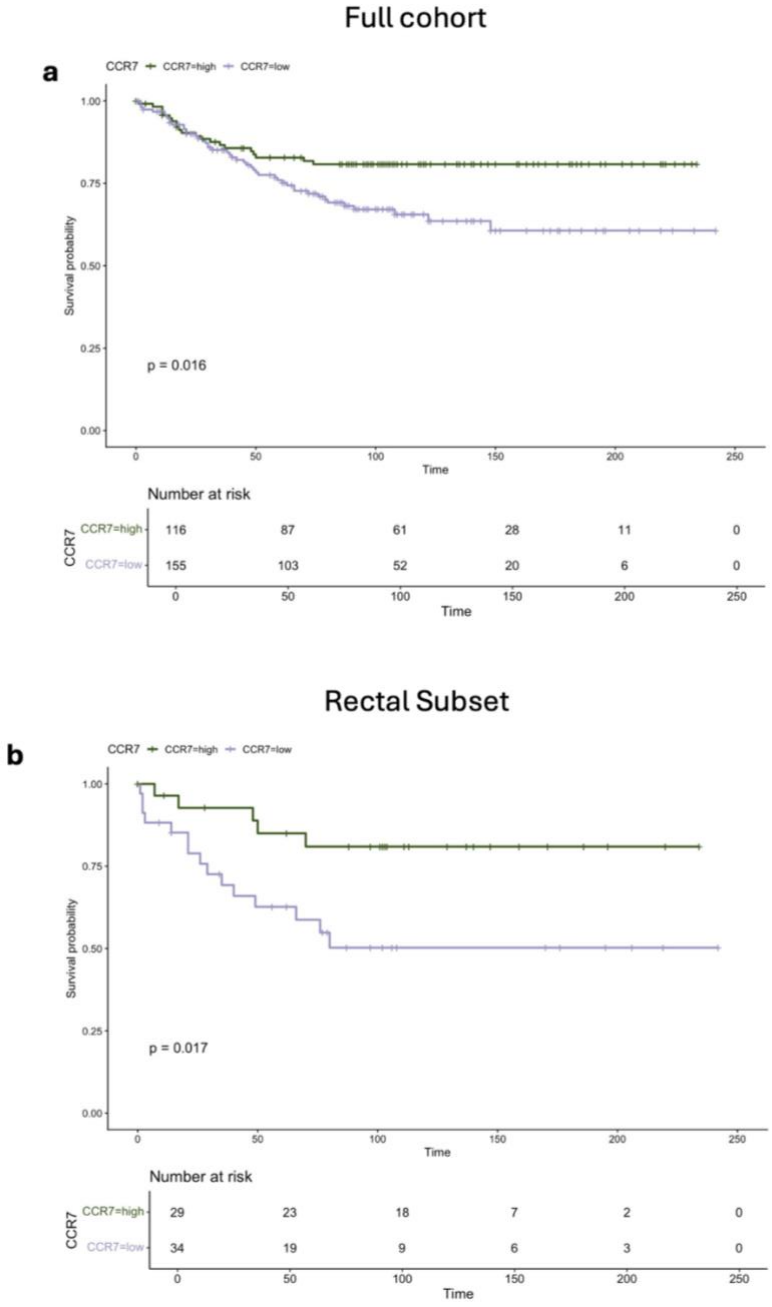

Figure 8 – Survival stratification using optimal CCR7 expression cutpoints.
Kaplan-Meier curves for CSS using the optimal cutpoint in CCR7 expression (determined by survminer) in the ***(a)*** *full cohort and* ***(b)*** *rectal-only group. These cutpoints yield statistically significant separation in survival ($p < 0.05$).*

This method identified thresholds in CCR7 expression that maximally separated patients into high and low survival probability groups, resulting in statistically significant differences ($p < 0.05$) in both the full cohort ($p = 0.016$) and rectal subset ($p = 0.017$). In both groups, patients classified as having high CCR7 expression demonstrated higher survival probabilities across the 10-year follow up period. The observed improvement in curve separation following optimisation

supports a quantifiable relationship between CCR7 expression and patient survival in both colorectal and rectal cancer subsets.

In addition to survival analyses, CCR7 expression was evaluated using fisher's exact tests to identify statistically significant relationships between CCR7 expression and invasive tumour characteristics. In the full cohort, high CCR7 expression was significantly associated with venous invasion (p = 0.020, OR = 1.81, 95% CI: 1.08–3.02), a key route for haematogenous metastasis, while in the rectal subgroup, CCR7 expression was strongly associated with lymph node metastasis (p = 0.030, OR = 3.99, 95% CI: 1.12–16.72). These findings support a possible role for CCR7 in facilitating tumour dissemination and systemic spread.

To complement this primary dataset and further evaluate CCR7 gene expression and its prognostic implications, publicly available data from the Human Protein Atlas (HPA) was analysed (Fig. 9,10). Specifically, CRC samples from colon and rectum adenocarcinoma validation cohorts were analysed and stratified by tumour stage to compare non-metastatic (early stage; T1/T2) and metastatic (late stage; T3/T4) disease. This provided an independent context to assess the biological consistency and clinical relevance of CCR7 expression as a prognostic biomarker.

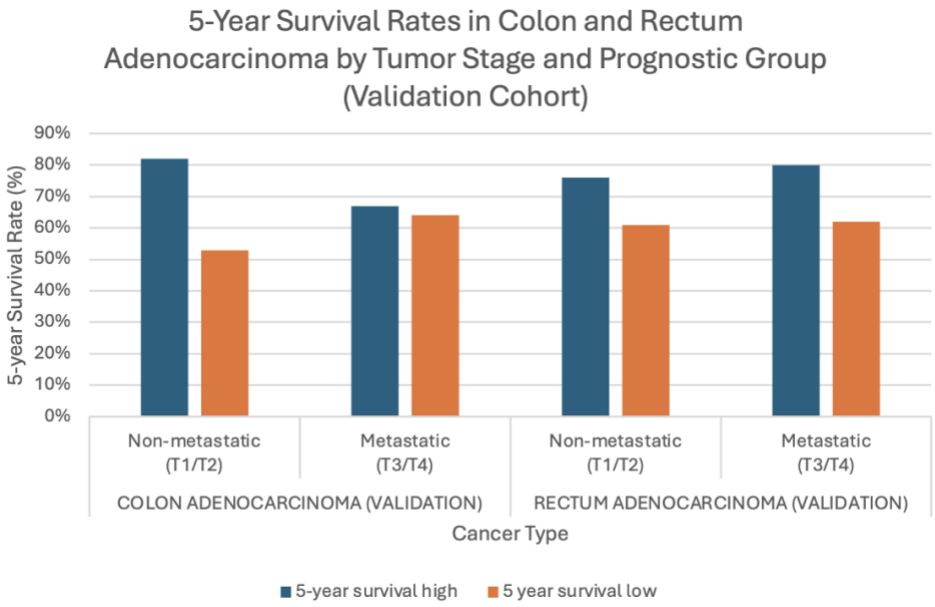

Figure 9 – CCR7 expression and survival stratification in colon and rectum adenocarcinoma validation cohorts obtained from the Human Protein Atlas.
5-year survival rates by tumour stage (T1/T2 vs T3/T4) and CCR7 expression group (high vs low), for colon and rectum adenocarcinoma patients.

Across both colon and rectum adenocarcinoma groups, survival stratification by CCR7 expression demonstrated similar patterns when grouped by tumour stage. In colon adenocarcinoma, high CCR7 expression was associated with better 5-year survival in early-stage tumours (T1/T2: 82% high vs 53% low), whereas in more advanced tumours (T3/T4), this survival rate decreased (67% high vs 64% low) (Fig. 9). Similarly, in rectal adenocarcinoma, high CCR7 expression correlated with better 5-year survival in both stages (T1/T2: 76% high vs 61% low; T3/T4: 80% high vs 62% low), suggesting a possible protective effect or immunological role in both early and late stages of this cancer. However, none of these comparisons reached statistical significance ($p > 0.1$ in all cases), which is consistent with the findings in the clinical and pre-clinical colorectal dataset.

4.1.2 CCR7 Gene Expression and Prognostic Analysis of Human Protein Atlas Datasets

To further investigate the prognostic value of CCR7 in CRC, survival curves from the HPA colon adenocarcinoma validation cohort (Fig. 10) and rectum adenocarcinoma validation cohort (Fig. 11) were analysed. Kaplan-Meier plots stratified by tumour stage and CCR7 expression provided additional insight into the relationship between gene expression and clinical outcomes, specifically survival probability.

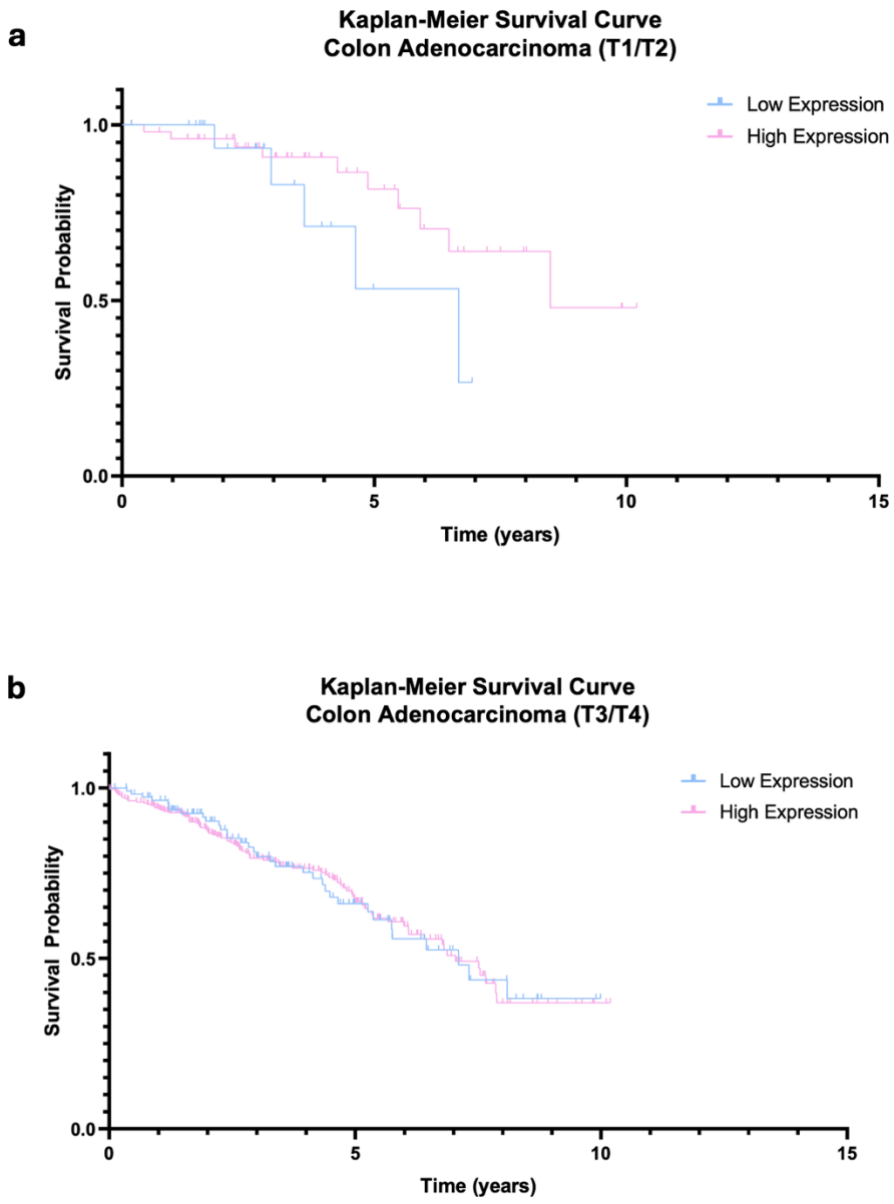

Figure 10 – Kaplan-Meier survival analysis for CCR7 expression in colon adenocarcinoma validation cohort (Human Protein Atlas).

Kaplan-Meier plots showing 10-year survival probability for patients with colon adenocarcinoma, stratified by tumour stage and CCR7 expression group (high vs low).

***(a)** T1/T2 (early-stage) tumours: Patients with high CCR7 expression demonstrate improved survival compared to those with low expression (Log-rank p = 0.1426; Gehan–Breslow–Wilcoxon p = 0.4282).*

***(b)** T3/T4 (late-stage) tumours: No clear survival difference is observed between high and low CCR7 expression groups (Log-rank p = 0.9314; Gehan–Breslow–Wilcoxon p = 0.7428).*

In early-stage colon adenocarcinoma (T1/T2) (Fig. 10a), high CCR7 expression was associated with improved survival, with a visibly higher survival probability maintained over the 10-year

follow up period compared to the low expression group. This is consistent with the trends observed in the CRC patient cohort (Fig. 7a,8), where higher CCR7 expression was linked to improved CSS.

In contrast, in late-stage tumours (T3/T4) (Fig. 10b), survival curves for high and low CCR7 expression groups overlapped, indicating no measurable difference in long-term survival outcomes based on CCR7 expression level at this stage. Similar patterns were also observed in the rectum adenocarcinoma validation cohort (Fig. 11).

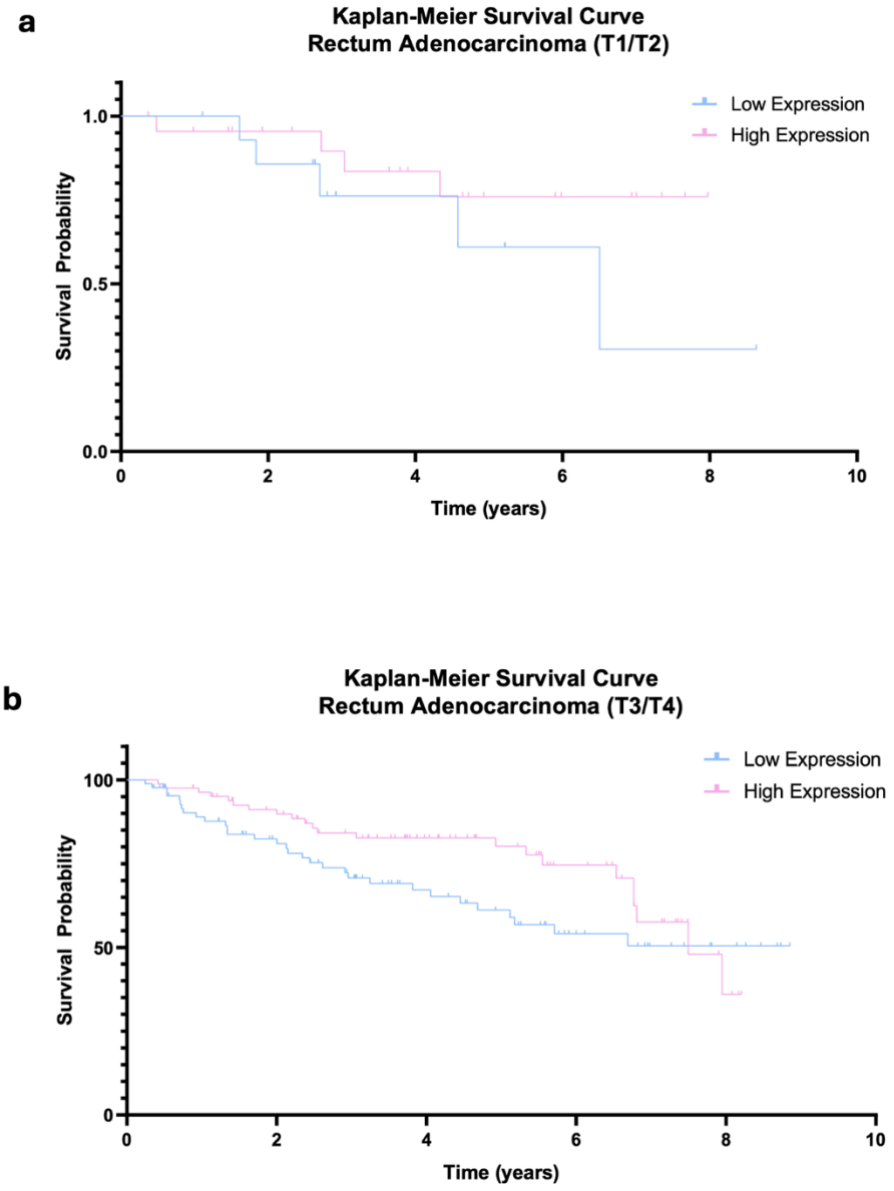

Figure 11 – Kaplan-Meier survival analysis for CCR7 expression in rectum adenocarcinoma validation cohort (Human Protein Atlas).

Kaplan-Meier plots showing 10-year survival probability for patients with colon adenocarcinoma, stratified by tum our stage and CCR7 expression group (high vs low).

***(a)** T1/T2 (early-stage) tumours: Patients with high CCR7 expression demonstrate improved survival compared to those with low expression (Log-rank p = 0.1891; Gehan-Breslow-Wilcoxon p = 0.3416).*

***(b)** T3/T4 (late-stage) tumours: Patients with high CCR7 expression demonstrate improved survival until ~7.5 years compared to those with low expression (Log-rank p = 0.1058; Gehan-Breslow-Wilcoxon p = 0.0247 *).*

In the rectum adenocarcinoma cohort, high CCR7 expression in early-stage (T1/T2) tumours (Fig. 11a) was associated with higher survival probability across the 10-year follow up period, consistent with trends observed in the CRC patient dataset (Fig. 7a,8).

In late-stage (T3/T4) rectum adenocarcinoma (Fig. 11b), the high CCR7 expression group maintained higher survival probability throughout the majority of the follow-up period, with the two curves converging after ~7.5 years. While the Log-rank test did not reach significance (p = 0.1058), the Gehan–Breslow–Wilcoxon test indicated a modest difference between the groups (p = 0.0247 *).

To further contextualise these findings, CCR7 gene expression levels and the corresponding cutpoints between high and low expression were examined from the HPA dataset to assess survival stratification (Fig. 12).

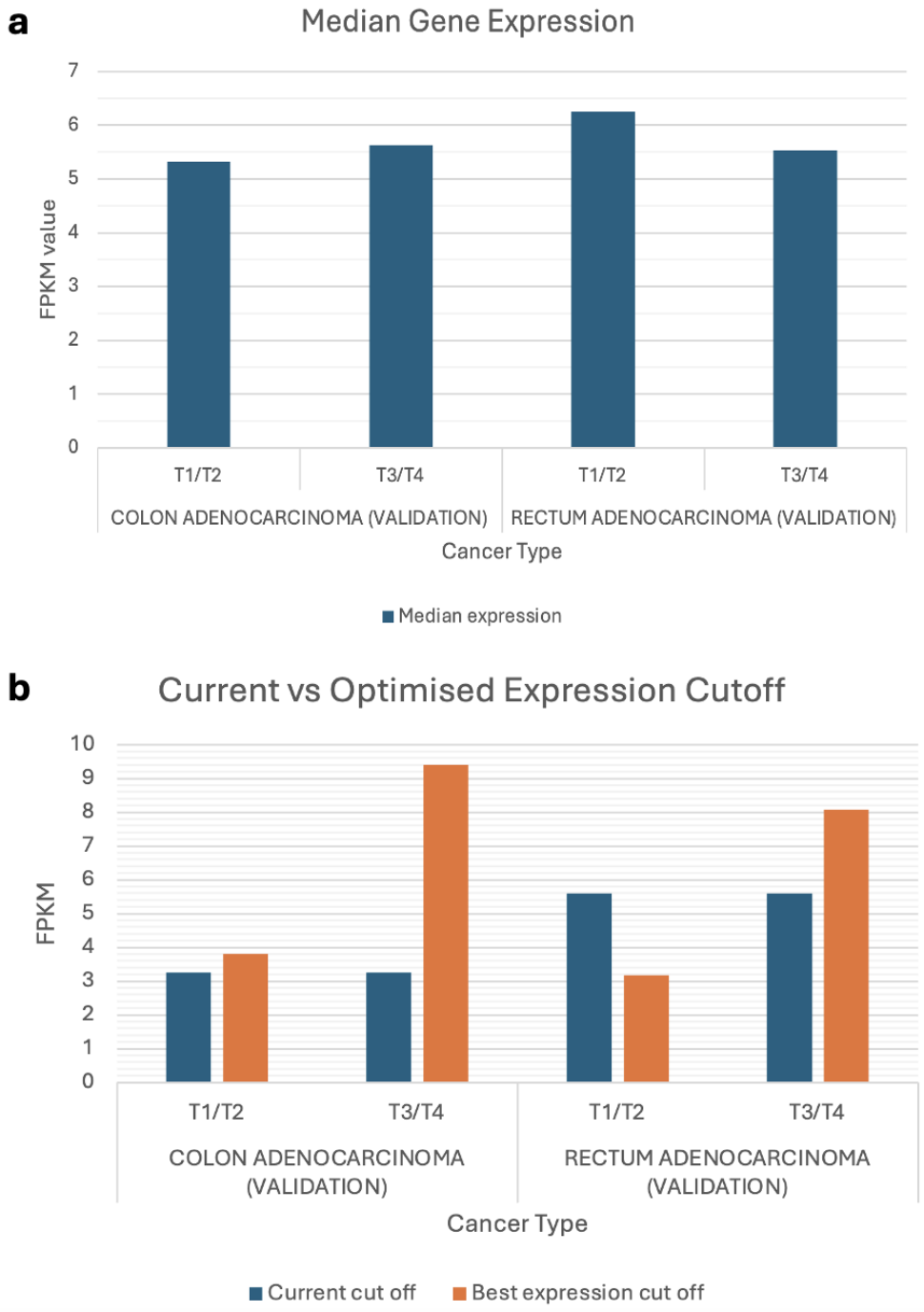

Figure 12 – CCR7 expression levels and optimised cutpoints by tumour stage and cancer type in colon and rectum adenocarcinoma validation cohorts obtained from the Human Protein Atlas.

Data sourced from the Human Protein Atlas. FPKM = Fragments Per Kilobase of transcript per Million mapped reads.

***(a)** Median CCR7 RNA expression (FPKM) across cancer type and stage.*

***(b)** Comparison of current versus optimised CCR7 expression cut-off values used for survival stratification, by cancer type and stage.*

The median expression levels of CCR7 (Fig. 12a) did not significantly vary across tumour stages or cancer type, indicating that CCR7 is broadly expressed across colorectal tumours. However, the optimal cutpoints for survival stratification, as determined by the HPA algorithm, showed considerable variation between stages (Fig. 12b). For instance, in colon adenocarcinoma, the optimised cutpoint increased from 3.81 (T1/T2) to 9.41 (T3/T4), and in rectal cancer from 3.17 to 8.08.

4.2 Development of CCR7 Overexpression Model

4.2.1 Plasmid Design and Validation of CCR7 Expression Construct

To generate sufficient quantities of the pcDNA3.1(+)-N-DYK CCR7 expression plasmid (Fig. 13a), the construct was propagated in competent E. coli DH5-α cells and extracted via miniprep or maxiprep.

Plasmid integrity and the successful incorporation of the CCR7 insert were initially assessed by PCR amplification of a 743bp internal region encompassing part of the CCR7 coding sequence and the FLAG-tag region, followed by agarose gel electrophoresis (Fig. 13b) and Sanger sequencing (Fig. 14). This molecular validation ensured construct integrity before transient transfection into HEK293 cells.

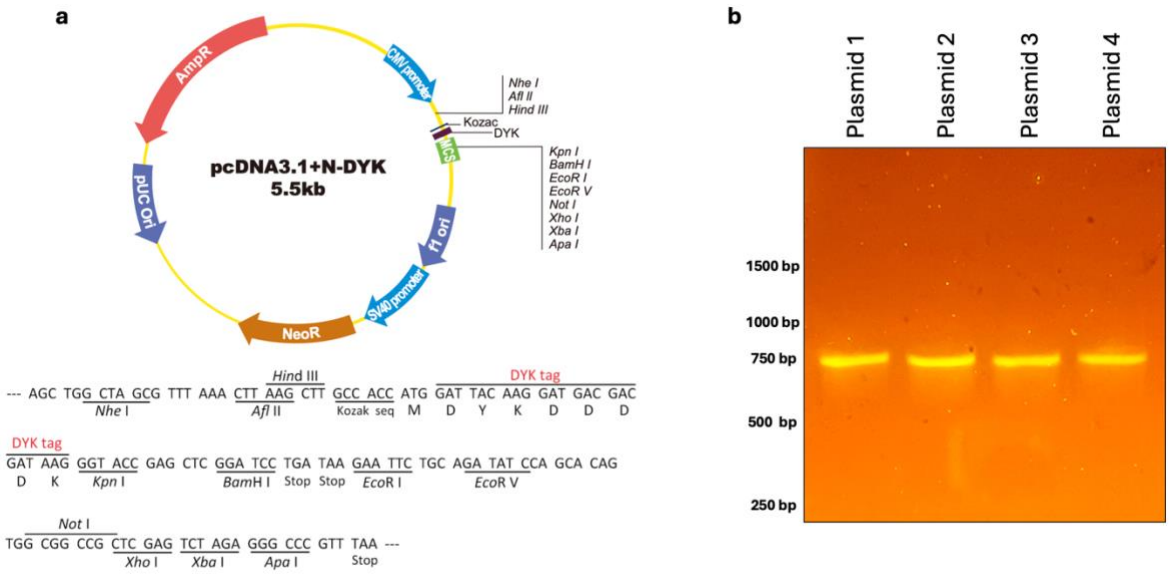

Figure 13 – Design and validation of CCR7 expression plasmid.

(a) *Map of CCR7 Expression Plasmid pcDNA3.1+N-DYK5.5kb, showing insertion of the human CCR7 gene between the KpnI and BamHI restriction sites, and presence of the N-terminal DYK (FLAG) tag. The ampicillin resistance gene (AmpR) and CMV promoter are also indicated.*

(b) *1% agarose gel electrophoresis of purified PCR products amplified from the CCR7 plasmid using FLAG-inclusive primers. Lanes 1-4 show amplicons from four separate plasmid preparations, each producing a single band of 743bp, corresponding to the expected size of the targeted internal validation amplicon. A 1 kb DNA ladder was used to assess molecular weight (not shown, though labelled).*

The successful validation of the CCR7 expression construct was a crucial initial step to establish a CCR7-overexpression cellular model. Transformation into competent E. coli DH5-α cells demonstrated optimal efficiency at a plasmid concentration of 10 ng/µl, which had the most robust colony formation. Colonies picked from this plate yielded sufficient plasmid for both mini and maxiprep procedures, indicating stable propagation and replication of the construct.

The PCR employed specific primers designed to amplify a 743bp internal region of the CCR7 insert that incorporated the FLAG-tag region, as opposed to the full-length (1137bp) CCR7 coding sequence. All eight independently prepared plasmid samples yielded a clean single band of 743bp upon 1% agarose gel electrophoresis (Fig. 13b), confirming successful amplification of the targeted region across multiple plasmid clones.

The size of the amplicon matched the expected length of the designed internal PCR target region, which was further confirmed by Sanger sequencing (Fig. 14). Returned sequences were aligned against the referenced CCR7 FASTA coding sequence using the NCBI BLAST tool.

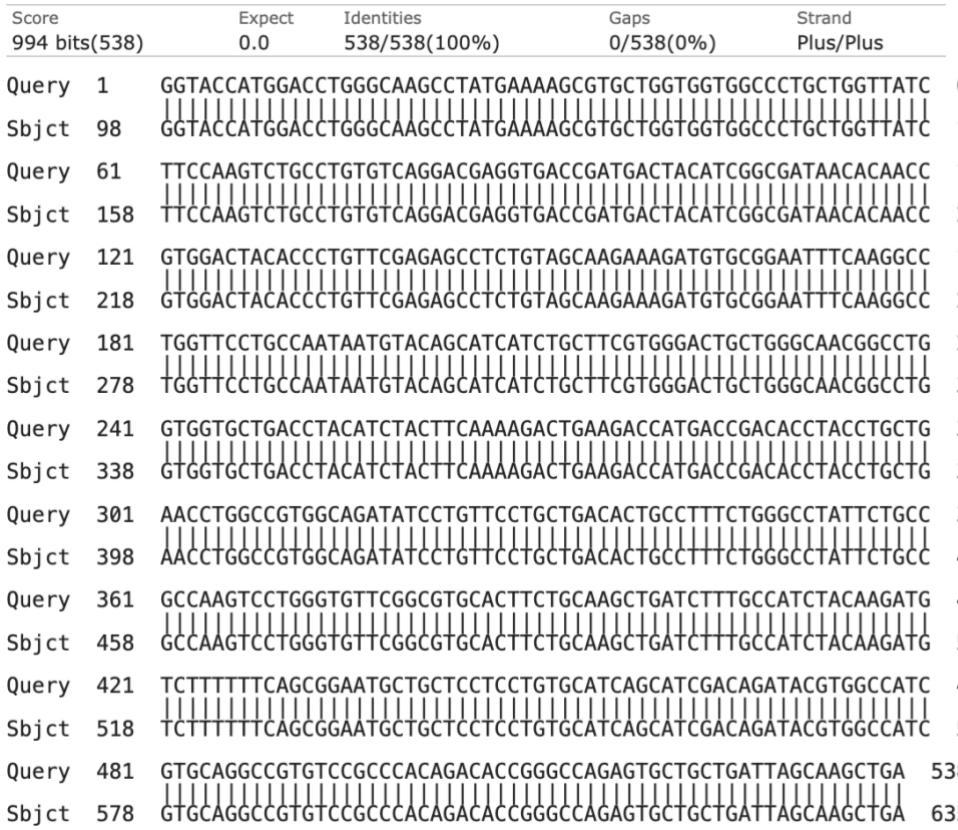

Score	Expect	Identities	Gaps	Strand
994 bits(538)	0.0	538/538(100%)	0/538(0%)	Plus/Plus

```
Query  1    GGTACCATGGACCTGGGCAAGCCTATGAAAAGCGTGCTGGTGGTGGCCCTGCTGGTTATC  60
            ||||||||||||||||||||||||||||||||||||||||||||||||||||||||||||
Sbjct  98   GGTACCATGGACCTGGGCAAGCCTATGAAAAGCGTGCTGGTGGTGGCCCTGCTGGTTATC  157

Query  61   TTCCAAGTCTGCCTGTGTCAGGACGAGGTGACCGATGACTACATCGGCGATAACACAACC  120
            ||||||||||||||||||||||||||||||||||||||||||||||||||||||||||||
Sbjct  158  TTCCAAGTCTGCCTGTGTCAGGACGAGGTGACCGATGACTACATCGGCGATAACACAACC  217

Query  121  GTGGACTACACCCTGTTCGAGAGCCTCTGTAGCAAGAAAGATGTGCGGAATTTCAAGGCC  180
            ||||||||||||||||||||||||||||||||||||||||||||||||||||||||||||
Sbjct  218  GTGGACTACACCCTGTTCGAGAGCCTCTGTAGCAAGAAAGATGTGCGGAATTTCAAGGCC  277

Query  181  TGGTTCCTGCCAATAATGTACAGCATCATCTGCTTCGTGGGACTGCTGGGCAACGGCCTG  240
            ||||||||||||||||||||||||||||||||||||||||||||||||||||||||||||
Sbjct  278  TGGTTCCTGCCAATAATGTACAGCATCATCTGCTTCGTGGGACTGCTGGGCAACGGCCTG  337

Query  241  GTGGTGCTGACCTACATCTACTTCAAAAGACTGAAGACCATGACCGACACCTACCTGCTG  300
            ||||||||||||||||||||||||||||||||||||||||||||||||||||||||||||
Sbjct  338  GTGGTGCTGACCTACATCTACTTCAAAAGACTGAAGACCATGACCGACACCTACCTGCTG  397

Query  301  AACCTGGCCGTGGCAGATATCCTGTTCCTGCTGACACTGCCTTTCTGGGCCTATTCTGCC  360
            ||||||||||||||||||||||||||||||||||||||||||||||||||||||||||||
Sbjct  398  AACCTGGCCGTGGCAGATATCCTGTTCCTGCTGACACTGCCTTTCTGGGCCTATTCTGCC  457

Query  361  GCCAAGTCCTGGGTGTTCGGCGTGCACTTCTGCAAGCTGATCTTTGCCATCTACAAGATG  420
            ||||||||||||||||||||||||||||||||||||||||||||||||||||||||||||
Sbjct  458  GCCAAGTCCTGGGTGTTCGGCGTGCACTTCTGCAAGCTGATCTTTGCCATCTACAAGATG  517

Query  421  TCTTTTTTCAGCGGAATGCTGCTCCTCCTGTGCATCAGCATCGACAGATACGTGGCCATC  480
            ||||||||||||||||||||||||||||||||||||||||||||||||||||||||||||
Sbjct  518  TCTTTTTTCAGCGGAATGCTGCTCCTCCTGTGCATCAGCATCGACAGATACGTGGCCATC  577

Query  481  GTGCAGGCCGTGTCCGCCCACAGACACCGGGCCAGAGTGCTGCTGATTAGCAAGCTGA  538
            ||||||||||||||||||||||||||||||||||||||||||||||||||||||||||
Sbjct  578  GTGCAGGCCGTGTCCGCCCACAGACACCGGGCCAGAGTGCTGCTGATTAGCAAGCTGA  635
```

Figure 14 - Validation of CCR7 amplicon sequence by NCBI BLAST alignment.
The consensus sequence obtained from Sanger sequencing of the 743 bp PCR-amplified internal CCR7 fragment (query) was aligned against the reference CCR7 coding sequence (subject) using the NCBI BLAST tool.

The BLAST alignment (Fig. 14) demonstrated 100% identity across all 538 aligned base pairs, with no gaps or mismatches, indicating that the amplified sequence corresponds exactly to the reference CCR7 sequence. The alignment yielded a high bit score of 994 and an E-value of 0.0, reflecting the high significance and reliability of the match. Additionally, the plus/plus strand orientation confirmed that the sequenced amplicon aligned in the correct direction. This validation confirmed the fidelity of the amplification and cloning process, ensuring that subsequent functional or expression studies were based on an accurate and verified construct.

Overall, these results established that the CCR7 plasmid was successfully amplified, extracted, and verified by both molecular weight and nucleotide identity.

4.2.2 Validation of CCR7 Overexpression in HEK293 Cells

To evaluate the exogenous overexpression of CCR7 following transient transfection, HEK293 cells were selected as a suitable model due to their low endogenous expression when compared to other readily available mammalian cell lines [as previously reported by Masters Student of Professor George Baillie: *Joe Graystone*].

Initially, HEK293 cells were transiently transfected using Lipofectamine LTX with increasing concentrations of plasmid DNA (0.5–4 µg) and analysed under various conditions to optimise FLAG-tagged protein detection using Western immunoblotting (Fig. 15).

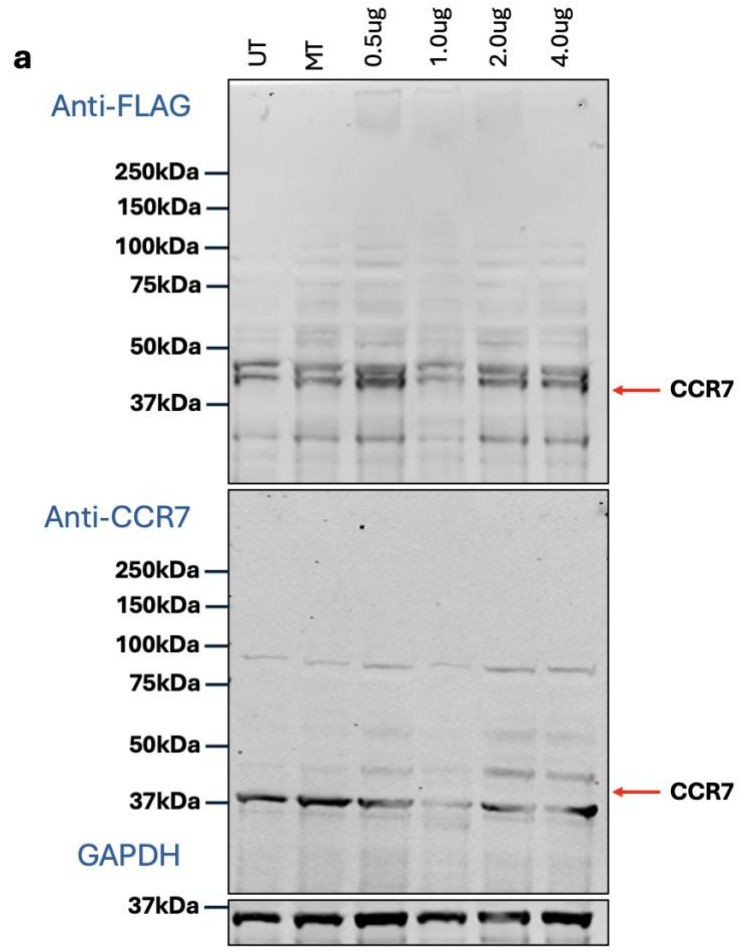

b

Cell Line	HEK293
Transfection Media	OptiMEM
Lipofectamine Reagent	LTX
Incubation	24h
Lysis Conditions	RIPA

Figure 15 – Western Blot Analysis of FLAG-tagged CCR7 expression in HEK293 cells under standard conditions.

(a) Western blot probed with anti-FLAG, anti-CCR7, and GAPDH antibodies. Image analysed using ImageJ.

(b) Table summarising corresponding transfection and lysis conditions. Table created using Excel.

Initial analysis using anti-FLAG and anti-CCR7 antibody staining revealed no discrete bands at the expected molecular weight of FLAG-tagged CCR7 (~43 kDa) in any of the transfected samples (Fig. 15a) under baseline conditions (Fig. 15b). Bands were observed around this molecular weight, though minimal differences were observed between the negative controls and transfected conditions, implying non-specific antibody binding rather than true detection of FLAG-tagged CCR7. GAPDH bands were observed at consistent intensity across all lanes, validating sample integrity and equal loading.

There did, however, appear to be weak high molecular weight smearing in CCR7-transfected lanes (0.5–2.0 µg) following anti-FLAG staining, which was absent from control lanes. This migration profile is consistent with that reported for glycosylated GPCRs, suggesting that CCR7

expression had occurred but that membrane extraction and protein solubilisation remained suboptimal under these conditions.

These results suggest that while CCR7 expression was being achieved, the receptor was not efficiently solubilised and therefore unable to migrate through the gel, prompting further optimisation of transfection and lysis conditions (Fig. 16).

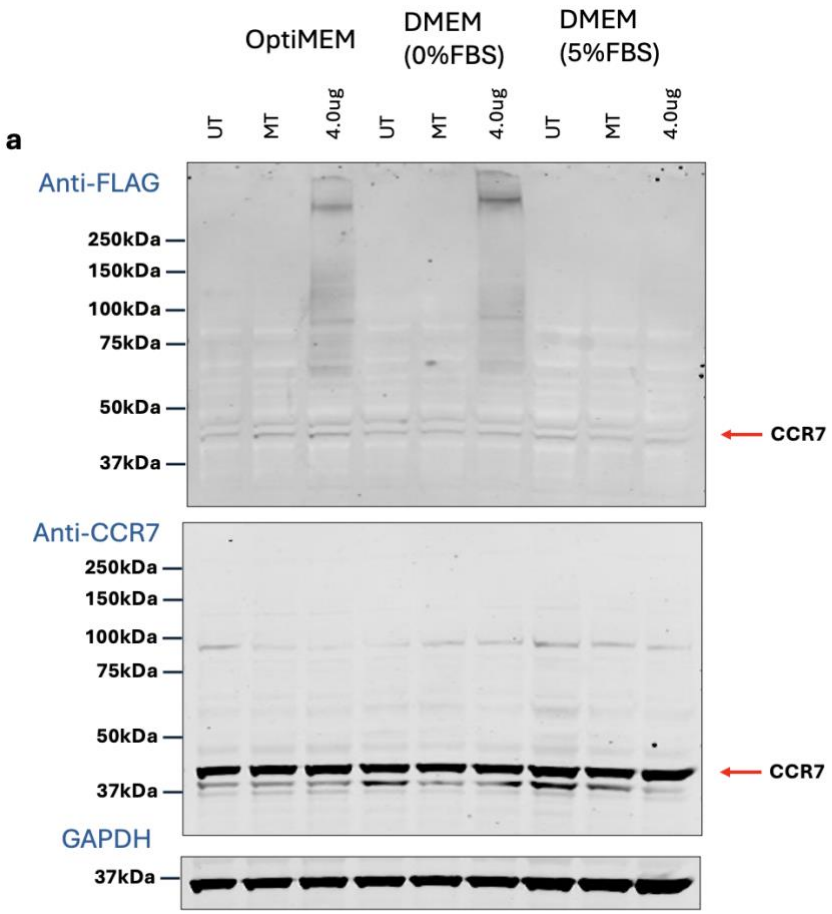

b

Cell Line	HEK293
Transfection Media	OptiMEM DMEM (0%FBS) DMEM (5% FBS)
Lipofectamine Reagent	LTX
Incubation	24h
Lysis Conditions	IP

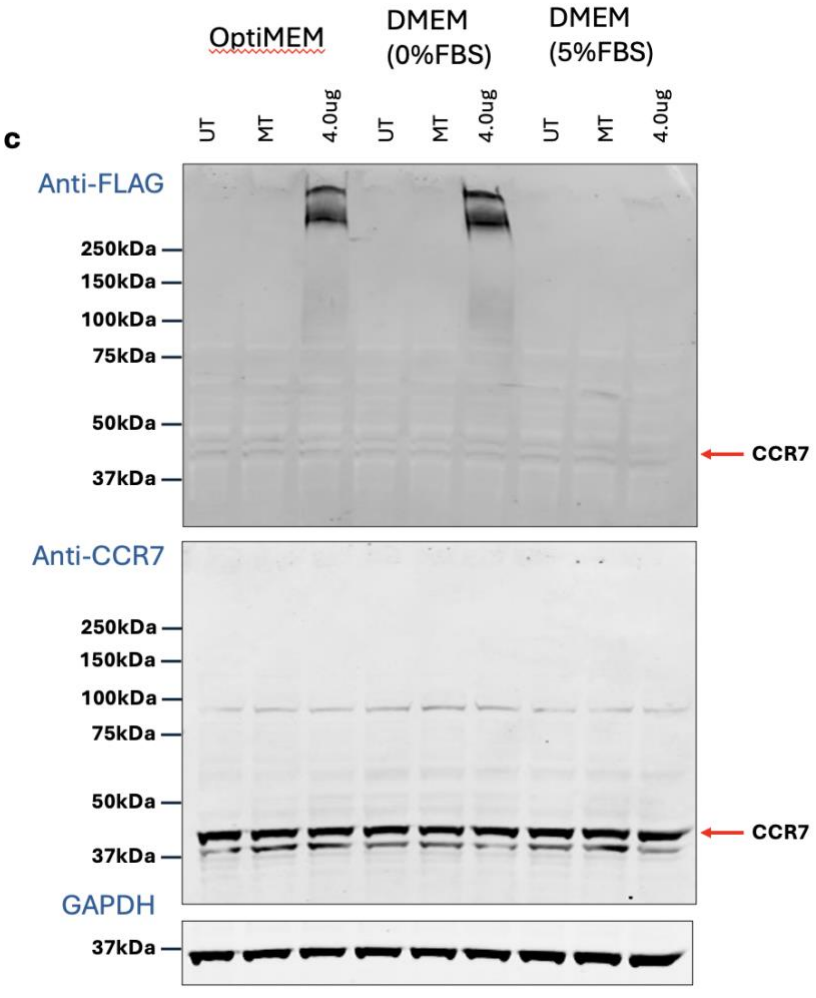

d

Cell Line	HEK293
Transfection Media	OptiMEM DMEM (0%FBS) DMEM (5%FBS)
Lipofectamine Reagent	LTX
Incubation	24h
Lysis Conditions	RIPA

Figure 16 – Western Blot Analysis of FLAG-tagged CCR7 expression in HEK293 cells under varying media and lysis conditions.
(a) *Western blot probed with anti-FLAG, anti-CCR7, and GAPDH antibodies, and lysed using IP Lysis Buffer.*
(b) *Table summarising corresponding transfection and lysis conditions.*
(c) *Western blot probed with anti-FLAG, anti-CCR7, and GAPDH antibodies, and lysed with RIPA Lysis Buffer.*
(d) *Table summarising corresponding transfection and lysis conditions.*

To determine whether solubilisation or serum content influenced FLAG-tag detection, transfections were repeated using three different media conditions – OptiMEM, DMEM (0% FBS), and DMEM (5% FBS) – and lysed using either IP Lysis Buffer (Fig. 16a,b) or RIPA Lysis Buffer (Fig. 16c,d).

When lysed using IP Lysis Buffer (Fig. 16a,b), FLAG signal remained visually weak across all media conditions, with high molecular weight smears present in the transfected lanes previously identified as potential FLAG-tagged CCR7.

In contrast, lysates prepared using RIPA Lysis Buffer (Fig. 16c,d) produced noticeably stronger FLAG-associated smearing, particularly in DMEM (0% FBS), suggesting that the higher detergent content of RIPA improved membrane protein extraction. Despite this improvement, discrete bands corresponding to exogenous CCR7 expression (~43 kDa) were still not observed.

In both blots (Fig. 16a,c), FLAG signal was noticeably reduced in the presence of DMEM (5% FBS), suggesting that serum components may reduce transfection efficiency, or interfere with FLAG-tag exposure or detection. These findings identified DMEM (0% FBS) and RIPA Lysis Buffer as optimal conditions and were therefore used for subsequent experiments with an alternate Lipofectamine reagent (Fig. 17).

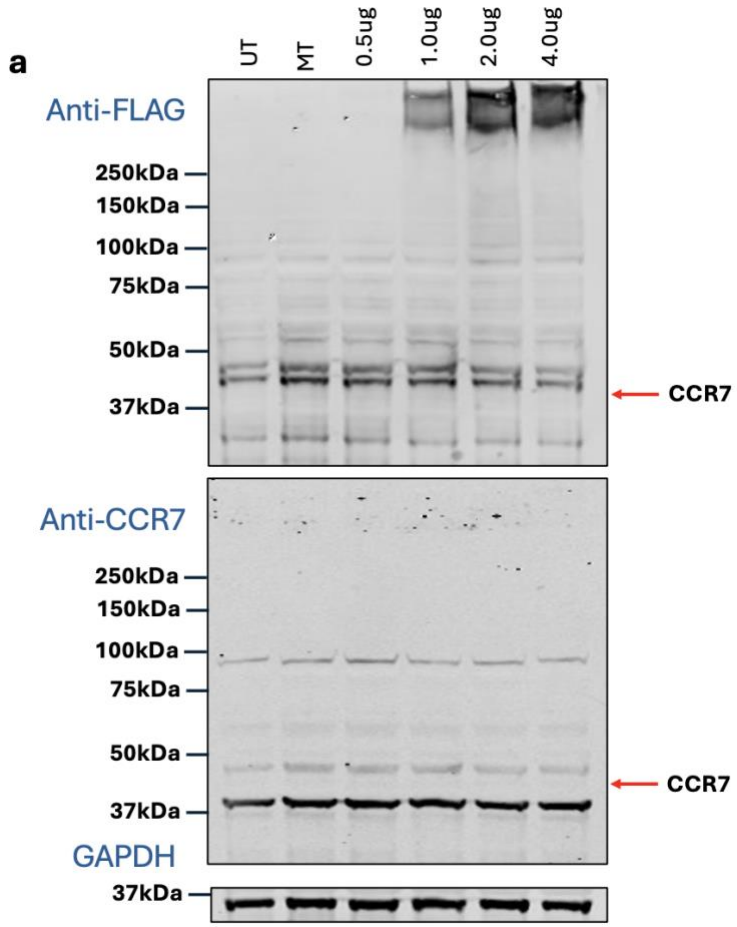

b

Cell Line	HEK293
Transfection Media	DMEM (0%FBS)
Lipofectamine Reagent	3000
Incubation	24h
Lysis Conditions	RIPA

Figure 17 – Western Blot Analysis of FLAG-tagged CCR7 expression in HEK293 cells using Lipofectamine 3000.

(a) *Western blot probed with anti-FLAG, anti-CCR7, and GAPDH antibodies.*

(b) *Table summarising corresponding transfection and lysis conditions.*

To test whether transfection efficiency could be enhanced, Lipofectamine 3000 was used to compare against previous Lipofectamine LTX reagent blots (Fig. 15,16). Transient transfection using Lipofectamine 3000 resulted in more intense FLAG signal smears (Fig. 17a) compared to previous LTX conditions, suggesting improved expression or extraction of FLAG-tagged CCR7.

Consistent high molecular weight anti-FLAG smearing was observed at the top of the gel across all transfected samples, particularly at higher plasmid concentrations (1.0–4.0 µg) (Fig. 17a), further supporting successful expression of exogenous CCR7 despite the continued absence of a sharply resolved band at the expected molecular weight.

To test whether extended incubation improved solubilisation or would allow for more complete processing of FLAG-tagged CCR7, a time course analysis was performed (Fig. 18).

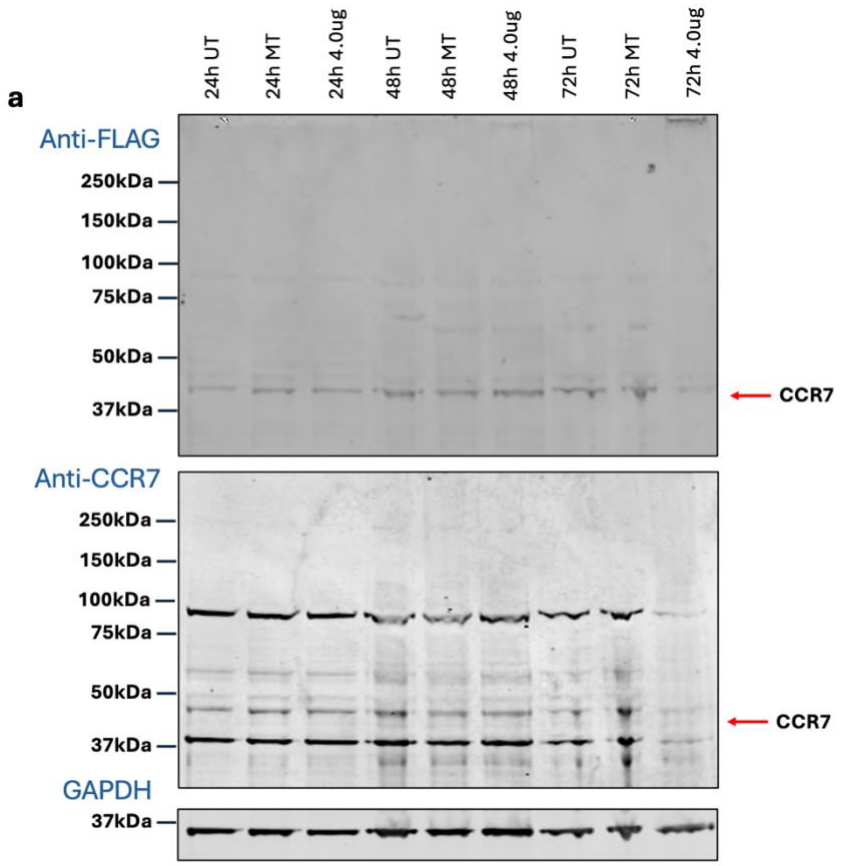

b

Cell Line	HEK293
Transfection Media	DMEM (0%FBS)
Lipofectamine Reagent	3000
Incubation	24h, 48h, 72h
Lysis Conditions	RIPA

Figure 18 – Western Blot Analysis of FLAG-tagged CCR7 expression in HEK293 cells at different time points post-transfection.

(a) *Western blot probed with anti-FLAG, anti-CCR7, and GAPDH antibodies. Lysates obtained 24 h, 48 h, 72 h post-transfection.*

(b) *Table summarising corresponding transfection and lysis conditions.*

Transfected HEK293 cells were harvested 24, 48, and 72 h post-transfection under identical conditions (Fig. 18b). Despite prolonged incubation, FLAG signal intensity remained relatively weak across all time points (Fig. 18a), with no clear trend. CCR7 band intensity did not vary substantially between controls and CCR7-transfected samples. The 24 h sample displayed a more visually prominent anti-CCR7 band pattern compared with later time points, although this was not accompanied by corresponding FLAG detection, suggesting potential non-specific CCR7 antibody binding. In addition, high-weight molecular smears were also absent when using anti-FLAG antibody staining.

Overall, extended incubation did not substantially improve the appearance of discrete FLAG- or CCR7-positive bands, suggesting that prolonged post-transfection incubation alone was insufficient to resolve the heterogeneous migration pattern observed across transfected samples. This indicates that factors such as membrane extraction efficiency, plasmid

concentration, or post-translational modification likely contributed more substantially to the observed smear patterns than incubation time alone. Therefore, alternate CCR7 plasmid concentrations were attempted at varying time points (Fig. 19).

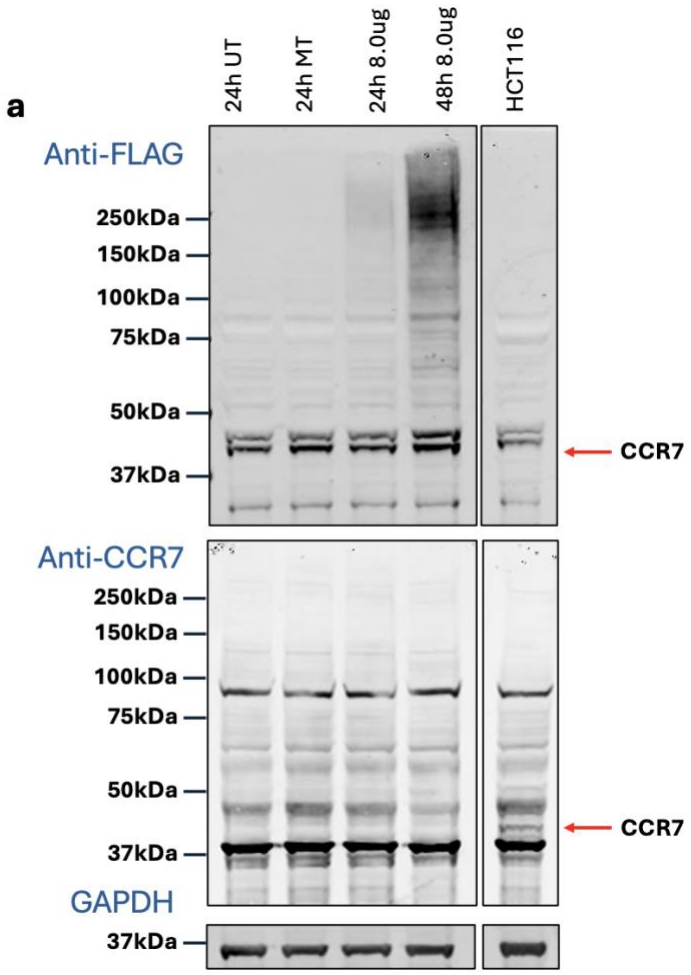

b

Cell Line	HEK293
Transfection Media	DMEM (0%FBS)
Lipofectamine Reagent	3000
Incubation	24h, 48h
Lysis Conditions	RIPA

Figure 19 – Western Blot Analysis of FLAG-tagged CCR7 expression in HEK293 cells using increased plasmid concentration.

(a) *Western blot probed with anti-FLAG, anti-CCR7, and GAPDH antibodies.*

(b) *Table summarising corresponding transfection and lysis conditions.*

This Western blot assessed whether increased plasmid concentrations could enhance CCR7 or FLAG signal, by transfecting HEK293 cells with 8.0 µg of plasmid and harvesting at varying time points (Fig. 19b).

FLAG smearing was again observed in both transfected conditions, with the 48 h sample showing visibly increased intensity at 48 h compared with 24 h (Fig. 19a). The persistence of these high molecular weight FLAG-reactive species across transfection conditions further supported successful expression of exogenous CCR7, despite the absence of a sharply resolved monomeric band.

An HCT116 lysate positive anti-CCR7 control was included in this blot and a discrete CCR7 band at 43kDa was achieved, validating the CCR7 antibody. To determine whether improved cell

attachment could stabilise expression or aid solubility, transfections were next conducted on collagen-coated and uncoated plates (Fig. 20).

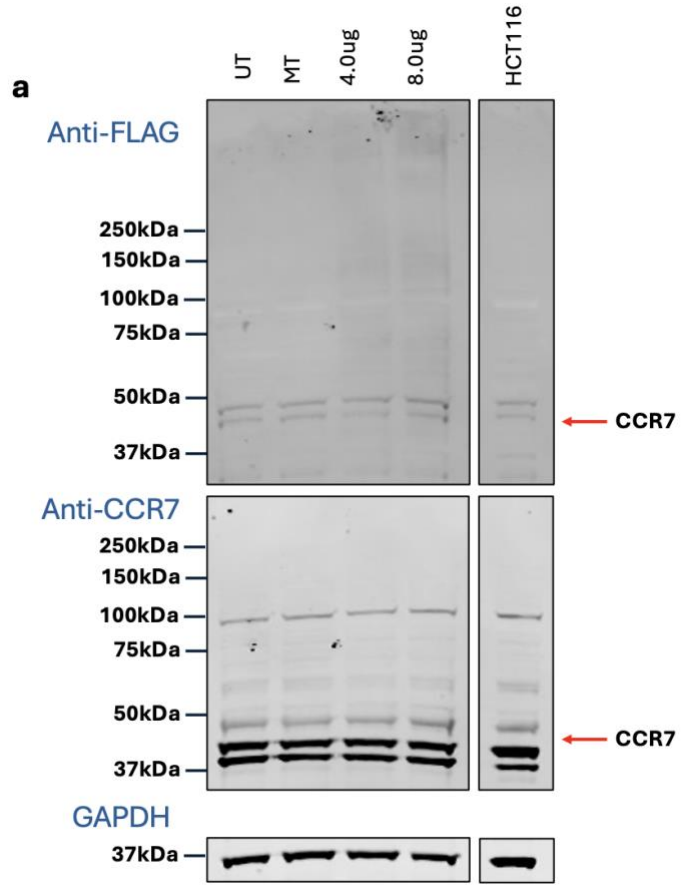

b

Cell Line	HEK293
Transfection Media	DMEM (0%FBS)
Lipofectamine Reagent	3000
Incubation	24h
Lysis Conditions	RIPA
Collagen	No

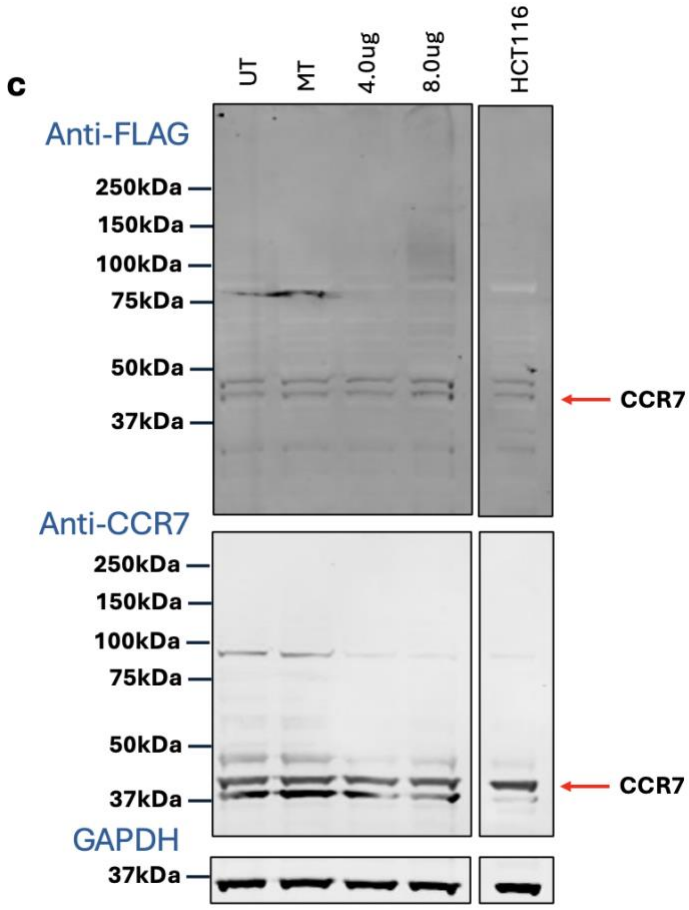

d

Cell Line	HEK293
Transfection Media	DMEM (0%FBS)
Lipofectamine Reagent	3000
Incubation	24h
Lysis Conditions	RIPA
Collagen	Yes

Figure 20 – Western Blot Analysis of FLAG-tagged CCR7 expression in HEK293 cells using collagen and collagen-free plates.

***(a)** Western blot probed with anti-FLAG, anti-CCR7, and GAPDH antibodies.*
***(b)** Table summarising corresponding transfection and lysis conditions, not including collagen.*
***(c)** Western blot probed with anti-FLAG, anti-CCR7, and GAPDH antibodies.*
***(d)** Table summarising corresponding transfection and lysis conditions, including collagen.*

HEK293 cells were transfected with 4.0 µg or 8.0 µg plasmid DNA and cultured on either a collagen-coated or uncoated plate for 24 h (Fig. 20b,d). FLAG and CCR7 signal intensity remained largely unchanged between coated and uncoated conditions (Fig. 20a,c), indicating that collagen-mediated improvements in cell attachment did not substantially alter either FLAG or CCR7 detection.

Collectively, these findings demonstrate that FLAG-tagged CCR7 expression was achieved under multiple transfection and experimental conditions, as evidenced by the reproducible FLAG-associated smear patterns selectively observed in transfected samples. However, CCR7 predominantly migrated as high molecular weight smears rather than producing discrete bands at the expected molecular weight (~43kDa), which is consistent with the known biochemical behaviour of membrane-associated and glycosylated GPCRs. Although optimisation of transfection, lysis, and culture conditions improved signal detection, efficient resolution of CCR7 expression was not achieved under the conditions tested.

Given the successful detection of endogenous CCR7 in the HCT116 positive control and the consistent GAPDH loading across samples to confirm sample integrity, this motivated the decision to focus on direct visualisation of the membrane-bound CCR7 as opposed to extracting it from the membrane itself.

Confocal imaging, specifically immunocytochemistry (ICC), offers direct visualisation of CCR7 and its FLAG-tag within intact cells (Fig. 21). Consistent with the preceding optimisation experiments, HEK293 cells were used due to their adherent growth properties, high transfection efficiency, and suitability for high-resolution imaging of exogenous membrane protein expression. Cells were transiently transfected with either 4 µg or 8 µg of the CCR7 expression plasmid and fixed at 24, 48, and 72 hours post-transfection (Fig. 21b). Cells were then stained with antibodies targeting CCR7 (detected using Alexa Fluor 647, magenta) and FLAG-tag (Alexa Fluor 488, yellow), with nuclei counterstained using DAPI (cyan).

Each condition was imaged across four channels, DAPI, FLAG, CCR7, and a merged composite, with consistent acquisition parameters and min/max scaling for each fluorophore to ensure consistency across samples. Controls included un-transfected cells stained with only primary or only secondary antibodies, or both primary and secondary antibodies, as well as mock-transfected cells treated with transfection reagent alone and then stained with both primary and secondary antibodies (Fig. 21a).

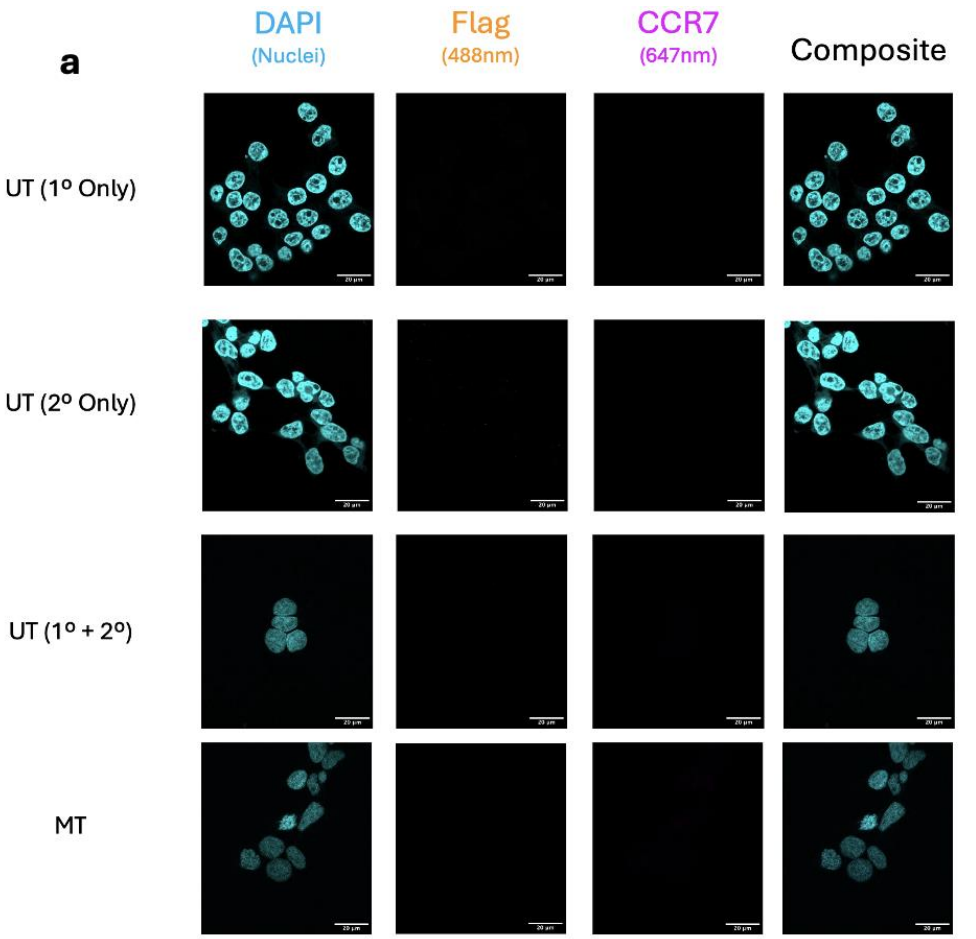
a
DAPI
(Nuclei)
Flag
(488nm)
CCR7
(647nm)
Composite
UT (1º Only)
UT (2º Only)
UT (1º + 2º)
MT

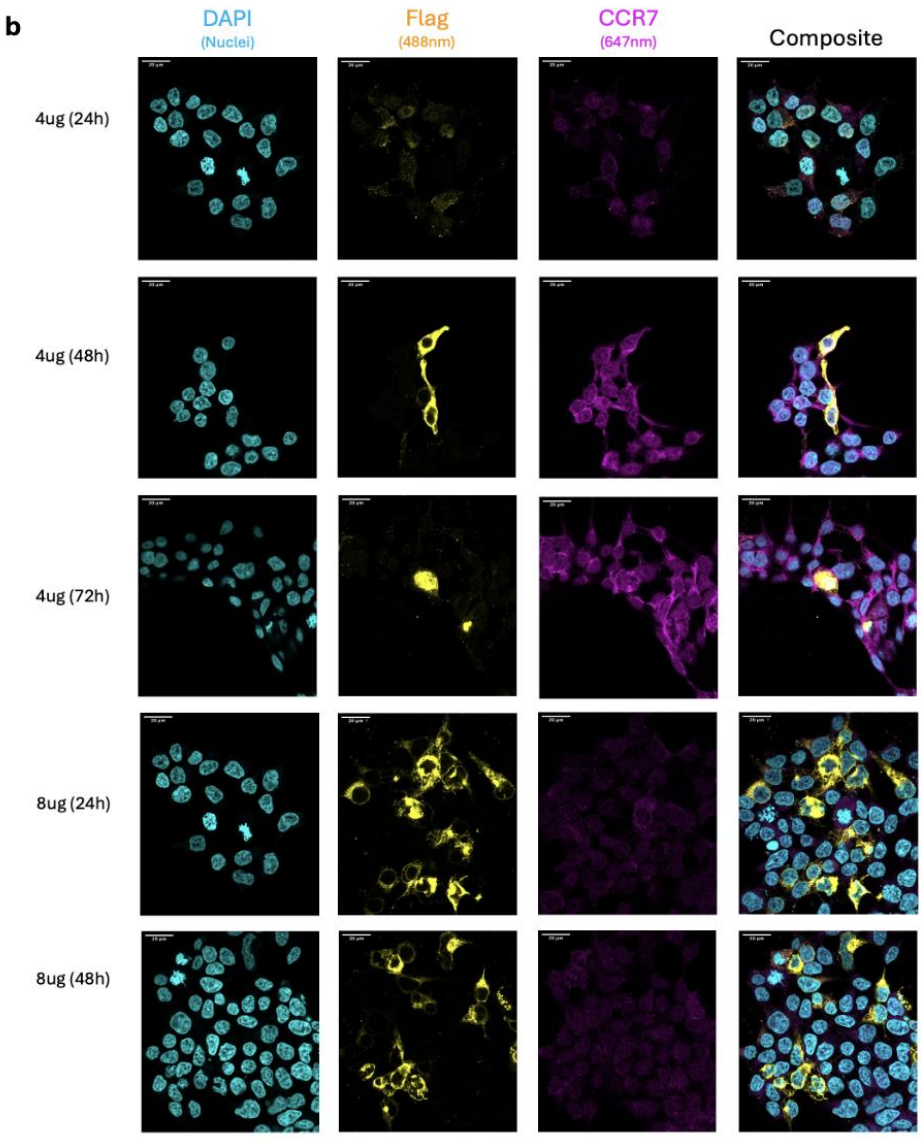
b
DAPI
(Nuclei)
Flag
(488nm)
CCR7
(647nm)
Composite
4ug (24h)
4ug (48h)
4ug (72h)
8ug (24h)
8ug (48h)

Figure 21 – Immunocytochemistry analysis of CCR7 overexpression in HEK293 cells.
HEK293 cells were transiently transfected with CCR7 expression plasmid and stained with anti-FLAG (yellow, Alexa Fluor 488) and anti-CCR7 (magenta, Alexa Fluor 647) antibodies. Nuclei were counterstained with DAPI (cyan).
Each condition includes DAPI, FLAG, CCR7, and merged composite channels.
Imaging parameters were held constant across all samples for direct comparison: FLAG (340–40000), CCR7 (130–44500).
***(a)** Control slides: un-transfected cells stained with either primary antibody only, secondary antibody only, or both. Mock-transfected cells were stained with both primary and secondary antibodies. No FLAG or CCR7 signal was detected, confirming specificity of staining.*
***(b)** Transfected conditions: cells were transfected with 4 µg or 8 µg of CCR7 expression plasmid and fixed at 24, 48, or 72 hours post-transfection.*

Control slides exhibited no detectable FLAG-tag or CCR7 signal, indicating antibody specificity and low background staining (Fig. 21a). This confirmed that any signal in the transfected conditions (Fig. 21b) could be attributed to exogenous expression of the CCR7 protein.

In CCR7-transfection conditions (Fig. 21b), FLAG-tag and CCR7 staining were observed at the plasma membrane, consistent with the known localisation of CCR7. FLAG-tag expression appeared to be most robust at 24 h post-transfection, with 8 µg of plasmid yielding the strongest and most consistent staining across cells. CCR7 signal intensity, however, did not follow the same trend. Despite higher FLAG expression with 8 µg DNA, CCR7 signal intensity appeared reduced compared to cells transfected with 4 µg.

Quantification of transfection efficiency of each condition tested (Fig. 22), revealed a peak of 44% when 8 µg of plasmid DNA was transfected for 24 hours.

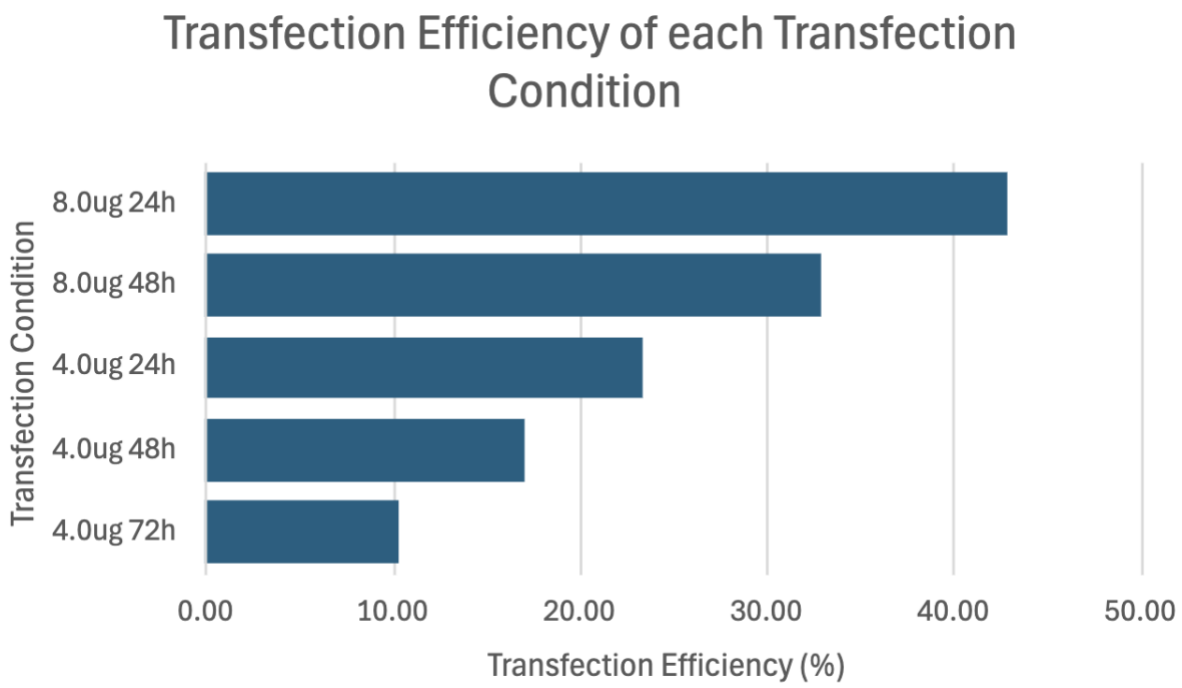

Figure 22 - Quantification of transfection efficiency in HEK293 cells based on FLAG-positive cell counts.

Transfection efficiency is expressed as the percentage of FLAG-positive cells relative to the total number of DAPI-stained nuclei.

There was a notable decrease in transfection efficiency as incubation time increased, irrespective of plasmid concentration, with efficiency dropping to as low as 11% by 72 h when transfected with 4 µg of plasmid. Based on these findings, transfection with 8 µg of plasmid for 24 h was identified as the optimal transient transfection condition for FLAG-tagged CCR7 expression.

4.3 Functional Validation of CCR7 Overexpression Model

To assess whether the transiently transfected HEK293 cells were overexpressing functionally active CCR7, a series of Transwell Migration Assays were performed in response to CCR7's two ligands, CCL19 and CCL21. Prior to functional analysis, the recombinant ligands were validated by western blot to confirm protein integrity and identity (Fig. 23).

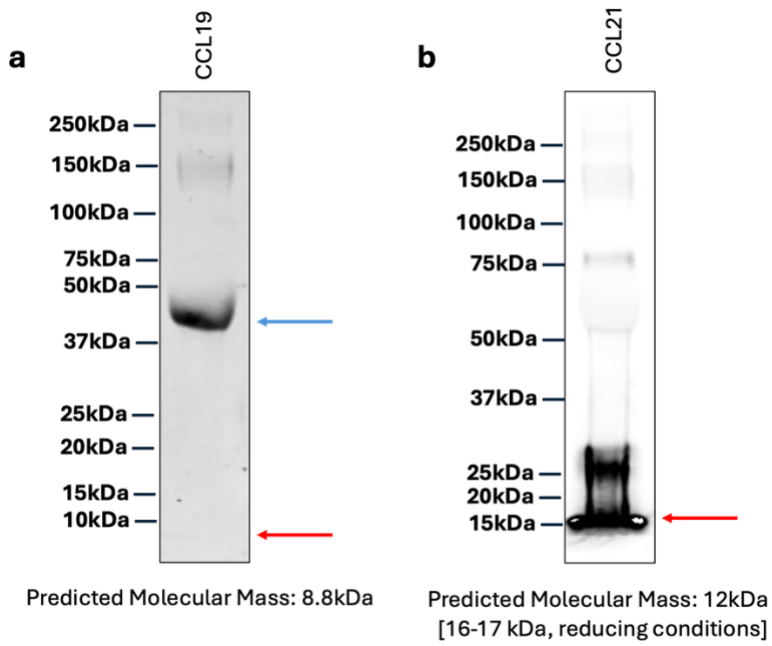

Figure 23 – Western blot validation of recombinant human CCL19 and CCL21 ligands used in migration assays.

Each ligand was run separately under reducing conditions.

(a) *WB of recombinant human CCL19 probed with anti-CCL19 antibody. The predicted molecular weight of CCL19 was 8.8 kDa (indicated by red arrow), however, a band was detected at ~40 kDa (indicated by blue arrow).*

(b) *WB of recombinant human CCL21 probed with anti-CCL21 antibody. A band was detected at the expected molecular weight of 16-17 kDa (indicated by red arrow) under reducing conditions.*

The CCL19 blot revealed a single band at ~40 kDa, higher than the predicted molecular weight of 8.8 kDa. This discrepancy may reflect the presence of carrier proteins within the supplied preparation. In contrast, CCL21 was detected at the expected molecular weight of 16–17 kDa, with mild smearing observed across the 15–30 kDa range, and regions of high signal intensity at the edges of the lane. Despite the altered migration profile observed for CCL19, both recombinant ligands demonstrated detectable antibody reactivity prior to their use in transwell migration assays.

Following ligand validation, migration assays were performed using the previously determined optimal transfection condition (8 µg of plasmid for 24 h), and cell migration was evaluated in response to CCL19 and CCL21 at increasing concentrations (0–200 ng/mL).

For each ligand, two experimental conditions were established, one using serum free media (DMEM (100 U/mL P/S, 0% FBS)) (Fig. 24,25), and one using low serum media (DMEM (100 U/mL P/S, 1% FBS)) (Fig. 26,27). Each medium was used in both the upper and lower chamber of the assay to mitigate any confounding effects of serum gradients.

To directly compare CCR7-mediated migration, mock-transfected and CCR7-transfected cells were seeded in adjacent wells, three wells for each ligand concentration, of the same 24-well plate under identical ligand concentrations. Migration was assessed by CVS, with representative images having been captured (Fig. 24a,25a,26a,27a) to qualitatively assess migration, followed by solubilisation of the stain and quantification of its absorbance at 595 nm (Fig. 24b-c,25b-c,26b-c,27b-c). Technical triplicates for each condition were averaged, normalised, and used to calculate mean values and standard deviations across all biological replicates.

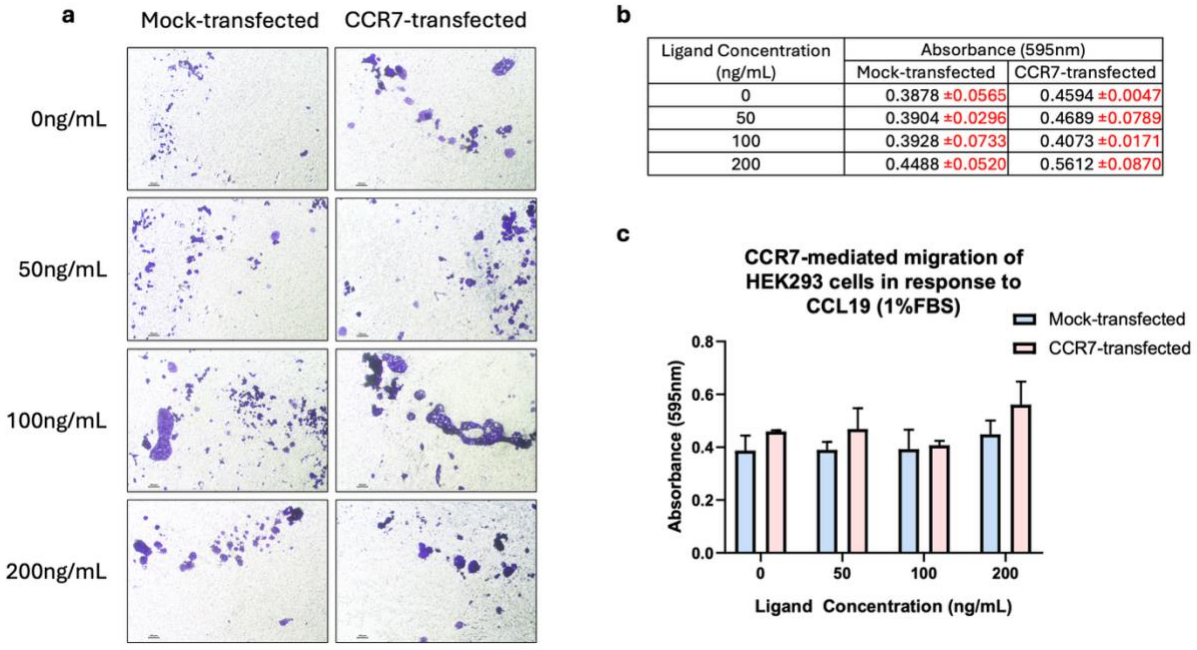

b

Ligand Concentration (ng/mL)	Absorbance (595nm)	
	Mock-transfected	CCR7-transfected
0	0.3878 ±0.0565	0.4594 ±0.0047
50	0.3904 ±0.0296	0.4689 ±0.0789
100	0.3928 ±0.0733	0.4073 ±0.0171
200	0.4488 ±0.0520	0.5612 ±0.0870

Figure 24 – CCR7-mediated chemotactic migration of HEK293 cells in response to CCL19 in a Transwell migration assay.

Assay was performed using low serum media: DMEM (1% FBS, 100 U/mL P/S).

***(a)** Representative images of Crystal Violet-stained HEK293 cells that migrated through the membrane after 24h incubation. Mock-transfected (left) and CCR7-transfected (right) cells were exposed to increasing concentrations of CCL19 (0–200 ng/mL) in the lower chamber. Images were captured at 4x magnification using a NIS-Elements microscope equipped with a Canon digital camera. A 100µm scale bar is shown in the bottom left corner.*

***(b)** Quantification of migrated cells following stain solubilisation, measured by absorbance at 595 nm. Values represent mean ± SD from three independent biological replicates, each performed in technical triplicate*

***(c)** Graphical summary of cell migration in response to CCL19 gradient, generated using GraphPad Prism 8. Statistical analysis was performed using two-way ANOVA followed by Sidak's multiple comparisons test (ns = not significant; * $p < 0.05$).*

Representative images of migrated cells (Fig. 24a) showed a modest increase in migration towards CCL19 under low serum media conditions in CCR7-transfected cells when compared with mock controls, particularly at higher ligand concentrations (100 ng/mL).

Quantitative analysis (Fig. 24b,c) confirmed this trend, with the absorbance values in CCR7-transfected cells (0.474 ± 0.02 AU) being generally higher than that of the mock-transfected cells (0.405 ± 0.02 AU). Two-way ANOVA revealed significant main effect of ligand

concentration (p = 0.0319) and transfection status (p = 0.0092), but no significant interaction (p = 0.5362) between the two factors, which, indicates that CCL19 concentration and CCR7 expression each independently influenced migration.

Sidak's post hoc comparisons test found no significant pairwise differences at specific ligand concentrations (all $p > 0.05$), but the overall trend supports a CCR7-mediated chemotactic response to CCL19 in this condition.

These findings indicated a subtle but measurable enhancement of migration with CCR7 expression in response to CCL19 under low-serum conditions, and therefore the chemotactic response toward CCL21 was next examined under identical conditions (1% FBS) (Fig. 25).

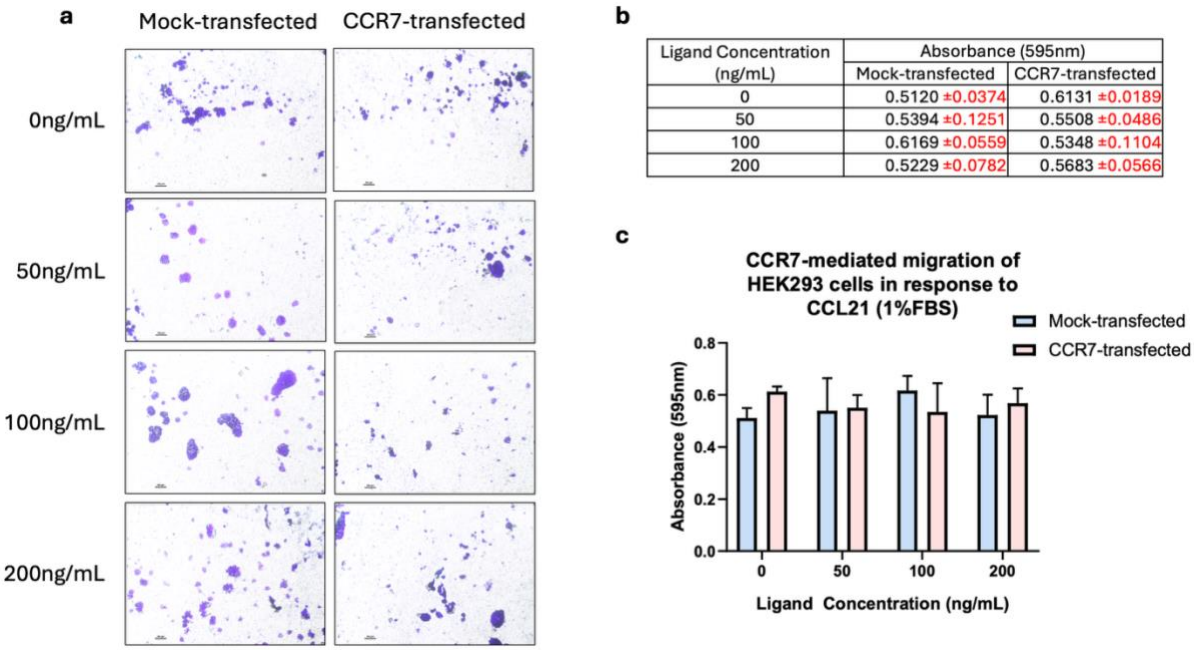

Ligand Concentration (ng/mL)	Absorbance (595nm)	
	Mock-transfected	CCR7-transfected
0	0.5120 ±0.0374	0.6131 ±0.0189
50	0.5394 ±0.1251	0.5508 ±0.0486
100	0.6169 ±0.0559	0.5348 ±0.1104
200	0.5229 ±0.0782	0.5683 ±0.0566

Figure 25 – CCR7-mediated chemotactic migration of HEK293 cells in response to CCL21 in a Transwell migration assay.

Assay was performed using low serum media: DMEM (1% FBS, 100 U/mL P/S).

***(a)** Representative images of Crystal Violet-stained HEK293 cells that migrated through the membrane after 24h incubation. Mock-transfected (left) and CCR7-transfected (right) cells were exposed to increasing concentrations of CCL21 (0–200 ng/mL) in the lower chamber. Images were captured at 4x magnification using a NIS-Elements microscope equipped with a Canon digital camera. A 100µm scale bar is shown in the bottom left corner.*

***(b)** Quantification of migrated cells following stain solubilisation, measured by absorbance at 595 nm. Values represent mean ± SD from three independent biological replicates, each performed in technical triplicate*

***(c)** Graphical summary of cell migration in response to CCL21 gradient, generated using GraphPad Prism 8. Statistical analysis was performed using two-way ANOVA followed by Sidak's multiple comparisons test (ns = not significant; * $p < 0.05$).*

In contrast, CCR7-transfected cells showed no noticeable change in migration towards CCL21 in low serum conditions. Representative images (Fig. 25a) and absorbance data (Fig. 25c) both indicate similar levels of migration between CCR7-transfected cells and mock controls, across all CCL21 concentrations.

Two-way ANOVA (Fig. 25b,c) indicated no significant effects of ligand concentration (p = 0.8696), transfection status (p = 0.5421), or their interaction (p = 0.2294), suggesting that

neither increasing CCL21 concentration nor CCR7 expression significantly altered migration under these conditions. Additionally, the mean absorbance values for both CCR7-transfected (0.567 ± 0.03 AU) and mock-transfected cells (0.548 ± 0.03 AU) revealed little difference. This data suggests that, unlike CCL19, CCL21 did not induce a significant CCR7-mediated chemotactic response in low serum conditions (1% FBS).

To determine whether serum content influenced CCR7-mediated migration, these migration assays were repeated using serum free media (DMEM (0% FBS)) (Fig. 26).

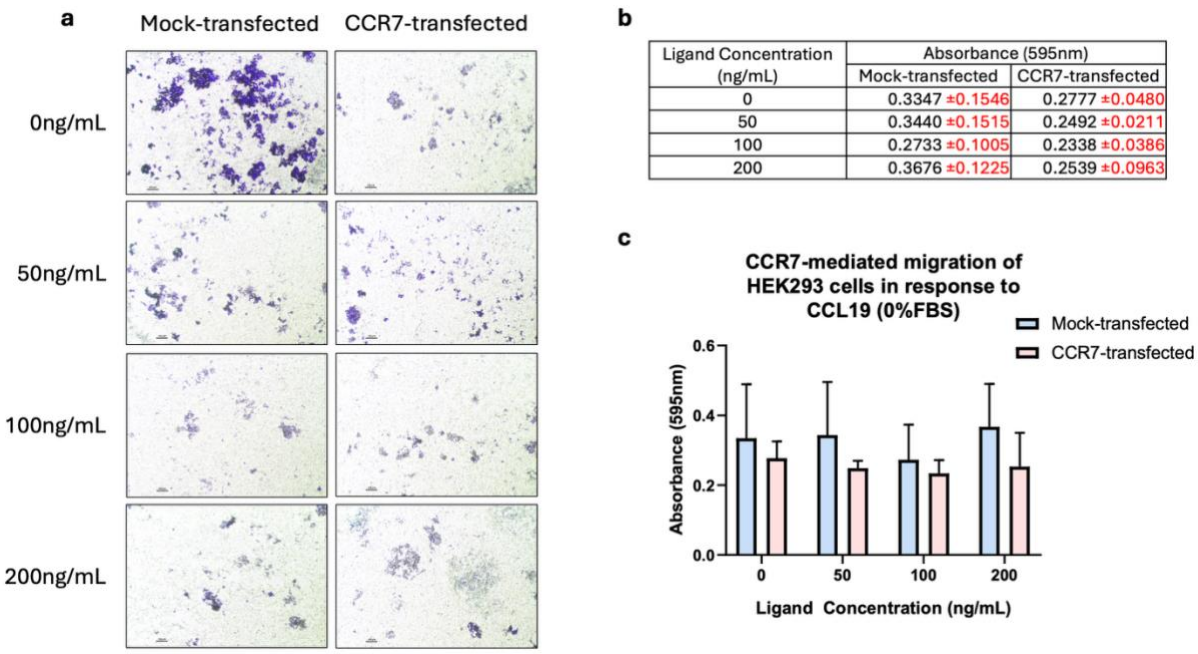

Ligand Concentration (ng/mL)	Absorbance (595nm)	
	Mock-transfected	CCR7-transfected
0	0.3347 ±0.1546	0.2777 ±0.0480
50	0.3440 ±0.1515	0.2492 ±0.0211
100	0.2733 ±0.1005	0.2338 ±0.0386
200	0.3676 ±0.1225	0.2539 ±0.0963

Figure 26 – CCR7-mediated chemotactic migration of HEK293 cells in response to CCL19 in a Transwell migration assay.

Assay was performed using low serum media: DMEM (0% FBS, 100 U/mL P/S).

***(a)** Representative images of Crystal Violet-stained HEK293 cells that migrated through the membrane after 24h incubation. Mock-transfected (left) and CCR7-transfected (right) cells were exposed to increasing concentrations of CCL19 (0-200 ng/mL) in the lower chamber. Images were captured at 4x magnification using a NIS-Elements microscope equipped with a Canon digital camera. A 100µm scale bar is shown in the bottom left corner.*

***(b)** Quantification of migrated cells following stain solubilisation, measured by absorbance at 595 nm. Values represent mean ± SD from three independent biological replicates, each performed in technical triplicate*

***(c)** Graphical summary of cell migration in response to CCL19 gradient, generated using GraphPad Prism 8. Statistical analysis was performed using two-way ANOVA followed by Sidak's multiple comparisons test (ns = not significant; * $p < 0.05$).*

Representative images (Fig. 26a) revealed low overall migration across all conditions. However, at 0 ng/mL CCL19 concentration, mock-transfected cells appeared to migrate more than the CCR7-transfected cells.

Quantitative analysis of mean migration levels (Fig. 26) revealed that they were low overall, though there was a slight increase in absorbance values between CCR7-transfected cells (0.254 ± 0.04 AU) and the mock control (0.330 ± 0.04 AU). Despite this, two-way ANOVA analysis revealed no significant main effects of ligand concentration (p = 0.7662), transfection status (p

= 0.0897), or interaction between factors (p = 0.9204). Additionally, post hoc analysis revealed no significant pairwise differences across concentrations (all $p > 0.05$) either. These findings indicate that serum deprivation noticeably reduces cell migration and the effect of any CCR7-mediated chemotaxis towards to CCL19, contrasting what was seen in low serum media (Fig. 27).

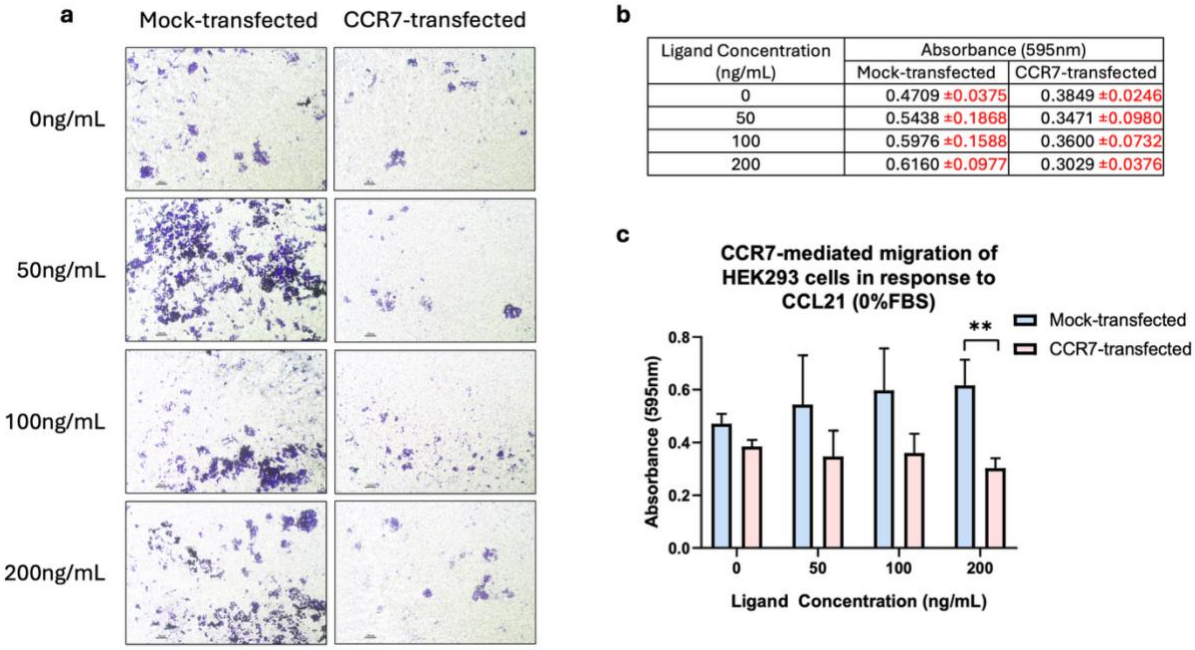

Ligand Concentration (ng/mL)	Absorbance (595nm)	
	Mock-transfected	CCR7-transfected
0	0.4709 ±0.0375	0.3849 ±0.0246
50	0.5438 ±0.1868	0.3471 ±0.0980
100	0.5976 ±0.1588	0.3600 ±0.0732
200	0.6160 ±0.0977	0.3029 ±0.0376

Figure 27 – CCR7-mediated chemotactic migration of HEK293 cells in response to CCL21 in a Transwell migration assay.

Assay was performed using low serum media: DMEM (0% FBS, 100 U/mL P/S).

***(a)** Representative images of Crystal Violet-stained HEK293 cells that migrated through the membrane after 24h incubation. Mock-transfected (left) and CCR7-transfected (right) cells were exposed to increasing concentrations of CCL21 (0-200 ng/mL) in the lower chamber. Images were captured at 4x magnification using a NIS-Elements microscope equipped with a Canon digital camera. A 100µm scale bar is shown in the bottom left corner.*

***(b)** Quantification of migrated cells following stain solubilisation, measured by absorbance at 595 nm. Values represent mean ± SD from three independent biological replicates, each performed in technical triplicate*

***(c)** Graphical summary of cell migration in response to CCL21 gradient, generated using Pri GraphPad Prism 8. Statistical analysis was performed using two-way ANOVA followed by Sidak's multiple comparisons test (ns = not significant; * $p < 0.05$).*

When transfected cells were exposed to CCL21 under serum free conditions, mock-transfected cells were shown to migrate more than CCR7-transfected cells (Fig. 27a), particularly at the highest ligand concentration (200 ng/mL).

Quantitative results (Fig. 27b,c) confirmed this unexpected trend, with mock-transfected cells displayed higher migration (0.557 ± 0.04 AU) than CCR7-transfected cells (0.349 ± 0.04 AU) across all ligand concentrations. The two-way ANOVA also revealed a significant main effect of

transfection status (p = 0.0002), but not of ligand concentration (p = 0.8579) or their interaction (p = 0.3335). Sidak's multiple comparisons test identified a significant difference between CCR7-transfected and mock-transfected conditions at 200 ng/mL CCL21 (p = 0.0085) (Fig. 27b,c).

These results demonstrate that, under serum free conditions, CCR7-transfected cells exhibited significantly reduced migration toward CCL21 compared to mock-transfected controls, contrary to the expected chemotactic response.

Overall, this assay design enabled the quantitative comparison of CCR7-transfected HEK293 cells with mock controls, across a range of ligand concentrations and serum conditions. This approach allowed for distinct ligand specific effects (CCL19 vs. CCL21) to be determined, and for the evaluation as to whether serum supplementation had any impact on chemotaxis. These results provide a basis for further investigation into ligand and serum specific effects on CCR7-mediated chemotaxis.

5. Discussion

This study explored the expression and prognostic significance of CCR7 expression in CRC, integrating the bioinformatic analysis of patient and publicly available datasets, with in vitro validation experiments aimed at developing and characterising a CCR7-overexpressing HEK293 cellular model. Together, these findings provide insight into CCR7's complex and context-dependent role in colorectal tumorigenesis, cancer progression, and chemotactic behaviour, while establishing a foundational in vitro platform for future functional validation.

5.1 CCR7 as a Prognostic Biomarker in Colorectal Cancer

CCR7 gene expression displayed distinct stratification patterns in both the full CRC cohort and rectal subset, as evidenced by unsupervised k-means clustering (Fig. 6). These non-random expression patterns are consistent with CCR7's known role in immune cell trafficking via CCL19 and CCL21 chemokine gradients [2,4], and suggests that CCR7 may be biologically relevant in colorectal tumour stratification.

Although survival analysis using these clusters showed trends toward improved survival in high CCR7 groups, there was no significant associations between higher CCR7 expression and CSS (Fig. 7). This lack of clear prognostic value is consistent with previous studies, where CCR7 expression has been variably linked to both favourable and adverse outcomes depending on cancer type, stage, and immune microenvironment context [8,10,45]. This variability may reflect site-specific differences in tumour biology or immune-related factors, particularly in CRC, which often overlaps with inflammation associated with inflammatory bowel disease [7,16].

The application of cutpoint optimisation algorithms (Fig. 8) identified statistically significant survival outcomes, suggesting that CCR7 may hold prognostic value that is not captured by unsupervised clustering alone. However, while this supports the potential use of CCR7 as a prognostic marker, the use of algorithmically derived cutpoints inflates statistical significance due to multiple hypothesis testing, thus increasing the risk of overfitting. Therefore, these findings should be seen as exploratory, and further validation in larger, prospective cohorts and across alternative tumour types (Fig. 4) would be needed to establish clinical utility [46].

Complementary analysis using the HPA datasets (Fig. 9-12) reinforced the heterogeneity observed in the clinical datasets. In colon adenocarcinoma, high CCR7 expression correlated

with improved survival in early disease stages, while in more advanced stages this benefit diminished. A similar pattern was observed in rectum adenocarcinoma, with early-stage tumours showing high CCR7 expression was also associated with improved survival. However, unlike colon cancer, high CCR7 expression in late-stage rectal tumours continued to show a survival advantage until approximately 7.5 years of follow-up, after which the benefit declined.

This stage specific variation supports the implication that CCR7's role may be context-dependent and shift during tumour progression; initially supporting immune surveillance and then contributing towards metastatic dissemination at later disease stages. This dynamic functional shift has been previously described in other tumour types, such as breast cancer, where CCR7 facilitates lymph node metastasis by guiding tumour cells toward CCL21-rich environments [47,48].

The variation in optimal prognostic cutpoints across tumour sites and stages highlights the limitations of fixed high/low expression thresholds. Instead, context-specific stratification may more accurately reflect the underlying biology and better inform prognostic assessments. This reinforces the need for biomarker frameworks that incorporate disease stage, anatomical location, and immune context [7,10,31].

Furthermore, the significant association between high CCR7 expression and invasive tumour features, such as venous invasion and lymph node metastasis ($p = 0.020$ and $p = 0.030$ respectively), supports its recognised role in metastatic dissemination. This is consistent with previous studies identifying CCR7 as a key driver of lymphatic dissemination via chemotactic signalling through its ligands, CCL19 and CCL21 [26,45,48].

Overall, the bioinformatic findings reinforces the rationale for further exploration of CCR7 as a context-dependent biomarker in CRC. Its involvement in immune cell migration, combined with stage-specific and site-specific prognostic patterns, positions CCR7 as a possible candidate for personalised risk stratification. Future work should prioritise validation in larger, clinically annotated cohorts and investigate functional mechanisms using relevant in vivo and ex vivo CRC models [28,36].

5.2 Establishment of a CCR7-Overexpressing Cell Model

To facilitate future functional studies and therapeutic screening, a CCR7-overexpressing HEK293 model was developed. Following successful amplification of the CCR7 expression plasmid (Fig. 13,14), transient transfection experiments were performed across a range of DNA concentrations and time points to assess CCR7 protein expression.

While Western blot analysis using both anti-FLAG and anti-CCR7 antibodies failed to produce discrete bands at the expected molecular weight (~43 kDa), high molecular weight smears were observed (Fig. 15-20) in the transfected samples. This pattern is consistent with the known biochemical properties of GPCRs, like CCR7, which are highly hydrophobic, membrane bound proteins that tend to aggregate and resist solubilisation using standard lysis protocols [49]. Despite extensive troubleshooting, including modifications to lysis buffer composition, loading amounts, transfection reagent and medium, and blotting protocols, discrete CCR7 bands could not be resolved. These results likely reflect overexpression-induced stress, aberrant folding, or saturation of the cellular machinery involved in membrane protein trafficking and processing [50]. In particular, the high molecular weight smear pattern observed across transfected samples is consistent with heterogeneous glycosylation, a common feature of membrane-associated GPCRs that can alter electrophoretic mobility and reduce band resolution during SDS-PAGE analysis [49,50].

To improve biochemical detection in future studies, alternative strategies could be employed, such as using a different detergent (e.g. CHAPS, digitonin), membrane-specific extraction kits, or surface biotinylation approaches to enrich for properly folded and membrane-localised CCR7 [10,27]. Additionally, the use of alternative cell lines with higher intrinsic membrane protein handling capacity may also enhance protein recovery and detection [50].

In contrast, ICC provided clearer evidence of successful CCR7 overexpression and membrane localisation (Fig. 21). Staining with both anti-FLAG and anti-CCR7 antibodies demonstrated robust signalling at 24 h post-transfection using 8 µg of CCR7 plasmid, with quantification analysis revealing a peak transfection efficiency of 44% under these conditions (Fig. 22). However, signal intensity and transfection efficiency declined as incubation time increased (48-72 h), suggesting that CCR7 overexpression may promote detachment or migration of these cells, behaviours which are consistent with its known role in cell trafficking and chemotaxis, particularly within immune and metastatic contexts [2,3,10].

Furthermore, given that ICC only captures adherent monolayers, these observations could also suggest that CCR7-overexpressing cells may have physically detached from the coverslip surface over time, thus becoming underrepresented in the imaging fields. For future experiments, the use of adherence enhancing coatings, such as fibronectin or collagen, may mitigate CCR7-driven detachment and improve retention of migratory cells [21,23].

Functional activity of overexpressed CCR7 was assessed using Transwell migration assays in response to its ligands, CCL19 and CCL21, across both low serum (1% FBS) and serum-free (0% FBS) conditions. Under low-serum conditions, CCR7-transfected cells showed a modest increase in migration towards CCL19 compared with mock controls (Fig. 24). Although the magnitude of this effect was limited, it followed the expected chemotactic response of CCR7 interacting with CCL19. This is consistent with the established role of CCL19 as an activator of CCR7-driven cell migration and supports the functional competence of the overexpressed receptor in this model [2,4,10]. In contrast, CCL21 did not elicit a comparable migratory response under the same conditions (Fig. 25), suggesting ligand-specific receptor dynamics, such as variations in binding affinity, receptor internalisation, or activation of downstream signalling pathways [12,13,15,54]. Previous studies have demonstrated that, despite recognising the same receptor, CCL19 and CCL21 can induce divergent signalling outcomes, with CCL21 often promoting receptor retention at the plasma membrane and sustained signalling, whereas CCL19 favours rapid internalisation and transient activation [3,6,15,54].

In serum free conditions, overall migration was reduced for all experimental groups, indicating that serum derived components likely contribute to baseline motility and cell viability. Notably, CCR7-transfected cells migrated significantly less toward CCL21 compared with mock controls (Fig. 27), suggesting that ligand engagement in the absence of serum factors may induce receptor desensitisation or impaired cytoskeletal responses. Such ligand-dependent inhibition has been reported in other GPCR systems, where sustained receptor activation leads to internalisation and downstream signalling attenuation [17,49,50,54].

These findings validate the use of HEK293 cells as a platform for CCR7 overexpression, though future work may benefit from using more physiologically relevant cancer cell lines.

5.3 Limitations

While this study provides valuable insights into the role and expression of CCR7 in cancer, specifically CRC, it has several limitations. The initial clinical and pre-clinical analysis was

comprised of a relatively small sample size, particularly the rectal subgroup (n = 63), which limits its statistical power and could increase the risk of random error and potential bias within these findings, such as false negatives. Moreover, tumour heterogeneity within the CRC cohort may have further confounded associations between CCR7 expression and clinical parameters, as tumour heterogeneity is a recognised challenge in transcriptomic analyses [51].

Furthermore, although the HEK293 overexpression model served as a useful tool to establish CCR7 protein localisation and expression feasibility, it does not mimic the epithelial or immune cell context relevant to colorectal or lymphoid malignancies [10,31]. Moreover, transient transfection methods introduce variability in transgene expression and temporal kinetics, limiting the reproducibility and physiological relevance of functional assays [53].

Technical difficulties in detecting CCR7 protein expression via Western blotting further constrained biochemical validation. As a hydrophobic GPCR, CCR7 is prone to aggregation and poor solubilisation in standard lysis conditions, an issue that frequently complicates GPCR research [49]. Despite extensive troubleshooting, the inability to resolve distinct bands highlights the need for more specialised protocols for membrane protein extraction and detection [50]. In addition, these technical challenges prevented consistent signal detection across replicates, limiting the ability to perform reliable quantitative analyses and report standardised mean and standard deviation values.

5.4 Future Directions

Building on these findings, several avenues for future investigation are warranted. Validation of CCR7's prognostic and biological relevance should be investigated in larger, independent cohorts. These datasets would, ideally, include stage-specific and molecular subtype annotations, as well as immune profiling, particularly given the differing trends observed between colon and rectal cancers and between early and late disease stages. Given the higher statistical expression of CCR7 observed in lymphatic and myeloid malignancies (Fig. 3), additional investigations into these cancer types may yield clearer functional insights and stronger clinical associations, making CCR7 a more appropriate biomarker [14,33,36].

Mechanistic studies using patient cell lines could also be used to determine whether CCR7 actively promotes invasive and metastatic behaviour or acts via immunomodulatory pathways. CRISPR/Cas9-mediated gene editing and lentiviral systems for stable overexpression or knockdown would provide controlled models for dissecting CCR7's functional contributions in a

cancer-relevant context. These refined models would also serve as valuable tools for preclinical evaluation of CCR7-targeted therapies, including ADCs and PDCs, helping bridge the gap between biomarker discovery and translational drug development [21,36,52].

Technically, optimisation of CCR7 detection, particularly via Western blotting, should be prioritised. Approaches such as detergent-resistant membrane fractionation, surface biotinylation, or cross-linking immunoprecipitation may improve yield and resolution of GPCRs like CCR7 in biochemical assays [10,49]. Alternatively, fluorescently tagged CCR7 constructs, and flow cytometry-based quantification may offer complementary data to Western blotting and ICC [3,19].

Furthermore, the establishment of a stable CCR7-overexpressing cell line using HEK293 cells would provide a more robust and reliable platform for both the mechanistic investigation and preclinical evaluation of CCR7-targeted therapeutics. While the transient transfection approaches used throughout this project enabled preliminary functional insights, CCR7-overexpression remained variable across each experiment. Generating a stably transfected cell model via lentiviral transduction or antibiotic selection would ensure consistent and sustained CCR7 overexpression across cell passages, thereby improving experimental reproducibility [55,56].

Collectively, these directions offer a more robust and translationally relevant exploration of CCR7 as a prognostic biomarker and therapeutic target in cancer.

6. Conclusion

This study demonstrates that CCR7 expression in colorectal cancer stratifies patient subgroups and correlates with invasive features, though its prognostic significance is context dependent, varying by tumour site and disease stage. While Western blot analysis was unable to visualise discrete CCR7 bands, ICC confirmed successful CCR7 overexpression in vitro, providing a valuable platform for future therapeutic screening. Transwell migration assays revealed ligand and serum dependent effects of CCR7 on cell migration, further highlighting its complex functional role in chemotaxis. Together, these findings support CCR7 as a biologically relevant, albeit complex, biomarker and potential therapeutic target in cancer.

Appendix A. Annotated CCR7 Plasmid Sequence

Annotated features:

- Full CCR7 Coding Insert (blue text)
- Forward Primer (blue)
- Sequencing Primer (purple)
- DYK (FLAG)-tag (yellow)
- Kpn I restriction site (green)
- Start Codon (red)
- Reverse Primer complement (pink)
- BamHI site (dark green)
- Multiple cloning site end (grey)

>2_CCR7_pcDNA3.1(+)-N-DYK

GACGGATCGGGAGATCTCCCGATCCCCTATGGTGCACTCTCAGTACAATCTGCTCTGATGCCGCATAGTT

AAGCCAGTATCTGCTCCCTGCTTGTGTGTTGGAGGTCGCTGAGTAGTGCGCGAGCAAAATTTAAGCTACA

ACAAGGCAAGGCTTGACCGACAATTGCATGAAGAATCTGCTTAGGGTTAGGCGTTTTGCGCTGCTTCGC

GATGTACGGGCCAGATATACGCGTTGACATTGATTATTGACTAGTTATTAATAGTAATCAATTACGGGGT

CATTAGTTCATAGCCCATATATGGAGTTCCGCGTTACATAACTTACGGTAAATGGCCCGCCTGGCTGACC

GCCCAACGACCCCCGCCCATTGACGTCAATAATGACGTATGTTCCCATAGTAACGCCAATAGGGACTTTC

CATTGACGTCAATGGGTGGAGTATTTACGGTAAACTGCCCACTTGGCAGTACATCAAGTGTATCATATGC

CAAGTACGCCCCCTATTGACGTCAATGACGGTAAATGGCCCGCCTGGCATTATGCCCAGTACATGACCTT

ATGGGACTTTCCTACTTGGCAGTACATCTACGTATTAGTCATCGCTATTACCATGGTGATGCGGTTTTGGC

AGTACATCAATGGGCGTGGATAGCGGTTTGACTCACGGGGATTTCCAAGTCTCCACCCCATTGACGTCAA

TGGGAGTTTGTTTTGGCACCAAAATCAACGGGACTTTCCAAAATGTCGTAACAACTCCGCCCCATTGACG

CAAATGGGCGGTAGGCGTGTACGGTGGGAGGTCTATATAAGGAGCTCTCTGGCTAACTAGAGAACCCAC

TGCTTACTGGCTTATCGAAATTAATACGACTCACTATAGGGAGACCCAAGCTGGCTAGCGTTTAAACTTA

AGCTTGCCACCATGGATTACAAGGATGACGACGATAAGGGTACCATGGACCTGGGCAAGCCTATGAAAA

GCGTGCTGGTGGTGGCCCTGCTGGTTATCTTCCAAGTCTGCCTGTGTCAGGACGAGGTGACCGATGACT

ACATCGGCGATAACACAACCGTGGACTACACCCTGTTCGAGAGCCTCTGTAGCAAGAAAGATGTGCGGA

ATTTCAAGGCCTGGTTCCTGCCAATAATGTACAGCATCATCTGCTTCGTGGGACTGCTGGGCAACGGCCT

GGTGGTGCTGACCTACATCTACTTCAAAAGACTGAAGACCATGACCGACACCTACCTGCTGAACCTGGCC

GTGGCAGATATCCTGTTCCTGCTGACACTGCCTTTCTGGGCCTATTCTGCCGCCAAGTCCTGGGTGTTCGG
CGTGCACTTCTGCAAGCTGATCTTTGCCATCTACAAGATGTCTTTTTTCAGCGGAATGCTGCTCCTCCTGT
GCATCAGCATCGACAGATACGTGGCCATCGTGCAGGCCGTGTCCGCCCACAGACACCGGGCCAGAGTGC
TGCTGATTAGCAAGCTGAGCTGCGTGGGCATCTGGATTCTGGCCACCGTGCTGTCTATCCCTGAGCTGCT
GTACAGCGACCTGCAGAGGTCCAGCAGCGAGCAGGCCATGAGATGTTCTCTGATCACCGAGCACGTGGA
AGCCTTTATCACAATCCAGGTTGCTCAGATGGTGATCGGCTTCCTGGTCCCCCTGCTGGCCATGAGCTTTT
GCTACCTGGTGATCATCAGAACCCTGCTGCAAGCTAGAAATTTCGAACGGAACAAGGCCATTAAGGTGA
TCATCGCCGTGGTCGTGGTCTTCATCGTGTTCCAGCTGCCTTACAACGGAGTGGTGCTGGCCCAGACAGT
GGCTAATTTCAACATCACCAGCAGCACCTGCGAGCTCTCTAAACAGCTGAACATCGCTTACGACGTGACA
TATAGCCTGGCTTGTGTGCGGTGCTGCGTGAACCCCTTCCTGTACGCCTTTATCGGCGTTAAGTTCAGAA
ACGACCTGTTCAAGCTGTTTAAGGATTTGGGCTGCCTGAGCCAGGAGCAGCTGAGACAGTGGTCCTCCT
GCAGACATATCCGCCGGAGCTCTATGAGCGTGGAAGCTGAAACCACCACAACATTCAGCCCTTGAGGAT
CCTGATAAGAATTCTGCAGATATCCAGCACAGTGGCGGCCGCTCGAGTCTAGAGGGCCCGTTTAAACCC
GCTGATCAGCCTCGACTGTGCCTTCTAGTTGCCAGCCATCTGTTGTTTGCCCCTCCCCCGTGCCTTCCTTGA
CCCTGGAAGGTGCCACTCCCACTGTCCTTTCCTAATAAAATGAGGAAATTGCATCGCATTGTCTGAGTAG
GTGTCATTCTATTCTGGGGGGTGGGGTGGGGCAGGACAGCAAGGGGGAGGATTGGGAAGACAATAGC
AGGCATGCTGGGGATGCGGTGGGCTCTATGGCTTCTGAGGCGGAAAGAACCAGCTGGGGCTCTAGGGG
GTATCCCCACGCGCCCTGTAGCGGCGCATTAAGCGCGGCGGGTGTGGTGGTTACGCGCAGCGTGACCGC
TACACTTGCCAGCGCCCTAGCGCCCGCTCCTTTCGCTTTCTTCCCTTCCTTTCTCGCCACGTTCGCCGGCTTT
CCCCGTCAAGCTCTAAATCGGGGGCTCCCTTTAGGGTTCCGATTTAGTGCTTTACGGCACCTCGACCCCAA
AAAACTTGATTAGGGTGATGGTTCACGTAGTGGGCCATCGCCCTGATAGACGGTTTTTCGCCCTTTGACG
TTGGAGTCCACGTTCTTTAATAGTGGACTCTTGTTCCAAACTGGAACAACACTCAACCCTATCTCGGTCTA
TTCTTTTGATTTATAAGGGATTTTGCCGATTTCGGCCTATTGGTTAAAAAATGAGCTGATTTAACAAAAAT
TTAACGCGAATTAATTCTGTGGAATGTGTGTCAGTTAGGGTGTGGAAAGTCCCCAGGCTCCCCAGCAGG
CAGAAGTATGCAAAGCATGCATCTCAATTAGTCAGCAACCAGGTGTGGAAAGTCCCCAGGCTCCCCAGC
AGGCAGAAGTATGCAAAGCATGCATCTCAATTAGTCAGCAACCATAGTCCCGCCCCTAACTCCGCCCATC
CCGCCCCTAACTCCGCCCAGTTCCGCCCATTCTCCGCCCCATGGCTGACTAATTTTTTTTATTTATGCAGAG
GCCGAGGCCGCCTCTGCCTCTGAGCTATTCCAGAAGTAGTGAGGAGGCTTTTTTGGAGGCCTAGGCTTTT
GCAAAAAGCTCCCGGGAGCTTGTATATCCATTTTCGGATCTGATCAAGAGACAGGATGAGGATCGTTTCG
CATGATTGAACAAGATGGATTGCACGCAGGTTCTCCGGCCGCTTGGGTGGAGAGGCTATTCGGCTATGA
CTGGGCACAACAGACAATCGGCTGCTCTGATGCCGCCGTGTTCCGGCTGTCAGCGCAGGGGCGCCCGGT

TCTTTTTGTCAAGACCGACCTGTCCGGTGCCCTGAATGAACTGCAGGACGAGGCAGCGCGGCTATCGTG
GCTGGCCACGACGGGCGTTCCTTGCGCAGCTGTGCTCGACGTTGTCACTGAAGCGGGAAGGGACTGGCT
GCTATTGGGCGAAGTGCCGGGGCAGGATCTCCTGTCATCTCACCTTGCTCCTGCCGAGAAAGTATCCATC
ATGGCTGATGCAATGCGGCGGCTGCATACGCTTGATCCGGCTACCTGCCCATTCGACCACCAAGCGAAAC
ATCGCATCGAGCGAGCACGTACTCGGATGGAAGCCGGTCTTGTCGATCAGGATGATCTGGACGAAGAGC
ATCAGGGGCTCGCGCCAGCCGAACTGTTCGCCAGGCTCAAGGCGCGCATGCCCGACGGCGAGGATCTC
GTCGTGACCCATGGCGATGCCTGCTTGCCGAATATCATGGTGGAAAATGGCCGCTTTTCTGGATTCATCG
ACTGTGGCCGGCTGGGTGTGGCGGACCGCTATCAGGACATAGCGTTGGCTACCCGTGATATTGCTGAAG
AGCTTGGCGGCGAATGGGCTGACCGCTTCCTCGTGCTTTACGGTATCGCCGCTCCCGATTCGCAGCGCAT
CGCCTTCTATCGCCTTCTTGACGAGTTCTTCTGAGCGGGACTCTGGGGTTCGAAATGACCGACCAAGCGA
CGCCCAACCTGCCATCACGAGATTTCGATTCCACCGCCGCCTTCTATGAAAGGTTGGGCTTCGGAATCGT
TTTCCGGGACGCCGGCTGGATGATCCTCCAGCGCGGGGATCTCATGCTGGAGTTCTTCGCCCACCCCAAC
TTGTTTATTGCAGCTTATAATGGTTACAAATAAAGCAATAGCATCACAAATTTCACAAATAAAGCATTTTT
TTCACTGCATTCTAGTTGTGGTTTGTCCAAACTCATCAATGTATCTTATCATGTCTGTATACCGTCGACCTC
TAGCTAGAGCTTGGCGTAATCATGGTCATAGCTGTTTCCTGTGTGAAATTGTTATCCGCTCACAATTCCAC
ACAACATACGAGCCGGAAGCATAAAGTGTAAAGCCTGGGGTGCCTAATGAGTGAGCTAACTCACATTAA
TTGCGTTGCGCTCACTGCCCGCTTTCCAGTCGGGAAACCTGTCGTGCCAGCTGCATTAATGAATCGGCCA
ACGCGCGGGGAGAGGCGGTTTGCGTATTGGGCGCTCTTCCGCTTCCTCGCTCACTGACTCGCTGCGCTCG
GTCGTTCGGCTGCGGCGAGCGGTATCAGCTCACTCAAAGGCGGTAATACGGTTATCCACAGAATCAGGG
GATAACGCAGGAAAGAACATGTGAGCAAAAGGCCAGCAAAAGGCCAGGAACCGTAAAAAGGCCGCGTT
GCTGGCGTTTTTCCATAGGCTCCGCCCCCCTGACGAGCATCACAAAAATCGACGCTCAAGTCAGAGGTGG
CGAAACCCGACAGGACTATAAAGATACCAGGCGTTTCCCCCTGGAAGCTCCCTCGTGCGCTCTCCTGTTC
CGACCCTGCCGCTTACCGGATACCTGTCCGCCTTTCTCCCTTCGGGAAGCGTGGCGCTTTCTCATAGCTCA
CGCTGTAGGTATCTCAGTTCGGTGTAGGTCGTTCGCTCCAAGCTGGGCTGTGTGCACGAACCCCCCGTTC
AGCCCGACCGCTGCGCCTTATCCGGTAACTATCGTCTTGAGTCCAACCCGGTAAGACACGACTTATCGCC
ACTGGCAGCAGCCACTGGTAACAGGATTAGCAGAGCGAGGTATGTAGGCGGTGCTACAGAGTTCTTGA
AGTGGTGGCCTAACTACGGCTACACTAGAAGAACAGTATTTGGTATCTGCGCTCTGCTGAAGCCAGTTAC
CTTCGGAAAAAGAGTTGGTAGCTCTTGATCCGGCAAACAAACCACCGCTGGTAGCGGTGGTTTTTTTGTT
TGCAAGCAGCAGATTACGCGCAGAAAAAAAGGATCTCAAGAAGATCCTTTGATCTTTTCTACGGGGTCTG
ACGCTCAGTGGAACGAAAACTCACGTTAAGGGATTTTGGTCATGAGATTATCAAAAAGGATCTTCACCTA
GATCCTTTTAAATTAAAAATGAAGTTTTAAATCAATCTAAAGTATATATGAGTAAACTTGGTCTGACAGTT

ACCAATGCTTAATCAGTGAGGCACCTATCTCAGCGATCTGTCTATTTCGTTCATCCATAGTTGCCTGACTC
CCCGTCGTGTAGATAACTACGATACGGGAGGGCTTACCATCTGGCCCCAGTGCTGCAATGATACCGCGA
GACCCACGCTCACCGGCTCCAGATTTATCAGCAATAAACCAGCCAGCCGGAAGGGCCGAGCGCAGAAGT
GGTCCTGCAACTTTATCCGCCTCCATCCAGTCTATTAATTGTTGCCGGGAAGCTAGAGTAAGTAGTTCGCC
AGTTAATAGTTTGCGCAACGTTGTTGCCATTGCTACAGGCATCGTGGTGTCACGCTCGTCGTTTGGTATG
GCTTCATTCAGCTCCGGTTCCCAACGATCAAGGCGAGTTACATGATCCCCCATGTTGTGCAAAAAAGCGG
TTAGCTCCTTCGGTCCTCCGATCGTTGTCAGAAGTAAGTTGGCCGCAGTGTTATCACTCATGGTTATGGCA
GCACTGCATAATTCTCTTACTGTCATGCCATCCGTAAGATGCTTTTCTGTGACTGGTGAGTACTCAACCAA
GTCATTCTGAGAATAGTGTATGCGGCGACCGAGTTGCTCTTGCCCGGCGTCAATACGGGATAATACCGC
GCCACATAGCAGAACTTTAAAAGTGCTCATCATTGGAAAACGTTCTTCGGGGCGAAAACTCTCAAGGATC
TTACCGCTGTTGAGATCCAGTTCGATGTAACCCACTCGTGCACCCAACTGATCTTCAGCATCTTTTACTTTC
ACCAGCGTTTCTGGGTGAGCAAAAACAGGAAGGCAAAATGCCGCAAAAAAGGGAATAAGGGCGACACG
GAAATGTTGAATACTCATACTCTTCCTTTTTCAATATTATTGAAGCATTTATCAGGGTTATTGTCTCATGAG
CGGATACATATTTGAATGTATTTAGAAAAATAAACAAATAGGGGTTCCGCGCACATTTCCCCGAAAAGTG
CCACCTGACGTC

REFERENCES

1. Yan, C., Du, W., Kirkwood, K.L., Wang, Y., Zhou, W., Li, Z., Tian, Y., Lin, S., Zheng, L., Maged Ali Al-Aroomi, Gao, J., Jiang, S., Sun, C. and Liu, F. (2024). CCR7 affects the tumour microenvironment by regulating the activation of naïve CD8+ T cells to promote the proliferation of oral squamous cell carcinoma. *Translational Oncology*, 44, pp.101924–101924. doi:https://doi.org/10.1016/j.tranon.2024.101924.
2. Förster, R., Davalos-Misslitz, A. & Rot, A. CCR7 and its ligands: balancing immunity and tolerance. *Nat Rev Immunol* 8, 362–371 (2008). https://doi.org/10.1038/nri2297
3. Purvanov, Vladimir et al. "Fluorescently Tagged CCL19 and CCL21 to Monitor CCR7 and ACKR4 Functions." *International journal of molecular sciences* vol. 19,12 3876. 4 Dec. 2018, doi:10.3390/ijms19123876
4. Sanjiv A. Luther, Afshin Bidgol, Diana C. Hargreaves, Andrea Schmidt, Ying Xu, Jyothi Paniyadi, Mehrdad Matloubian, Jason G. Cyster; Differing Activities of Homeostatic Chemokines CCL19, CCL21, and CXCL12 in Lymphocyte and Dendritic Cell Recruitment and Lymphoid Neogenesis[1]. *J Immunol* 1 July 2002; 169 (1): 424–433. https://doi.org/10.4049/jimmunol.169.1.424
5. Menzel, Lutz et al. "Lymphocyte access to lymphoma is impaired by high endothelial venule regression." Cell reports vol. 37,4 (2021): 109878. doi:10.1016/j.celrep.2021.109878
6. Noelia Sánchez-Sánchez, Lorena Riol-Blanco, José Luis Rodríguez-Fernández; The Multiple Personalities of the Chemokine Receptor CCR7 in Dendritic Cells[1]. *J Immunol* 1 May 2006; 176 (9): 5153–5159. https://doi.org/10.4049/jimmunol.176.9.5153
7. Brandum, Emma Probst et al. "Dendritic Cells and CCR7 Expression: An Important Factor for Autoimmune Diseases, Chronic Inflammation, and Cancer." *International journal of molecular sciences* vol. 22,15 8340. 3 Aug. 2021, doi:10.3390/ijms22158340
8. Rizeq, Balsam, and Mohammed Imad Malki. "The Role of CCL21/CCR7 Chemokine Axis in Breast Cancer Progression." *Cancers* vol. 12,4 1036. 23 Apr. 2020, doi:10.3390/cancers12041036
9. Y.K. Mburu, K. Abe, L.K. Ferris, S.N. Sarkar, R.L. Ferris. Human beta-defensin 3 promotes NF-kappaB-mediated CCR7 expression and anti-apoptotic signals in squamous cell carcinoma of the head and neck. Carcinogenesis, 32 (2011), pp. 168-174
10. Bill, C.A.; Allen, C.M.; Vines, C.M. C-C Chemokine Receptor 7 in Cancer. *Cells* 2022, *11*, 656. https://doi.org/10.3390/cells11040656
11. Seyfried, Thomas N, and Leanne C Huysentruyt. "On the origin of cancer metastasis." *Critical reviews in oncogenesis* vol. 18,1-2 (2013): 43-73. doi:10.1615/critrevoncog.v18.i1-2.40

12. Hong, W., Yang, B., He, Q., Wang, J. and Weng, Q. (2022). New Insights of CCR7 Signaling in Dendritic Cell Migration and Inflammatory Diseases. *Frontiers in Pharmacology*, 13. doi:https://doi.org/10.3389/fphar.2022.841687.
13. Jørgensen, A.S., Rosenkilde, M.M. and Hjortø, G.M. (2018). Biased signalling of G protein-coupled receptors – From a chemokine receptor CCR7 perspective. *General and Comparative Endocrinology*, 258, pp.4–14. doi:https://doi.org/10.1016/j.ygcen.2017.07.004.
14. Cuesta-Mateos, Carlos et al. "Of Lymph Nodes and CLL Cells: Deciphering the Role of CCR7 in the Pathogenesis of CLL and Understanding Its Potential as Therapeutic Target." *Frontiers in immunology* vol. 12 662866. 24 Mar. 2021, doi:10.3389/fimmu.2021.662866
15. Rodríguez-Fernández, José Luis, and Olga Criado-García. "The Chemokine Receptor CCR7 Uses Distinct Signalling Modules With Biased Functionality to Regulate Dendritic Cells." *Frontiers in immunology* vol. 11 528. 15 Apr. 2020, doi:10.3389/fimmu.2020.00528
16. Hong, Wenxiang et al. "New Insights of CCR7 Signalling in Dendritic Cell Migration and Inflammatory Diseases." *Frontiers in pharmacology* vol. 13 841687. 25 Feb. 2022, doi:10.3389/fphar.2022.841687
17. Allaire, Marc-André, and Nancy Dumais. "Involvement of the MAPK and RhoA/ROCK pathways in PGE2-mediated CCR7-dependent monocyte migration." *Immunology letters* vol. 146,1-2 (2012): 70-3. doi:10.1016/j.imlet.2012.05.002
18. Schaeuble, Karin et al. "Cross-talk between TCR and CCR7 signaling sets a temporal threshold for enhanced T lymphocyte migration." *Journal of immunology (Baltimore, Md. : 1950)* vol. 187,11 (2011): 5645-52. doi:10.4049/jimmunol.1101850
19. Tejchman, Anna et al. "Tumor hypoxia modulates podoplanin/CCL21 interactions in CCR7+ NK cell recruitment and CCR7+ tumor cell mobilization." *Oncotarget* vol. 8,19 (2017): 31876-31887. doi:10.18632/oncotarget.16311
20. Moschovakis, G.L., Bubke, A., Friedrichsen, M. *et al*. The chemokine receptor CCR7 is a promising target for rheumatoid arthritis therapy. *Cell Mol Immunol* 16, 791–799 (2019). https://doi.org/10.1038/s41423-018-0056-5
21. Xu, Bing et al. "CCR7 mediates human breast cancer cell invasion, migration by inducing epithelial-mesenchymal transition and suppressing apoptosis through AKT pathway." *Cancer medicine* vol. 6,5 (2017): 1062-1071. doi:10.1002/cam4.1039
22. Liu, Yun et al. "Modulation of tumor microenvironment for immunotherapy: focus on nanomaterial-based strategies." *Theranostics* vol. 10,7 3099-3117. 10 Feb. 2020, doi:10.7150/thno.42998

23. Ma, Huiying et al. “CCR7 enhances TGF-β1-induced epithelial-mesenchymal transition and is associated with lymph node metastasis and poor overall survival in gastric cancer.” *Oncotarget* vol. 6,27 (2015): 24348-60. doi:10.18632/oncotarget.4484
24. Ribatti, Domenico et al. “Epithelial-Mesenchymal Transition in Cancer: A Historical Overview.” *Translational oncology* vol. 13,6 (2020): 100773. doi:10.1016/j.tranon.2020.100773
25. Roche J. The Epithelial-to-Mesenchymal Transition in Cancer. Cancers (Basel). 2018 Feb 16;10(2):52. doi: 10.3390/cancers10020052. Erratum in: Cancers (Basel). 2018 Mar 19;10(3):E79. doi: 10.3390/cancers10030079. PMID: 29462906; PMCID: PMC5836084.
26. Mishan, M.A., Ahmadiankia, N. and Bahrami, A.R. (2016) ‘CXCR4 and CCR7: Two eligible targets in targeted cancer therapy’, *Cell Biology International*, 40(9), pp. 955–967. Available at: https://doi.org/10.1002/cbin.10631
27. Schall, T., Proudfoot, A. Overcoming hurdles in developing successful drugs targeting chemokine receptors. *Nat Rev Immunol* 11, 355–363 (2011). https://doi.org/10.1038/nri2972
28. CCR7 as a therapeutic target in Cancer. (2020). *Biochimica et Biophysica Acta (BBA) - Reviews on Cancer*, [online] p.188499. doi:https://doi.org/10.1016/j.bbcan.2020.188499
29. Gowhari Shabgah, Arezoo et al. “Does CCL19 act as a double-edged sword in cancer development?.” *Clinical and experimental immunology* vol. 207,2 (2022): 164-175. doi:10.1093/cei/uxab039
30. Hughes, Catherine E, and Robert J B Nibbs. “A guide to chemokines and their receptors.” *The FEBS journal* vol. 285,16 (2018): 2944-2971. doi:10.1111/febs.14466
31. Alrumaihi, Faris. “The Multi-Functional Roles of CCR7 in Human Immunology and as a Promising Therapeutic Target for Cancer Therapeutics.” *Frontiers in molecular biosciences* vol. 9 834149. 6 Jul. 2022, doi:10.3389/fmolb.2022.834149
32. Vela M, Aris M, Llorente M, Garcia-Sanz JA, Kremer L. Chemokine receptor-specific antibodies in cancer immunotherapy: achievements and challenges. Front Immunol. 2015 Jan 30;6:12. doi: 10.3389/fimmu.2015.00012. PMID: 25688243; PMCID: PMC4311683
33. Catapult Therapeutics. (2024). *Catapult Therapeutics ~ Targeted Therapy for Cancer*. [online] Available at: https://www.catapult-therapeutics.com/ [Accessed Jan. 2025].
34. Mateu-Albero, Tamara et al. “Evaluation of the novel therapeutic anti-CCR7 antibody CAP-100 as an add-on therapy in chronic lymphocytic leukemia patients receiving venetoclax.” *Hematological oncology* vol. 41,5 (2023): 869-876. doi:10.1002/hon.3213

35. *NCI Drug Dictionary* (2024) *Cancer.gov*. Available at: https://www.cancer.gov/publications/dictionaries/cancer-drug/def/anti-ccr7-monoclonal-antibody-cap-100 (Accessed: November 2024).
36. Cuesta-Mateos, Carlos & Juárez-Sánchez, Raquel & Mateu-Albero, Tamara & Loscertales, Javier & Mol, Wim & Terrón, Fernando & Muñoz, Cecilia. (2021). Targeting cancer homing into the lymph node with a novel anti-CCR7 therapeutic antibody: the paradigm of CLL. mAbs. 13. 1917484. 10.1080/19420862.2021.1917484
37. Pau Abrisqueta, Marks, R., Irit Avivi, Wermke, M., Lim, F., Tae Min Kim, Alba Cabirta Touzon, Kristiina Karihtala, Shinichi Makita, Werner, L., Tanaka, C., Dang, A., Chaudhury, A., Rice, S., Chowdhury, R., Knee, D., Belén Gomezcarrillo, Furutani, E., Koji Izutsu and Sirpa Leppä (2024). Abstract CT174: A phase 1 study of JBH492, an anti C-C chemokine receptor 7 antibody-drug conjugate (anti-CCR7 ADC), assessing safety and efficacy in lymphoid malignancies. *Cancer research*, 84(7_Supplement), pp.CT174–CT174. doi:https://doi.org/10.1158/1538-7445.am2024-ct174
38. Clinicaltrials.gov. (2025). Available at: https://clinicaltrials.gov/study/NCT05327114 [Accessed Jan. 2025].
39. Lindberg, J.; Nilvebrant, J.; Nygren, P.-Å.; Lehmann, F. Progress and Future Directions with Peptide-Drug Conjugates for Targeted Cancer Therapy. *Molecules* 2021, *26*, 6042. https://doi.org/10.3390/molecules26196042
40. Endpoints Contributor (2024) *PDCs vs. ADCs: A New Frontier in Targeted Cancer Therapies and the Potential for Development Partnerships*, *Endpoints News*. Available at: https://endpts.com/sp/pdcs-vs-adcs-a-new-frontier-in-targeted-cancer-therapies-and-the-potential-for-development-partnerships/ (Accessed: November 2024).
41. Shiravand Y, Khodadadi F, Kashani SMA, Hosseini-Fard SR, Hosseini S, Sadeghirad H, Ladwa R, O'Byrne K, Kulasinghe A. Immune Checkpoint Inhibitors in Cancer Therapy. Curr Oncol. 2022 Apr 24;29(5):3044-3060. doi: 10.3390/curroncol29050247. PMID: 35621637; PMCID: PMC9139602.
42. Li, Bin et al. "Immune Checkpoint Inhibitors Combined with Targeted Therapy: The Recent Advances and Future Potentials." *Cancers* vol. 15,10 2858. 22 May. 2023, doi:10.3390/cancers15102858
43. Zhu, S., Zhang, T., Zheng, L. *et al*. Combination strategies to maximize the benefits of cancer immunotherapy. *J Hematol Oncol* 14, 156 (2021). https://doi.org/10.1186/s13045-021-01164-5

44. Mahmoodi Chalbatani, Ghanbar et al. “Small interfering RNAs (siRNAs) in cancer therapy: a nano-based approach.” *International journal of nanomedicine* vol. 14 3111-3128. 2 May. 2019, doi:10.2147/IJN.S200253
45. Kohjiro Mashino, Noriaki Sadanaga, Hiroshi Yamaguchi, Fumiaki Tanaka, Mitsuhiko Ohta, Kenji Shibuta, Hiroshi Inoue, Masaki Mori; Expression of Chemokine Receptor CCR7 Is Associated with Lymph Node Metastasis of Gastric Carcinoma1. *Cancer Res* 15 May 2002; 62 (10): 2937–2941.
46. Guan, R., Lyu, Q., Lin, A., Liang, J., Ding, W., Cao, M., Luo, P. and Zhang, J. (2021). Influence of Different Age Cutoff Points on the Prediction of Prognosis of Cancer Patients Receiving ICIs and Potential Mechanistic Exploration. Frontiers in oncology, 11. doi:https://doi.org/10.3389/fonc.2021.670927.
47. Müller, A., Homey, B., Soto, H. et al. Involvement of chemokine receptors in breast cancer metastasis. Nature 410, 50–56 (2001). https://doi.org/10.1038/35065016
48. Shields, J.D., Fleury, M.E., Yong, C., Tomei, A.A., Randolph, G.J. and Swartz, M.A. (2007). Autologous Chemotaxis as a Mechanism of Tumor Cell Homing to Lymphatics via Interstitial Flow and Autocrine CCR7 Signaling. Cancer Cell, 11(6), pp.526–538. doi:https://doi.org/10.1016/j.ccr.2007.04.020.
49. Rosenbaum, D., Rasmussen, S. & Kobilka, B. The structure and function of G-protein-coupled receptors. Nature 459, 356–363 (2009). https://doi.org/10.1038/nature08144
50. Duvernay, M.T., Filipeanu, C.M. and Wu, G. (2005). The regulatory mechanisms of export trafficking of G protein-coupled receptors. Cellular Signalling, 17(12), pp.1457–1465. doi:https://doi.org/10.1016/j.cellsig.2005.05.020.
51. Marusyk, A., Almendro, V. & Polyak, K. Intra-tumour heterogeneity: a looking glass for cancer?. Nat Rev Cancer 12, 323–334 (2012). https://doi.org/10.1038/nrc3261
52. Ran, F., Hsu, P., Wright, J. et al. Genome engineering using the CRISPR-Cas9 system. Nat Protoc 8, 2281–2308 (2013). https://doi.org/10.1038/nprot.2013.143
53. Yeong, W.-Y., Chua, C.-K., Leong, K.-F. and Chandrasekaran, M. (2004). Rapid prototyping in tissue engineering: challenges and potential. Trends in Biotechnology, 22(12), pp.643–652. doi:https://doi.org/10.1016/j.tibtech.2004.10.004.
54. Côté, S.C. et al. (2009) ‘CCR7-specific migration to CCL19 and CCL21 is induced by PGE2 stimulation in human monocytes: Involvement of EP2/EP4 receptors activation’, Molecular Immunology, 46(13), pp. 2682–2693. doi:10.1016/j.molimm.2008.08.269.
55. Elegheert, Jonathan et al. “Lentiviral transduction of mammalian cells for fast, scalable and high-level production of soluble and membrane proteins.” Nature protocols vol. 13,12 (2018): 2991-3017. doi:10.1038/s41596-018-0075-9

56. Mao, Yingying et al. “Lentiviral Vectors Mediate Long-Term and High Efficiency Transgene Expression in HEK 293T cells.” International journal of medical sciences vol. 12,5 407-15. 15 May. 2015, doi:10.7150/ijms.11270